INVESTIGATING THE ROLE OF POST-TRANSLATIONAL MODIFICATIONS IN THE CORE RAS GTPASE DOMAIN

Samantha Kathleen Kistler

A dissertation submitted to the faculty at the University of North Carolina at Chapel Hill in partial fulfillment of the requirements for the degree of Doctor of Philosophy in Chemical Biology and Medicinal Chemistry in the Eshelman School of Pharmacy.

Chapel Hill
2019

Approved by:

Sharon Campbell

Michael Jarstfer

Stephen Frye

David Williams

Adrienne Cox

Eric Brustad

ABSTRACT

Samantha Kathleen Kistler: Investigating the Role of Post-Translational Modifications in the Core Ras GTPase Domain
(Under the direction of Sharon Campbell)

Ras proteins are the most commonly mutated oncoproteins in cancer (~30%). Oncogenic, activating Ras mutations are known drivers of the deadliest human cancers, including lung, pancreatic and colorectal cancers. Ras proteins function as critical regulators of cellular growth by acting as molecular switches, cycling between active, GTP- and inactive, GDP-bound states. In their active form, Ras proteins signal through downstream pathways that regulate cellular growth, differentiation and apoptosis. Early attempts to target Ras proteins (farnesyltransferase inhibitors) were directed toward inhibiting key carboxyl (C)-terminal lipid post-translational modifications (PTMs), which are crucial for proper Ras localization and function at the cellular membrane. Despite their failure, FTIs represent the first direct targeting efforts of Ras proteins.

Promising new classes of anti-cancer drugs directed at targeting the dysregulation of PTM status in cancers (kinase inhibitors, histone deacetylase inhibitors, HDACi and methyltransferase inhibitors) have demonstrated multiple clinical successes in recent years. PTMs have been demonstrated to alter protein stability and localization as well as protein-protein interactions in several non-histone cancer-related proteins. While PTMs have been extensively studied in the C-terminus of Ras proteins, their role remains poorly understood in the core Ras guanine nucleotide binding domain (GTPase domain). Monoubiquitylation and acetylation within the core Ras GTPase domain have been demonstrated to modulate Ras protein activity,

signaling and tumorigenesis, suggesting that PTMs in this region are capable of regulating Ras behavior. Further, aberrant dysregulation in the balance of PTMs has been characterized in several cancer types, including the Ras-driven pancreatic cancer. It is therefore reasonable that Ras PTMs may present a novel avenue for therapeutic targeting in cancer. Despite more than three decades of research, Ras has remained an elusive target for cancer therapy.

We have recently identified novel sites of PTMs in Ras proteins at highly conserved residues within the core GTPase domain. Herein, we present highly innovative and novel methods of generating both acetyl- and methyl-lysine in intact Ras proteins. With the combined use of biochemical, structural, cellular and computational data, we provide mechanistic insight into the regulation Ras proteins by PTMs and also provide rationale for novel therapeutic targeting approaches in Ras-driven cancers.

TABLE OF CONTENTS

LIST OF TABLES

LIST OF FIGURES

LIST OF ABBREVIATIONS

BEZ235	Dactolisib, an ATP-competitive PI3K (phosphoinositide 3-kinase) and mTOR (mammalian target of rapamycin) inhibitor
BME	2-Mercaptoethanol
C-terminus	carboxyl-terminus
CD	circular dichroism
CFC	cardio-facio cutaneous syndrome
CRC	colorectal cancer
CS	Costello Syndrome
CSP	chemical shift perturbations
DTPA	diethylenetriaminepentaacetic acid
EGFR	Epidermal growth factor receptor
FTase	farnesyltransferase
FTI	farnesyltransferase inhibitor
GAP	GTPase activating protein
GDP	guanosine diphosphate
GEF	guanine nucleotide exchange factor
GMPPCP	Guanosine-5'-[(β,γ)-methyleno]triphosphate
GSK1120212	Trametinib, a reversible, selective MEK1/MEK2 kinase inhibitor
GTP	guanosine triphosphate
GTPγS	guanosine 5'-O-(gamma-thio)triphosphate
GTPase	guanosine triphosphatase

GTPase domain	G-domain, guanine nucleotide binding domain
H2	Helix 2 in Ras
HDACi	Histone deacetylase inhibitor
HEK-HT cells	Human embryonic kidney cells
HNSCC	Head and neck small cell carcinoma
HVR	Hypervariable region
K_D	Equilibrium dissociation constant
KDM	Histone lysine demethylase
KMT	Histone lysine methyltransferase
MANT-GDP	2'-(or-3')-O-(N-Methylanthraniloyl) Guanosine 5'-Diphosphate
MANT-GMPPCP	2'/3'-O-(N-Methyl-anthraniloyl)-guanosine-5'-((β,γ)-methyleno)triphosphate
MANT-GTPγS	2'/3'-O-(N-Methyl-anthraniloyl)-guanosine-5'-(γ-thio)-triphosphate
MAP3K2 (MEKK2)	Mitogen-activated protein kinase kinase kinase 2
MAPK	Mitogen-activated protein kinase
MD Simulations	Molecular dynamic simulations
MEFs	Rasless mouse embryo fibroblasts
MLA	Methyl-lysine analogues
N-terminus	Amino-terminal
NS	Noonan's Syndrome
P-loop	Phosphoryl binding loop
PARP	Poly ADP-ribose polymerase, cleaved PARP is a marker of cellular apoptosis

PDAC	Pancreatic ductal adenocarcinoma
PDX101	Belinostat, pan- (class I/II) histone deacetylase (HDAC) inhibitor
PI3K	Phosphoinositide 3-kinase
PLCε	Phospholipase C epsilon
PTM	Post-translational modification
Raf	A family of serine/threonine-specific protein kinases
RalGDS	Ral guanine nucleotide dissociation stimulator
RBD	Ras binding domain
Rce1	Ras and a-factor converting enzyme-1
RTK	Receptor tyrosine kinase
SAHA	Vorinostat, suberoyl+anilide+hydrozamic acid, pan- (class I/II) histone deacetylase (HDAC) inhibitor
SMYD3	SET and MYND domain containing protein 3
S_N2	Nucleophilic substitution reaction mechanism
SOS	Son of Sevenless exchange factor
SWI	Switch I
SWII	Switch II
TCEP	(tris(2-carboxyethyl)phosphine hydrochloride)
TEV	Tobacco Etch Virus
Tiam1	T-cell lymphoma invasion and metastasis-inducing protein 1
T_M	Melting temperature
TSA	Trichostatin A, pan- (class I/II) histone deacetylase (HDAC) inhibitor

XTT	A tetrazolium salt, which when used in a cell proliferation assay serves as a colorimetric analysis for quantification of cellular proliferation

Chapter 1 – Introduction to the Ras superfamily of GTPases and Ras proteins

Ras Proteins as GTPases

Ras proteins are members of the larger Ras superfamily of guanine nucleotide binding proteins, which are classified by a highly conserved structural domain *(1)*. The Ras subfamily contains approximately 40 members in humans *(2)–(4)*. The three human *Ras* genes encode for four Ras proteins (HRas, NRas, KRas-4A and KRas-4B). Two Ras isoforms, KRas-4A and KRas-4B, arise from alternate RNA splice variations of the same *Ras* gene. KRas-4B (further referred to as KRas) is the predominant Ras isoform expressed in human cells and is the most commonly mutated Ras isoform *(4),(5)*. These small (21 kDa) proteins are classified as guanosine triphosphatases, GTPases, as they bind GDP and GTP with high affinity and can slowly hydrolyze GTP to GDP. As the intrinsic rate of nucleotide dissociation and hydrolysis is slow *(6)*, Ras proteins interact with modulatory factors to fine-tune their activation status in cells. GEFs, guanine nucleotide exchange factors, and GAPS, GTPase activating proteins, serve as modulatory proteins to further aid in maintaining the proper GTP/GDP balance of Ras proteins *in vivo (7)–(9)* (**Figure 1.1**). GEFs activate Ras proteins by facilitating the release of GDP primarily through a restructuring of the nucleotide binding site and displacement of a critical magnesium ion, allowing for the subsequent loading of GTP *(10)*. GAPs play the opposite role of GEFs, aiding in the hydrolysis of GTP to GDP and thereby converting Ras proteins to an 'off' or inactive state *(9)*. In particular, the critical 'arginine finger' in GAPs inserts itself into the Ras active site, stabilizing the catalytic glutamine 61 and allowing for proper coordination of a water molecule for nucleophilic attack at the γ-phosphate of GTP *(11)–(13)*. In the unstimulated cell,

Ras proteins are predominately GDP-bound and inactive. After proper membrane localization, Ras proteins are capable of being activated. One mechanism of Ras activation involves upstream receptor tyrosine kinases (RTKs). Receptor activation via an external stimuli triggers phosphorylation of the internal portion of the receptor and subsequent recruitment of scaffolding and modulatory proteins to the cellular membrane, which in turn serves to activate Ras proteins at the membrane *(14)*. When bound to GTP, Ras proteins assume a conformation that confers high affinity binding to downstream effector proteins *(15),(16),* initiating signaling through downstream pathways to regulate multiple aspects of cellular growth, differentiation and apoptosis *(4),(17)* (**Figure 1.1**).

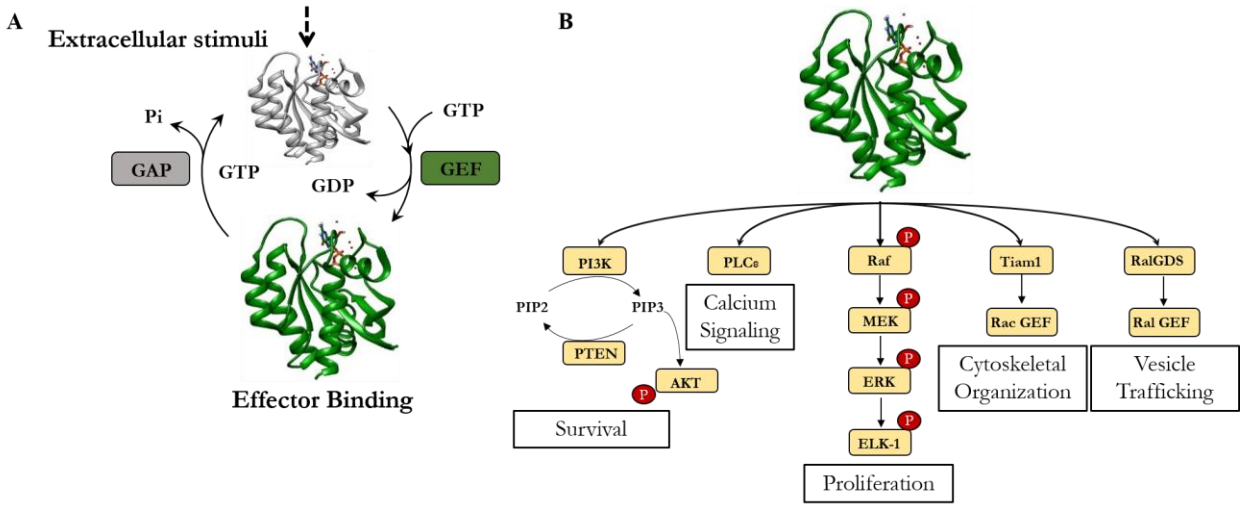

Figure 1.1. Ras Regulation and Effector Binding

Ras proteins cycle between "off" and "on" states with the aid of the modulatory factors, GEFs (guanine nucleotide exchange factors) and GAPs (GTPase activating proteins), A. In their active form, Ras proteins display significantly higher affinity to their downstream effector proteins, which promotes binding and signaling through Ras-mediated signaling cascades *(16)***, B.**

Ras History and Signaling in Cancer

The discovery and report of the previously 'unknown' rat retroviruses in the 1960s and

1970s were the first glimpses into what we now know as Ras oncoproteins *(18),(19)*. In hallmark discoveries in 1980s, *Ras* genes were discovered in human cancers and their role in driving oncogenic cancer cell transformation was first described *(20)–(23)*. This has triggered decades of extensive research, aimed at therapeutically targeting and understanding Ras oncoproteins as drivers of human cancers. To date, no clinically effective anti-Ras therapies have been developed *(24)*.

Ras proteins are some of the most commonly mutated oncoproteins in human cancers *(25)*. Oncogenic, gain-of-function mutations in *Ras* genes promote Ras protein hyper-activation and are present in approximately 30% of the most deadly human cancers, including melanoma, lung, pancreatic and colorectal cancers *(5),(17),(26)*. While the ability of wild-type Ras proteins to serve as tumor suppressors is still in debate *(27)*, 'hotspot' mutations in Ras proteins are known to be oncogenic drivers *(4)*. These 'hotspot' mutations are located at three primary residues in the highly conserved Ras core GTPase domain: glycine (G) 12, glycine (G) 13, and glutamine (Q) 61 (**Figure 1.2**) *(4),(5),(17)*. Mutations at these positions are known to activate Ras proteins by altering nucleotide binding and/or exchange directly or indirectly through altering the ability of GAPs to properly elicit their function *(5),(17),(26),(28)*. Interestingly, Ras-driven cancers display striking isoform- and mutation-specific preferences in each tissue type *(5)*. For example, KRas proteins are mutated predominately at glycine 12 whereas NRas proteins harbor glutamine 61 mutations *(4),(5),(29)*. HRas proteins on the other hand, have very similar mutation rates between the 'hotspot' G12, G13 and Q61 locations (**Figure 1.2**) *(4),(5),(26)*. It has also been demonstrated that different Ras oncogenic mutations exhibit unique activity profiles *(17),(28),(30),(31)* and differentially affect clinical outcome *(32)*. Historically, the majority of research on Ras proteins has been conducted on the HRas isoform *(1)*. However, this

is the least frequently mutated Ras isoform in human cancers (~4%). This is followed by NRas, which is mutated in approximately 11% of human cancers. KRas proteins are by far the most mutated of the isoforms, revealing an almost 85% mutation rate in Ras-driven cancers *(4),(5),(17)*. Ras-driven cancers also exhibit isoform preferences. Pancreatic ductal adenocarcinoma (PDAC) and colorectal cancers (CRC) are driven by oncogenic KRas proteins (nearly 100% of cases and ~86% of cases, respectively), whereas melanoma is driven by mutant NRas (~94% of cases) *(4),(5),(26),(28)*. While HRas proteins are the least mutated of the Ras isoforms, they are known drivers of bladder urothelial carcinoma and head and neck squamous cell carcinoma (HNSCC) *(4),(5),(26)*. Taken together, these data suggest a functionally unique role for each Ras isoform and mutation in cancer. Even though each of these mutations have a distinct mechanistic role in modulating Ras activity, the details of which are still under investigation, the outcome is similar in that they lead to a hyper-activated or constitutively activated form of Ras *(17)*. This leads to aberrant downstream signaling to effector proteins and an upregulation of signaling through Ras-mediated pathways, resulting in dysregulation of cellular growth, differentiation and apoptosis *(17),(26),(33)*.

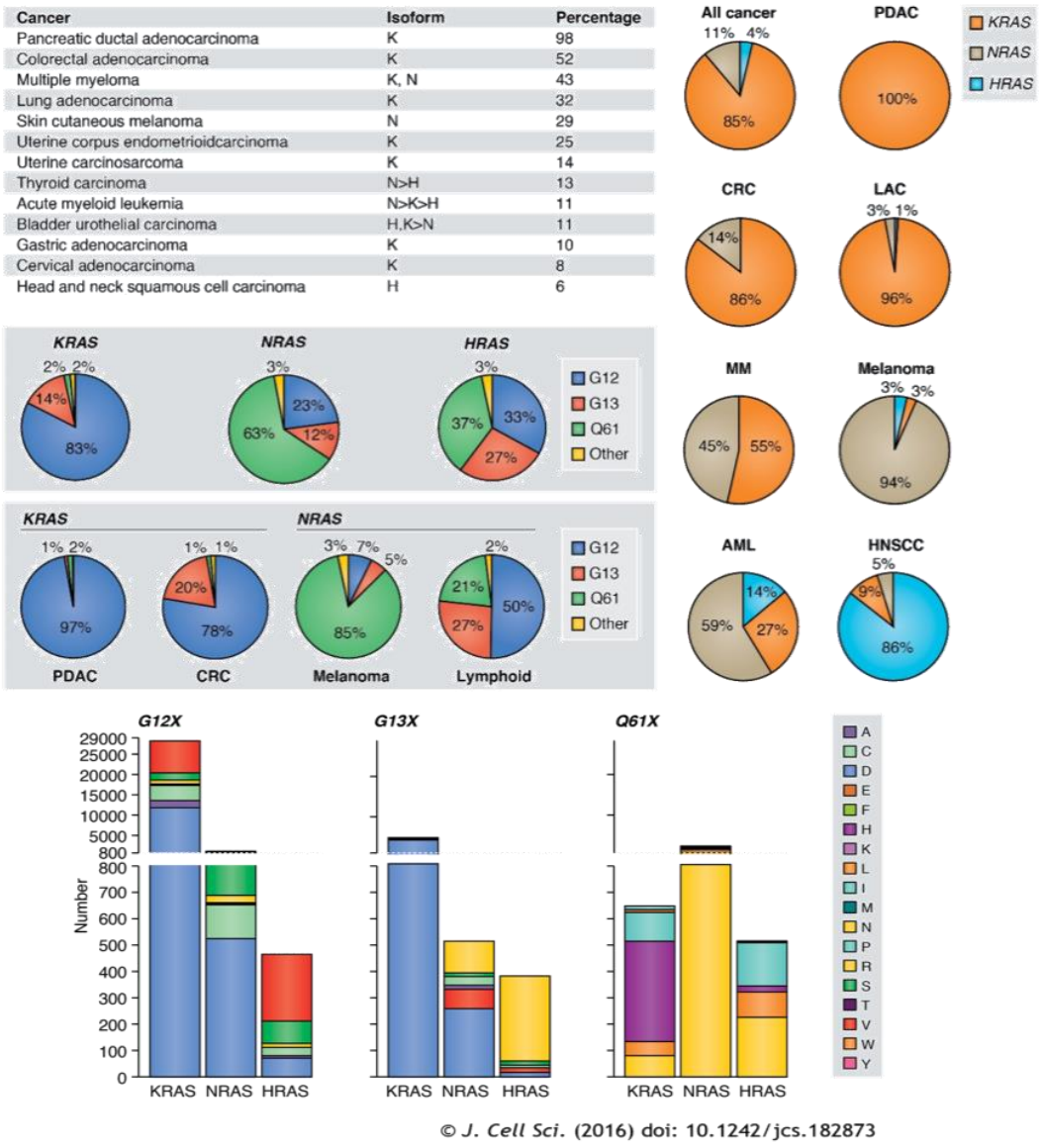

Figure 1.2 Ras Mutations in Cancer.

Ras proteins are oncogenic drivers in several of the deadliest cancers, including melanoma, lung (LAC), pancreatic (PDAC) and colorectal cancers (CRC). Strikingly, these cancers display tissue, mutation and isoform-specific preferences.

Reprinted (adapted) with permission from Hobbs, G. A., Der, C. J., & Rossman, K. L. (2016). RAS isoforms and mutations in cancer at a glance. *Journal of Cell Science*, *129*(7), 1287–1292. Copyright 2016 Journal of Cell Science.

Ras Structure and Dynamics

The superfamily of Ras proteins are classified by a commonly conserved structural domain, the guanine-nucleotide binding domain, as Ras proteins bind GDP and GTP, which is critical to their activity *(1)*. Ras isoforms are composed of a highly conserved core guanine nucleotide binding domain and a sequence divergent carboxy (C)-terminal hypervariable region (HVR). The C-terminal HVR is poorly conserved throughout the Ras isoforms (<10% sequence conservation) and undergoes isoform-specific post-translational modifications (PTMs) that facilitate proper membrane localization crucial for Ras activity *(4),(5),(34)*. The core GTPase domain within N-, H- and KRas is highly similar (~90% sequence identity) and is composed of the effector and allosteric lobes. The effector lobe (residues 1-86) is strictly conserved and contains sites critical for nucleotide binding as well as for effector and regulator protein recognition *(4),(26)*. Much less is known about the role of the allosteric lobe (residues 87-171) *(4),(26)*. Ras proteins exhibit isoform-specific sequence differences within their allosteric lobe. While the effector lobe is 100% conserved between the Ras isoforms, the allosteric lobe contains several sequence differences between the Ras isoforms. Within their allosteric lobe, Ras proteins display less than 80% sequence homology (**Figure 1.3A**) *(4),(5)*. Additionally, subsets of these sequence differences contain non-conservative substitutions. For example, α-helix 3 in KRas is composed of charged, polar amino acids while in NRas this region is primarily nonpolar and not charged. This changes the entire electrostatic and solvent-exposed face of α-helix 3. While the role of the allosteric lobe is poorly understood, this region may contribute to Ras isoform specificity and is postulated to play roles in effector recognition, regulator binding, membrane interactions and allosteric regulation of the Ras active site *(26),(34)–(40)*.

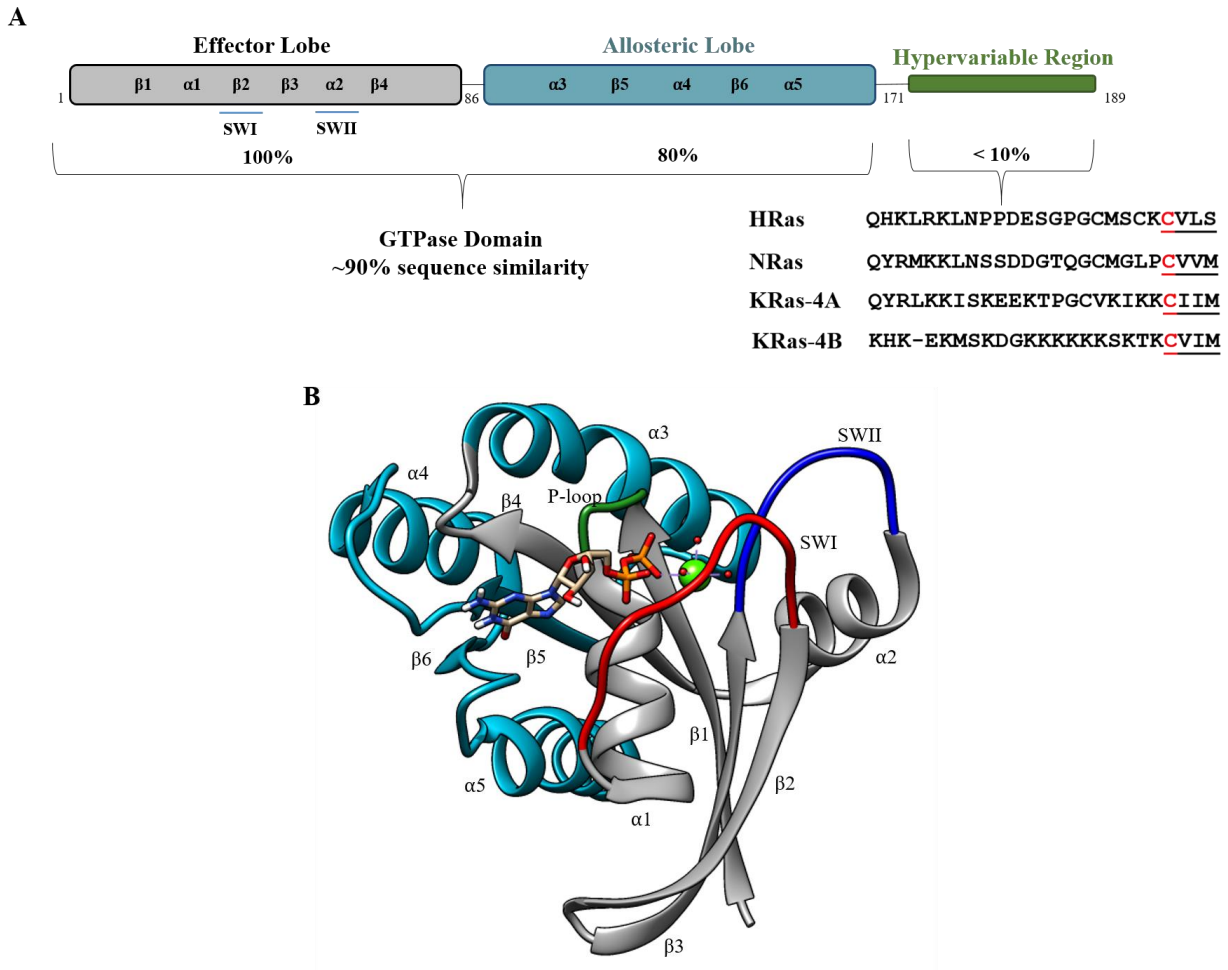

Figure 1.3. Ras Domain Architecture and Structure.

A. Ras isoforms share a highly similar core GTPase domain but a highly dissimilar C-terminal hypervariable region (HVR). The effector lobe is strictly conserved between Ras isoforms and plays roles in effector/modulatory protein binding. The allosteric lobe houses isoform-specific sequence differences between Ras proteins, the roles of which are currently unknown. The c-terminal HVR is highly post-translationally modified, allowing for proper Ras location and activity at the cellular membrane. B. The Ras core GTPase domain (PDB 4LPK) is shown in cartoon representation. Core structural elements are labeled. The effector lobe is represented in grey and is the primary location of effector and regulatory protein interactions. The role of the allosteric lobe (teal) is more poorly understood and may contribute to Ras isoform-specificity. The highly dynamic switch regions are colored in red and blue for SWI and SWII, respectively.

Structurally, the core GTPase domain is comprised of six β-sheets and 5 α-helices, taking

on a Rossmann-type fold of alternating α-helices and β-sheets (**Figure 1.3B**) *(1)*. It is further divided into five different structural motifs (G1-G5). G1 contains the phosphate binding loop (P-loop) that aids in coordinating the nucleotide within the Ras binding pocket. G2, more commonly termed 'switch I' (SWI, residues 32-38) is a highly dynamic region of Ras proteins that distinctly changes conformation upon nucleotide binding and exchange *(41)* (**Figure 1.4**). This region is also termed the 'effector region' as Ras effector proteins (such as the Raf kinases) are known to recognize and bind to Ras through this highly conserved region (**Figure 1.5**) *(1),(41)–(43)*. G3 comprises another highly dynamic region in Ras proteins, termed 'switch II' (SWII, residues 59-67). Together with switch I, these regions describe the nucleotide-bound state of Ras *(1)*. In an 'open' conformation, Ras is GDP-bound and inactive. However, in a closed conformation, SWI and SWII residues aid in binding and coordinating the β- and γ- phosphates of GTP, defining the active Ras conformation (**Figure 1.4**) *(1),(41),(44),(45)*. G4 contains the critical NKXD motif in Ras proteins. These residues are essential in coordinating the binding of and providing specificity for the guanine-nucleotide base. Mutations at these residues greatly destabilize Ras nucleotide binding, resulting in increased protein activation *(1),(46),(47)*. G5 is termed the SAK motif, where key interactions with the guanine nucleotide contribute to high affinity binding and nucleotide specificity *(1)*.

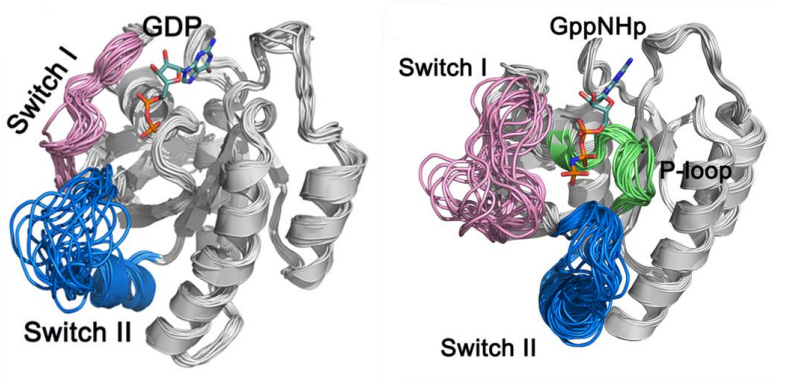

Figure 1.4. Ras switch dynamics.

Left, cartoon representation of the NMR structures of GDP-bound HRas (PDB 1CRP *(48)*). In the GDP-bound form, Ras proteins exist in a more 'open' conformation, as seen by the increased conformational dynamics of SWII. Right, cartoon representation of the lowest energy NMR structures of GppNHp (GTP analogue)-bound HRas^{T35S} *(49)*. In the active, GTP-bound form the switch regions exist in a closed conformation, facilitating contacts with the β- and γ-phosphates.

Reprinted (adapted) with permission from Lu, S., Jang, H., Muratcioglu, S., Gursoy, A., Keskin, O., Nussinov, R., & Zhang, J. (2016). Ras Conformational Ensembles, Allostery, and Signaling. *Chemical Reviews*. https://doi.org/10.1021/acs.chemrev.5b00542. Copyright 2016 Chemical Reviews ACS.

The ability to bind downstream effector proteins is also dependent upon the nucleotide-bound state of Ras proteins. In the active, GTP-bound form, Ras proteins exhibit a significantly higher affinity to downstream effector proteins *(15)*. Effector proteins such as the Raf kinases and PI3-kinases (phosphoinositide 3-kinase) bind Ras proteins within their Ras binding domain (RBD) through differential SWI and SWII residue engagement (**Figure 1.5**). These binding interfaces are often highly electrostatic in nature *(42),(50),(51)*. Binding will also be a result of β-strand pairing between Ras and the effector RBD *(52)*. Effector binding and engagement will result in downstream signaling through Ras-mediated pathways. Ras effector proteins are not unique in their engagement of the switch regions. Ras GEFs and GAPs also interface with SWI

and SWII and the surrounding regions to engage with Ras proteins *(13),(53),(54)*.

	Interacting Residues	
	Ras	Raf RBD
SWI	21	88
	25	89, 89, 90
	31	84
	33	84
	36	57, 69, 71
	37	59, 67, 69
	38	68, 89
	39	66, 67, 89
	40	66, 88, 89
	41	65, 64, 66
	54	67
	56	61

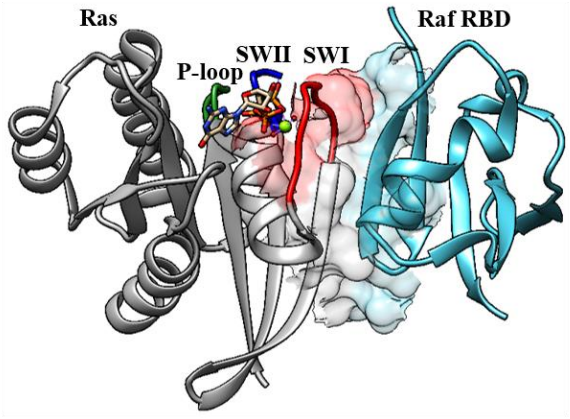

	Interacting Residues	
	Ras	PI3K RBD
SWI	25	257, 258
	33	251, 255
	38	251
	41	228
	39	230
	40	231
	37	223, 232
	36	221
SWII	64	234
	63	234
	73	919

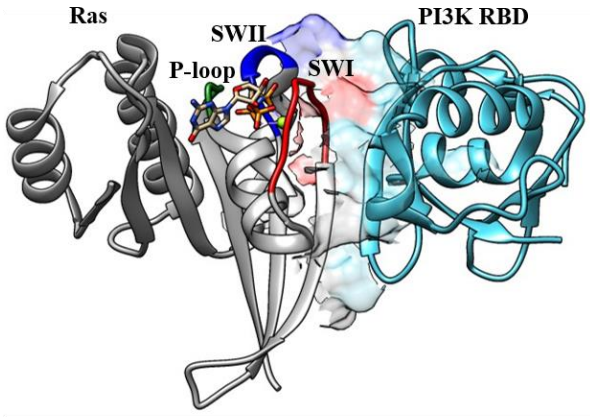

Figure 1.5. Ras interactions with Raf and PI3K RBDs.

Ras proteins interact with effector proteins primarily through the switch regions. Raf RBD (top figure, teal) interacts with Ras proteins (grey) through SWI (red) and β-strand pairing at the interaction interface (PDB 4G0N *(55)***). Interactions shown are < 4.0 Å** *(56)***. PI3Kγ RBD (teal, bottom figure) also displays an interaction interface with β-strand pairing but engages both SWI (red) and SWII (blue) of Ras (grey) for binding (PDB 1HE8** *(50)***). Binding interfaces in both models are shown as a surface. The switch regions are labeled accordingly.**

Beyond effector and modulatory protein binding, the switch regions in Ras have been

implicated in an allosteric modulation mechanism. Several groups of inter-connected residues have been identified through computational simulations that propagate structural and dynamic changes upon effector binding from the N-terminus to the C-terminus of Ras *(39)*. Results of these computational simulations indicate that the binding of effector proteins locked Ras in the active state, primarily due to the conformational restriction of SWI. Effector binding then stimulated conformational changes in unique residue groupings that stretch from the N- to C-terminus of Ras *(39),(40)*. While the dynamic switch regions are critical determinants of Ras activation state, their engagement in effector and regulatory protein binding can lead to larger global conformational and dynamic changes. These inside-out, allosteric structural changes are only beginning to be described in recent years and may serve to provide a more comprehensive understanding of Ras conformational and dynamic relationships alone and in complex with effector or regulatory proteins.

Ras and Post-Translational Modifications

Post-translational modifications (PTMs) in Ras have been primarily studied in the context of the C-terminal HVR, where they drive the differential localization of Ras isoforms *(4),(37)*. It is well accepted that Ras proteins must be properly membrane localized to order to become activated. The C-terminus of Ras proteins are heavily post-translationally modified. The critical CAAX box and hypervariable regions are sites of post-translational lipid modifications (**Figure 1.3A**). In all Ras proteins, the terminal cysteine (C) of the CAAX box is farnesylated followed by removal of the remaining –AAX by Rce1 (Ras and a-factor converting enzyme-1). This exposes the cysteine for carboxymethylation, and these actions promote weak membrane association *(4),(57)*. Interestingly, the Ras isoforms display differential secondary processing within their C-terminal HVR that further enhances membrane association. HRas can additionally

be palmitoylated at two other sites, while NRas can be palmitoylated at one other site. The KRas-4B HVR contains a polybasic lysine tail that is not further modified. This differential processing is thought to lead to isoform-specific trafficking at the cellular membrane *(57)–(59)*. Early attempts to target Ras proteins (farnesyltransferase inhibitors, FTIs) were directed toward inhibiting this key carboxyl (C)-terminal lipid modification, crucial for proper Ras localization and function at the cellular membrane. FTIs ultimately failed as NRas and KRas can undergo an alternative type of lipid modification (geranyl-geranylation) *(60)*.

Ras proteins are also post-translationally modified within their core GTPase domains *(61)* (**Figure 1.6**). However, the role of these PTMs has not been intensively studied. Importantly, PTMs in this region can directly regulate Ras activity. Monoubiquitylation has been identified at three sites within the core GTPase domain of Ras proteins: K104, K117 and K147 *(62),(63)*. K147 is located in the conserved G5 box, which plays a role in the stabilization of the guanine nucleotide *(1)*. Monoubiquitination at K147 has been demonstrated to up-regulate protein activity primarily through an insensitivity to GAP proteins, leading to persistent GTP-bound Ras *(63)*. This was further verified in cellular studies where an amplified population of GTP-bound Ras was identified in RBD pulldown experiments *(62)*. However, monoubiquitination at K147 significantly impaired binding of activated Ras to the downstream effectors PI3Kγ, CRaf and RalGDS RBDs *(64)*, which would seem to contradict the cellular findings. One possible explanation for increased RBD binding in cells could be due to an increased affinity of CRaf RBD to the GDP-bound from of monoubiquitinated Ras *(64)*. Monoubiquitination of K117 in Ras also led to an activated phenotype in cells; however, this occurred through a unique mechanism *(65)*. K117 is part of the NKxD motif and forms crucial interactions with the guanine nucleotide base *(1),(46),(47)*. Mutations at K117 (K117R, K117N) have been demonstrated to

increase rates of nucleotide exchange, in turn activating Ras proteins *(46),(47),(66)*. These mutations have been demonstrated to promote tumorigenesis in human cancers and have also been identified in 'Ras-opathies' (developmental disorders characterized by Ras germline mutations). It was determined that monoubiquitination of K117 lead to increased guanine nucleotide dissociation rates, which served to activate Ras *(65)*.

Beyond ubiquitination, Ras proteins are also capable of being acetylated in the core GTPase domain at K104 *(67)–(69)*. Lysine (K) 104 is a highly conserved residue in the Ras superfamily. Structurally, K104 is located in loop 7, following α-helix 3, in the Ras core G-domain. In molecular dynamic simulations using an acetylation mimetic, glutamine (Q), *Yang et al.* identified that K→Q mutation destabilized the α2 helix of SWII *(67)*. They determined that the destabilization was primarily due to a disruption in the electrostatic interactions resulting from the K→Q mutation *(67)*. Given that these regions are critical for GEF-mediated nucleotide exchange, it was not surprising that K104Q mutation disrupted SOS-mediated exchange *(67)*. Subsequent NMR studies using the same K104Q mutant indicated that the disruption of α2 was not as severe as predicted computationally, but partial helix disruption was able to be identified *(69)*. In addition to the GEF defect, K104Q mutation in Ras also demonstrated a GAP defect *(69)*. However, in cellular studies K104Q mutation in Ras did not significantly alter steady-state GTP levels, cellular growth or proliferation, leading to the conclusion that the GEF and GAP defects were compensatory in nature, and acetylation at K104 likely did not impact overall Ras activity *(69)*. However, the validity of using canonical amino acids as a mimetic of PTMs is still under debate *(70)*. Our lab and others were able to use a genetic approach to site specifically install Nε-acetyl-L-lysine into Ras proteins, generating natively acetylated lysine, and determined that natively acetylated Ras proteins exhibit much less of a harsh biochemical profile

than the acetylation mimetic, K104Q *(68),(69)*. In fact natively acetylated Ras at K104 displayed no significant defects in intrinsic or GEF-mediated nucleotide exchange relative to wild-type protein, while K104A/R/Q all demonstrated both intrinsic and GEF-mediated exchange defects *(68),(69)*. This work is described in detail in Chapter 4. Further, previous analysis using the acetylation mimetic K104Q identified HDAC6 and Sirt2 as the Ras deacetylates. However, these were not able to be verified when Ras proteins were natively acetylated at K104 *(68)*. As PTMs are highly regulated in the cellular milieu, introduction of a foreign amino acid likely disrupts recognition sequences for regulatory/effector proteins, which is exemplified by these findings. *Knyphausen et al.* were able to identify the acetyltransferases responsible for acetylating Ras at K104 as CBP and p300 and also identified acetylation sites at K101, K128 and K147 using natively acetylated protein *(68)*. In Chapter 2, we investigate the role of acetylation at a novel site, K5.

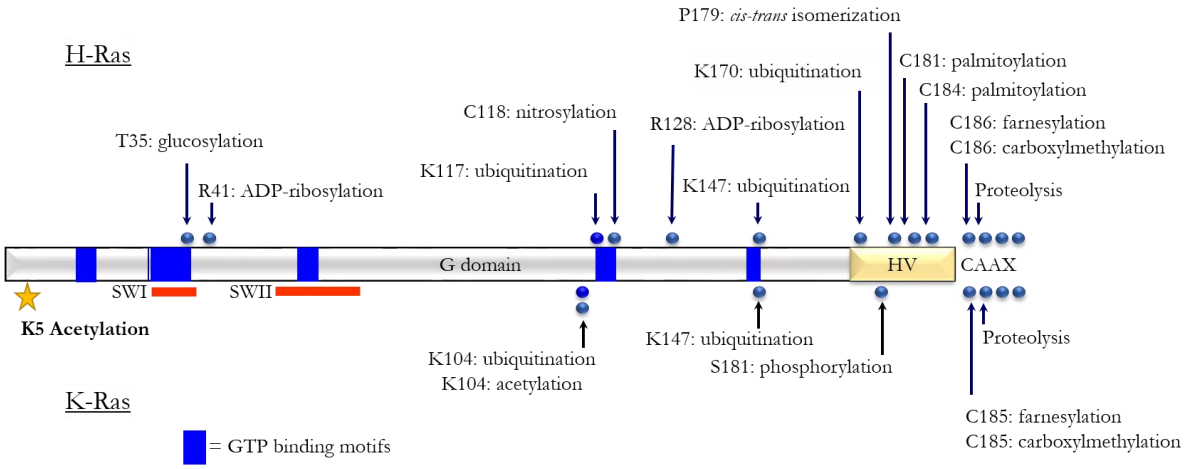

Figure 1.6. Ras proteins are extensively regulated by post-translational modifications.

Here, a schematic of the Ras core G-domain is shown with Ras PTMs reported. On the top, HRas PTMs are identified, where KRas is on the bottom. We can see that Ras proteins are highly post-translationally modified both within their core G-domain and also their carboxy-terminal hypervariable regions. Several of these PTMs are known to regulate Ras activity.

Reprinted (adapted) with permission from Ahearn, I. M., Haigis, K., Bar-Sagi, D., & Philips, M. R. (2012). Regulating the regulator: post-translational modification of RAS. *Nature Reviews Molecular Cell Biology*, *13*(1), 39–51. https://doi.org/10.1038/nrm3255. Copyright 2011, Springer Nature.

Research in our lab and others has eluded to the identification of novel methylation sites within the core Ras G-domain. Several methylation sites have been identified, but their roles in regulating Ras activity are not clear (manuscripts submitted, data not shown). Aberrant methylation patterns have been described in several Ras-mediated signaling pathways and of Ras effector or modulatory proteins *(71)–(75)*. Further, the Ras-driven cancer, pancreatic ductal adenocarcinoma (PDAC), displays strong dysregulation of crucial histone lysine methyltransferases (KMTs) and histone lysine demethylases (KDMs), which are responsible for modulating the methylation status *in vivo (76)*. In fact, knockout of the KMT SMYD3 inhibited Ras-mediated tumorigenesis in mouse models for PDAC and lung cancer *(77)*. MAP3K2 was

identified as a direct target of SMYD3 and its inhibition resulted in decreased MAPK signaling *(73),(77)*. Taken together this data suggests that lysine methylation may be a novel therapeutic target in Ras-driven cancers. While the functional role of Ras methylation remains unclear, the role of methylation regulating other cancer-related proteins is well established. Lysine methylation (or acetylation) of the tumor suppressor gene p53, fine-tunes its overall activity in cancer *(78),(79)*. Inhibitors of KMTs or KDMs present viable therapeutic opportunities in several cancer types *(80)*. If Ras methylation contributes to aberrant growth control, methyltransferase inhibitors may represent a potential targeting mechanism. As most lysine PTMs in Ras occur at conserved sites involved in structural integrity or nucleotide binding *(81)*, it is likely that these PTMs will alter the intrinsic function of the protein. In Chapter 5 I present novel methods to generate site-specifically methylated intact Ras proteins. This could be a crucial first step in understanding how methylation is capable of regulating Ras protein activity.

Taken together, these data demonstrate the complexity by which Ras proteins are regulated by post-translational modifications. While our lab and others have demonstrated that Ras protein activity can be modulated by PTMs, namely acetylation and monoubiquitination, the mechanisms behind this regulation are complicated in nature. PTMs in the C-terminal HVR presented therapeutic opportunities in Ras proteins with farnesyltransferase inhibitors *(60)*. This may also be the case with PTMs that occur in the core G-domain of Ras proteins. By understanding the distinct mechanisms by which PTMs elicit their activity in Ras proteins, we may develop novel therapeutic opportunities in Ras-driven cancers.

Strategies to Therapeutically Target Ras Proteins: A Broad Overview

Early anti-Ras drug efforts were targeted at the C-terminal HVR of Ras proteins (FTIs, farnesyltransferase inhibitors). All Ras isoforms are farnesylated in their C-terminal CAAX box.

Farnesylation of the C-terminal cysteine and subsequent proteolysis of -AAX leads to carboxymethylation of the terminal cysteine and facilitates proper Ras membrane localization, which is crucial for Ras activity *(4),(57)*. FTIs were designed to inhibit the farnesyltransferase (FTase) responsible for acting on Ras proteins, thereby rendering them cytosolic and inactive *(60)*. However, while FTIs were one of the first examples of rational drug design targeting Ras proteins, they were designed to be specific for the FTase and not for Ras itself. FTIs were successful at blocking the prenylation of HRas proteins, but this was not the case for N- or KRas proteins *(60)*. It was soon discovered that in the presence of FTIs, N- and KRas could undergo alternative prenylation in the form of geranylgeranylation, allowing them to be effectively trafficked to the cellular membrane where they could be activated *(4),(60),(82),(83)*. In recent years, the idea of blocking Ras membrane association has again become a topic of conversation. A salicylic acid derivative, Salirasib has been reported to dislodge prenylated Ras proteins from the cellular membrane. As a mimetic of farnesyl-cysteine, Salirasib has been reported to compete with farnesylated Ras binding sites at the cellular membrane *(84)–(86)*. In cellular studies using human hepatocellular carcinoma cell lines, Salirasib was demonstrated to reduce Ras expression and activation and decreased phosphorylation of Akt, a readout of PI3-kinase pathway activation *(85)*. In early preclinical trials in patient derived PDAC mouse xenograft studies, Salirasib in combination therapy demonstrated low overall toxicity, increased overall survival and decreased levels of signaling through both PI3-kinase and MAPK pathways as determined through western blotting *(87)*. Unfortunately, in human phase 2 clinical trials of Salirasib in non-small cell lung cancer, low drug toxicity and good tolerance were noted but no increase in progression free survival was demonstrated *(88)*. However, a more recent phase I clinical trial in Japanese patients with Ras positive solid tumors does indicate increased median progression-free survival

upon salirasib treatment *(89)*. While these are preliminary studies, they bring to light the previous strategy of targeting Ras membrane localization as a potentially effective anti-Ras therapy.

Since the failure of traditional FTIs, targeted Ras therapies are being pursued using both direct and indirect strategies. As *Papke & Der* outline, there are five general strategies for the development of anti-Ras therapeutics *(83)*. These strategies include: 1) small molecules that bind directly to Ras proteins, disrupting interactions with regulatory/effector proteins, 2) inhibition of Ras membrane association/localization, 3) inhibition of Ras downstream effector signaling cascades, 4) inhibition of genes whose functions are crucial for mutant Ras (synthetic lethal interactions) and 5) inhibition of Ras-mediated metabolic processes *(83),(86)*. Direct strategies to target Ras proteins have proven challenging as Ras proteins lack easily discernable druggable pockets on their surface, which greatly limits the efficacy of these approaches *(24),(82)*. In recent years, potentially druggable novel pockets have been identified in Ras, and the hunt is on for specific and selective Ras therapeutics *(24),(90),(91)*. One direct Ras targeting strategy that has garnered some initial successes has been the efforts to develop G12C-selective inhibitors. KRas G12C mutations have been identified in non-small cell lung cancer (NSCLC) and are associated with poor prognosis *(92)*. Using the thiol of the cysteine mutation, G12C-selective inhibitors form covalent adducts with small molecules, thereby inhibiting GTP binding and rendering Ras inactive *(83),(90),(93),(94)*. Currently there are 2 drugs that target Ras G12C in clinical trials for the treatment of G12C-specific Ras solid tumors. MRTX894 (clinical trial identifier NCT03785249) and AMG 510 (clinical trial identifier NCT03600883) are currently undergoing phase 1 and phase 2 clinical trials to determine safety and efficacy in human patients. These

drugs represent the first efforts for mutation-specific targeting of Ras proteins for the treatment of cancer.

The most clinically successful inhibitors to date have been those that target downstream Ras effector signaling pathways. Arguably, the most important downstream Ras signaling cascade is the Ras/Raf/MEK/ERK (MAPK) cascade, responsible for regulating cellular proliferation *(4),(82),(83),(95)*. However, given the multitude of Ras-regulated signaling pathways, targeting a specific pathway presents challenges due to significant pathway crosstalk and paradoxical activation *(83)*. Initial efforts focused on developing direct inhibitors of Raf and MEK as a means to inhibit downstream ERK activation. However, this approach was not successful, as targeting BRaf led to paradoxical MAPK pathway activation due to compensatory CRaf activity *(83)*. Since these initial findings, several generations of Raf, MEK and ERK-specific inhibitors have been developed and have demonstrated varying levels of clinical success *(83),(86)*. Pathway-specific inhibitors have also been developed for the PI3-kinase signaling cascade. However, there is contradicting evidence as to whether PI3K is a potent Ras effector or is its importance is situationally dependent *(82)*. As monotherapies, inhibitors of the PI3K-AKT-mTOR pathway have not demonstrated success in Ras-driven cancers *(82),(83)*. While dual therapies targeting both MAPK and PI3K pathways seems promising, they have demonstrated limited clinical efficacy due to toxicity and drug-resistance concerns *(83),(86)*.

Very promising emerging classes of anti-cancer drugs directed at targeting the frequent dysregulation of PTM status in cancers (i.e. kinase inhibitors, methyltransferase inhibitors and histone deacetylase inhibitors, HDACi) have gained much interest in recent years. Kinase inhibitors, HDACi and methyltransferase inhibitors have shown multiple early and later phase clinical successes in the treatment of a myriad of non-solid tumor cancers *(76),(96)–(99)*.

However, these drugs have not demonstrated successes as monotherapies in Ras-driven cancers. Ras proteins are known to be regulated by PTMs, and these PTMs has been demonstrated to modulate Ras activity *(67)–(69)*. Recently, several labs have been able to demonstrate that HDACi are successful in Ras-driven cancers when administered as combination therapies *(100)–(102)*. In particular, the combination of a MEK inhibitor (trametinib, GSK1120212)+ PI3K inhibitor (belinostat, BEZ-235)+ HDAC inhibitor (TSA,SAHA or PDX101) resulted in >99% inhibition of cellular proliferation and dramatic induction of cellular apoptosis in pancreatic cancer cells *(101)*. Additionally, a pan-HDAC inhibitor, Belinostat when combined with the MEK inhibitor, Trametinib functioned to synergistically decrease tumor formation in a mouse lung cancer xenograft model *(102)*. This data suggests that HDACi may represent an untapped therapeutic potential in Ras-driven cancers. In addition to acetylation, methylation may also represent a therapeutically targetable PTM in Ras. It was recently discovered that there are significant alterations in methylation patterns and signaling in the Ras-driven cancer, PDAC *(76)*. Additionally, the Ras-mediated MAPK signaling cascade has been demonstrated to be regulated by methylation. Methylation of MAP3K2 (MEKK2) by the methyltransferase SMYD3 is linked to increases in MAPK signaling and promotes the formation of Ras-driven carcinomas in mouse models of PDAC and lung cancer *(77)*. This effect was reversed in SMYD3 knock-out studies. This may suggest that lysine methylation is a tractable therapeutic target in Ras-driven cancers. HDACi and methyltransferase inhibitors have not been extensively studied in Ras-driven cancers. This is due in part to the lack of clinical knowledge surrounding the exact mechanisms of drug action in non-histone proteins. Traditionally, HDACi and methyltransferase inhibitors have been studied in the realm of histone regulation *(97),(103)–(106)*. However, it is becoming increasingly evident that PTMs are also capable of regulating non-histone proteins

(78),(79),(105). As such, PTMs may represent novel therapeutic opportunities in non-histone proteins and warrant further investigation.

Chapter 2. – HDACi treatment causes Ras acetylation, directing signaling through the MAPK pathway through a reordering of the Ras:Raf binding interface[1]

Introduction

Ras proteins are the most commonly mutated oncoproteins in cancer. They function as critical regulators of cellular growth by acting as molecular switches, cycling between active and inactive states *(4),(17),(33)*. In their active form, two highly dynamic regions of Ras proteins, termed switch I and switch II, assume a conformation that confers high affinity binding to downstream effectors *(15)–(17)*. Effector engagement then stimulates signaling through downstream pathways that regulate cellular growth, differentiation and apoptosis *(17),(33)*. Oncogenic, gain-of-function mutations in *Ras* genes promote Ras protein hyper-activation and are present in approximately 30% of the most deadly human cancers, including melanoma, lung, pancreatic and colorectal cancers *(5),(17)*. Mutationally activated Ras proteins have a well-validated role in driving oncogenic cancer cell transformation *(107)*, and mutations in Ras at position 12, 13 or 61 are particularly oncogenic, and are widely recognized as critical determinants of therapeutic response *(107)–(109)*. Despite more than three decades of research, Ras has remained an elusive target for cancer therapy and is commonly considered undruggable *(24)*. This has stimulated the search for comprehensive approaches to develop efficient therapeutic strategies to target mutant Ras proteins for cancer treatment. Early attempts to target Ras proteins (farnesyltransferase inhibitors, FTIs) were directed toward inhibiting a key carboxyl

[1] Figures 2.1-2.4 and corresponding methods provided by Sylvia Ispasanie and Dr. Christine Sers, Charité Universitätsmedizin Berlin, Berlin, Germany. Figure 2.5 and corresponding method provided by Dr. Erik Soderblom, Duke Core Proteomics Facility. Figures 2.12-2.17 and corresponding methods were developed in collaboration with Dr. Konstantin Popov, UNC – Chapel Hill.

(C)-terminal lipid modification, crucial for proper Ras localization and function at the cellular membrane *(4),(34),(60)*. Unfortunately, as NRas and KRas can undergo an alternative type of lipid modification (geranyl-geranylation), the use of FTIs as an anti-Ras targeted therapy was unsuccessful *(60)*. Current approaches to target oncogenic Ras proteins are more focused on indirect strategies, including disruption of regulator or effector protein interactions and inhibiting downstream effector signaling pathways *(83)*.

Histone deacetylase inhibitors (HDACi) are a very promising emerging class of anti-cancer drugs directed at targeting the frequent dysregulation of PTMs in cancers. Aberrant dysregulation of acetylation due to altered expression of HDACs or histone acetyl transferases (HATs) has been observed in several cancer types *(110)–(112)*. Additionally, HDACi have shown multiple clinical successes in the treatment of a myriad of primarily non-solid tumor cancers *(96)*. Historically, the effects of PTMs have been most extensively studied in histone regulation *(113)*; however, acetylation of non-histone proteins is known to alter protein stability and localization as well as protein-protein interactions *(105)*. While the role of acetylation in modulating protein activity in several cancer-related proteins such as p53 has been well established *(79),(105),(114)*, the role of acetylation has not been thoroughly investigated in Ras-driven cancers. Despite the early promise of HDACi, they have not proven to be a clinically viable monotherapy treatment option for Ras-driven solid tumors *(106),(115)*. The rationale for this ineffectiveness is currently unknown. However, the use of an HDACi as part of a combination therapy has been reported as a successful therapeutic strategy, causing Ras-driven cancer cell death and tumor regression *(100)–(102)*. In particular, when pancreatic cells were treated with a combination therapy of a MEK inhibitor (trametinib, GSK1120212)/ PI3K inhibitor (belinostat, BEZ-235)/ HDAC inhibitor (TSA,SAHA or PDX101), >99% of cellular

proliferation was inhibited and dramatic cellular apoptosis was induced *(101)*. Further, belinostat (HDACi) combination therapy with a MEK inhibitor (trametinib) synergistically acted to decrease tumor formation in a mouse lung cancer xenograft model *(102)*.

Ras proteins have been reported to be acetylated within their core GTPase domain, but it is unclear exactly how acetylation modulates Ras activity *(67)–(69),(116),(117)*. Acetylation of a receptor tyrosine kinase upstream of Ras, EGFR (epithelial growth factor receptor), causes enhanced signaling and sustained downstream activation, leading to resistance of tumor cells to HDACi treatment *(118)*. Also, HDAC2 overexpression has also been identified in colorectal cancer (CRC) *(96),(119)–(122)* and it is correlated with poor survival *(121)*. CRC is one of the leading causes of cancer deaths in the United States *(123)*, and Ras proteins are mutated in approximately 52% of CRCs *(5)*. These findings suggest that acetylation likely plays a role in regulating Ras-driven CRC, and therefore, HDACi may be an important and novel therapeutic option for Ras-driven cancers. Given the lack of clinical knowledge surrounding HDACi therapy in Ras-driven cancers, we have used cellular, biophysical and computational approaches to characterize the mechanism by which HDAC inhibitors display limited clinical utility as a monotherapy in Ras-driven CRC. This may lead to novel therapeutic approaches for the treatment of Ras-driven cancers.

Herein, we have demonstrated that treatment of CRC cells with the class I HDACi, Entinostat resulted in acetylation of Ras at a novel site, lysine (K) 5. We were further able to demonstrate that K5 acetylation led to increased MAPK signaling, while not significantly affecting PI3K signaling. Increased MAPK signaling is likely caused by an increased affinity of the acetylated protein to the Raf RBD, which was verified in binding studies. Molecular dynamic studies demonstrated the formation of novel electrostatic contacts between acetylated Ras and

the Raf RBD and an overall restructuring of the highly electrostatic binding network, consistent with the increased affinity for Raf and subsequent increased signaling.

Results

Oncogenic Ras is an effective predictor of resistance to HDACi treatment.

To gain insight into the limited clinical utilities of HDAC inhibitors as therapeutics in Ras-driven solid tumors the Sers lab conducted a drug sensitivity screen using a selection of HDACi on a panel of CRC cell lines that differ in their KRas or BRaf mutational status. Inhibitors that were chosen target either class I HDACs or both classes I and II, serving as pan-HDAC inhibitors. Three of the selected inhibitors in the include the pan-HDAC inhibitors panobinostat (LBH589), belinostat (PXD101) and vorinostat (SAHA), all of which are US Food and Drug Administration (FDA)-approved for the treatment of multiple myeloma (MM), peripheral T cell lymphoma (PTCL) and cutaneous T cell lymphoma (CTCL), respectively *(115),(124).* Additionally included in the screen were the two narrow- spectrum, class I HDAC inhibitors, entinostat (MS-275) and the FDA-approved romidepsin (FK228) *(115),(124)*. The CRC cell lines were treated with the HDACi for a total of 72 hours and the degree of cellular apoptosis was quantified as the percentage of cells that displayed cleaved caspase-3, a marker of cellular apoptosis, as analyzed by flow cytometry (**Figure 2.1A**). The extent of the apoptosis was further investigated based on the levels of cleaved PARP and visualized by immunoblotting (**Figure 2.1B**). Interestingly, upon treatment with the class I HDACi, MS-275 and FK228, they were able to observe two distinct cellular response profiles based on whether the CRC cells harbored KRas *WT* or oncogenic KRas. Cell lines that harbored KRas *WT* were unanimously more sensitive to HDACi treatment with more than 50% of the cells being apoptotic, while cells with oncogenic KRas exhibited a markedly more resistant phenotype with less than 20% of cells

being apoptotic (**Figures 2.1A, B**). They were further able to demonstrate that in the presence of the oncogenic BRaf *V600E* mutant, cells harboring KRas *WT* demonstrated no alterations in their sensitivity profiles. This suggested a mechanism dependent upon KRas and not the oncogenic BRaf *V600E*-mediated dysregulation of the downstream MAPK-signaling cascade. To confirm that oncogenic Ras is an adequate predictor of resistance to HDAC inhibitor treatment, in particular the class I HDACi MS-275 (Entinostat), an isogenic system using CaCO-2 cells transduced with either KRas *G12V* or KRas *WT* was employed to allow for conditional expression of the respective proteins. Upon expression of the oncogenic KRas *G12V*, a significant reduction in apoptotic cells and a subsequent dramatic shift towards a more resistant phenotype with close to a 5-fold increase in the IC_{50} was revealed. This phenomenon was not observed with an induced expression of KRas *WT*, which displayed a largely unchanged response profile. Taken together these results suggest that oncogenic KRas *G12V* is a predictor of negative therapeutic response to the class I HDACi, Entinostat.

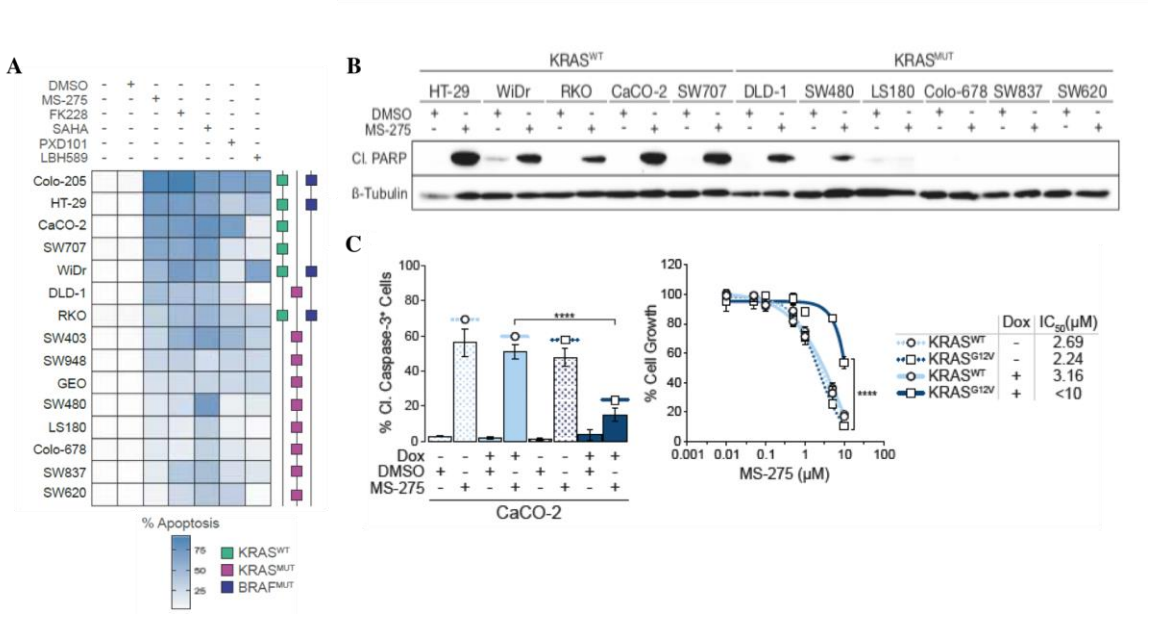

Figure 2.1. Oncogenic Ras is an effective predictor of resistance to HDAC inhibitors.

A. Heatmap representing the degree of sensitivity to HDAC inhibitors. 15 CRC cell lines were treated with either DMSO (0.1% v/v), MS-275 (5 μM), FK228 (5 nM), SAHA (5 μM), PXD101 (1 μM) or LBH589 (750 nM) for 72 hrs. The level of apoptosis was determined based on the percentage of cleaved capspase-3 positive cells as detected by flow cytometry. The white end of the spectrum denotes no detectable apoptosis (< 5%), while the blue end of the spectrum represents increasing to complete activation of apoptosis (100%). KRas and BRaf mutational status is indicated in left column. Data were compiled as mean ± standard deviation B. The mutational status of KRas determines the degree of MS-275-induced apoptosis as based on the level of cleaved PARP (poly ADP-ribose polymerase). 11 CRC cell lines from A, were treated with either DMSO (0.1% v/v) or MS-275 (5 μM) for a total of 72 hrs. Samples were immunoblotted with the indicated antibodies. C. A KRAS *G12V*-dependent decrease in sensitivity to MS-275 treatment. CaCO-2 KRAS *WT* and CaCO-2 KRAS *G12V* cells were treated with either DMSO (0.1% v/v), MS-275 (5 μM) (left) or increasing concentration of MS-275 (right) for 72 hrs. The ectopic expression of KRAS *WT* and KRAS *G12V* was initiated with doxycycline (2 μg/ml) 72 hrs prior and maintained for the full duration of the experiment. The level of apoptosis (left) was determined as in A, while growth inhibition was measured using XTT (tetrazolium salt) cell proliferation assay (colorimetric assay for quantification of cellular proliferation). For the latter, the IC50 values are indicated. *Data collected by the Sers lab.

KRas is acetylated at position K5 in response to MS-275 treatment.

KRas has been reported to be regulated via post-translational acetylation at lysine 104 (K104) and lysine 147 (K147), with HDAC6 and SIRT2 serving as the lysine deacetylases modulating these processes *(67)–(69),(125),(126)*. In order to investigate whether the resistance to the HDACi MS-275 observed upon expression of oncogenic KRas *G12V* protein is a consequence of modulation of the acetylation state of Ras, the Sers lab assessed the overall acetyl-lysine levels of immunoprecipitated Ras from CaCO-2 cells ectopically expressing either KRas *WT* or KRas *G12V*. Immunoblotting data demonstrated that irrespective of the mutational status of KRas, treatment with MS-275 resulted in elevated levels of detected acetyl-lysine (**Figure 2.2A**). This data suggests that MS-275 induced therapeutic resistance via modulation of acetylation state in oncogenic KRas *G12V* proceeds via a mechanism unique or perpetuated by oncogenic Ras that is distinct from KRas *WT*. In order to determine which residue was being acetylated in Ras proteins independent immunoprecipitation followed by protein shotgun LC-MS/MS analysis was conducted. Intriguingly, only one lysine residue, K5 where acetylation was detected as a consequence of treatment with MS-275 was identified (**Figure 2.2B**). To verify that acetylation of K5 was solely responsible for the observed increase in detectable levels of acetylated lysine identified in response to MS-275 treatment, substitution mutants were made at K5. K5 was substituted for either alanine (K5A) or arginine (K5R). This functioned to eliminate the detectable overall lysine acetylation, permanently locking KRas in a constitutively deacetylated state upon MS-275 treatment. This indicated that K5 is likely to be the only acetylated lysine residue in this context (**Figure 2.2C**). K5 has not been identified previously as a site of post-translational modification in Ras proteins. Here, the Sers lab has identified a novel, physiologic acetylation site in Ras proteins in response to MS-275 HDACi treatment. As this is a

previously unidentified acetylation site in Ras proteins, the functional consequence of acetylation at K5 are unknown.

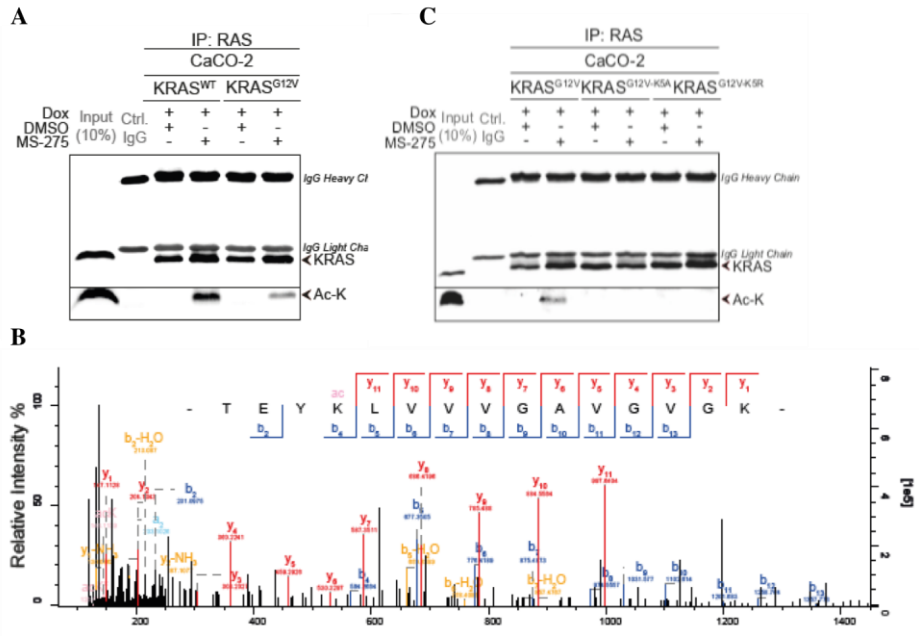

Figure 2.2. HDAC inhibition promotes KRas acetylation

A. Detection of acetyl-lysine of immunoprecipitated KRAS. CaCO-2 KRas *WT* and CaCO-2 KRas *G12V* cells, with an induced ectopic expression of the respective proteins, were treated with either DMSO (0.1% v/v) or MS-275 (5 µM) for 72 hrs. Total Ras was immunoprecipitated and acetyl-lysines (AcK) on KRas were detected by immunoblotting. B. Identification of the acetylated lysine residue by LC/MS/MS analysis of immunoprecipitated KRas *G12V*. C. Effect of K5A and K5R substitution mutations on overall lysine acetylation of KRas *G12V*. Ectopically expressed KRas *G12V*, KRas *G12V-K5A* and KRas *G12V-K5R* were immunoprecipitated form CaCO-2 cells treated as in A. Acetylated lysine on KRas was detected by immunoblotting. *Data collected by the Sers lab.

MS-275 induced acetylation of Ras increases the steady-state Ras-GTP levels in cells.

As the role of K5 acetylation has not been previously described in Ras proteins, we next assessed the impact that acetylation at K5 has on the biological function of KRas. We first

evaluated whether MS-275 treatment and Ras acetylation were capable of modulating the overall activation status of Ras in cells. As Ras proteins bind to their downstream effectors in a GTP-dependent manner *(15)*, Raf-RBD (Ras binding domain) pulldown assays can be used to evaluate the GTP-bound population of Ras proteins in cells *(127)*. The Raf-RBD pull-down assay revealed an immediate and persistent increase in the steady-state GTP-bound levels of KRas following treatment with MS-275. This effect was observed independent of KRas mutational status (**Figure 2.3A**). Although the steady-state GTP-bound level of KRas is expectedly significantly higher in the context of oncogenic KRas *G12V* relative to KRas *WT*, the magnitude of the change that occurs due to MS-275 treatment exhibits an overall similar tendency. To confirm that acetylation at K5 is solely responsible for the increase in the level of KRas-GTP complexed with the Raf RBD, the Sers lab assessed whether K5A or K5R substitution mutations would restore the KRas *WT*-GTP population in cells. However, in K5A and K5R KRas mutants, moderate increases in the steady-state GTP levels in cells relative to wild-type protein were observed (**Figure 2.3B**). Interestingly, KRas germline mutations at K5 have been identified in several Ras-driven genetic disorders, and these mutations have been demonstrated to increase the GTP-bound population of Ras in cells leading to increased downstream MAPK signaling *(128)*. However, the mechanism by which K5 mutations activate Ras proteins is unknown *(128)*. It is therefore likely that K5A and K5R KRas mutants are altering the relative GTP-bound population of cells that is unique from the effect of K5 acetylation due to MS-275 treatment.

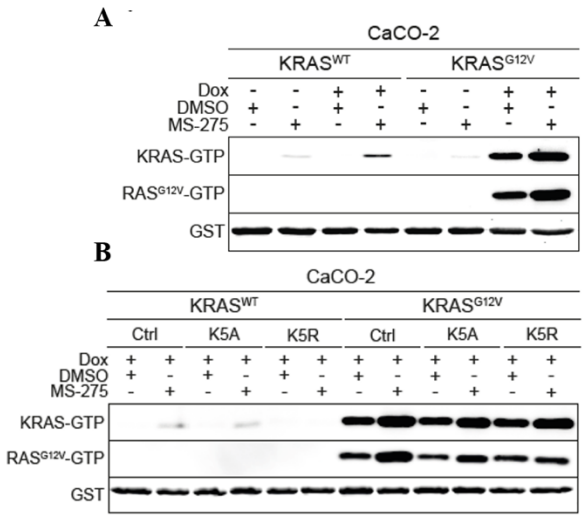

Figure 2.3. HDAC inhibition increases the steady-state levels of KRas-GTP complexed with Raf-RBD

A. MS-275-induced changes in steady-state GTP-bound KRas levels. Cells were treated with either DMSO (0.1% v/v) or MS-275 (5 µM) for 72 hrs. Changes in the levels of KRas *G12V*-GTP and KRas *WT*-GTP pulled-down with Raf1-RBD agarose beads were assayed in the absence and presence of an induced ectopic expression of the respective proteins and detected by immunoblotting analysis. B. Effect of K5A and K5R mutations on MS-275-induced changes in steady-state GTP-bound KRas levels. Changes in the levels of KRas *G12V*-GTP, KRas *G12V-K5A*-GTP and KRas *G12V-K5R*-GTP were assessed as described in A.

MS-275 induced acetylation of Ras results in preferential signaling through the downstream Raf-MAPK signaling cascade.

KRas K5 germline mutations are associated with increased GTP-levels in cells and potentiate signaling via the downstream Raf-MAPK signaling cascade in Ras-driven genetic disorders *(128)–(130)*. In addition, K5 is also highly conserved in the Ras superfamily of proteins *(4)*. Taken together, this suggests that K5 is an important site in regulating the function and activity of Ras proteins. Given this data and the identification of an increase in the GTP-bound population of Ras in Raf RBD pulldown assays, we would expect that acetylation at K5 would likely also lead to altered downstream signaling via Ras-mediated pathways. Therefore,

the Sers lab assessed whether MS-275 treatment and acetylation of Ras at K5 led to altered MAPK-mediated downstream signaling. They uncovered that only in the setting of an oncogenic KRas *G12V* were they able to observe hyper-activation of the downstream MAPK signaling cascade due to MS-275 treatment. This is marked by an increase in the phosphorylation of MEK1/2 and ERK1/2 (**Figure 2.4A**). In case of KRas *WT*, this remained largely unchanged. This identified disparity is not entirely unexpected as oncogenic KRas *G12V* is known to populate a constitutively activated phenotype primarily due to the lack of GAP-stimulated GTP hydrolysis *(4),(5),(27),(33).* In response to MS-275 treatment, acetylation of K5 in KRas *G12V* resulted in further increase in MAPK pathway activation. No observed defect was identified in PI3K signaling (data not shown).

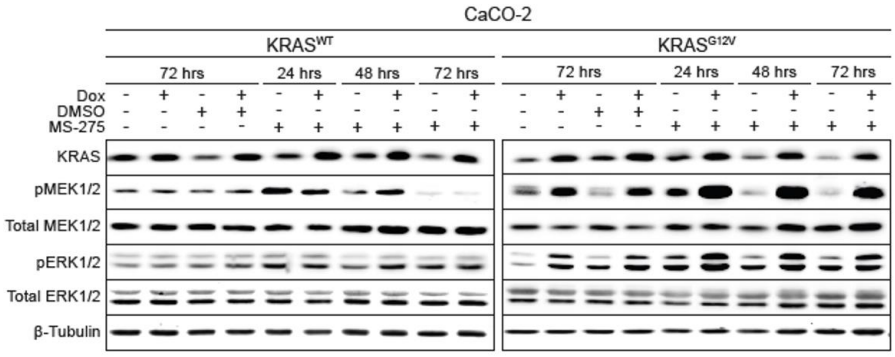

Figure 2.4. HDAC inhibitor treatment potentiates MAPK-mediated signaling

MS-275-induced hyperactivation of MAPK-signaling in KRas *G12V* expressing cells. CaCO-2 KRas *WT* and CaCO-2 KRas *G12V* were treated with either DMSO (0.1% v/v) or MS-275 (5 µM) for 24, 48 and 72 hrs. Changes in the levels of MAPK-signaling components were assayed in the absence and presence of an induced ectopic expression of the respective proteins. Samples were immunoblotted with the indicated antibodies.

In vitro acetylation of KRas results in mild GEF and GAP defects and thermal instability.

Despite being a highly conserved residue in the core GTPase domain of Ras proteins *(4),(34),* the functional role of K5 has until now remained an uncertainty. Structurally, K5 is

located in the β1 sheet of Ras and extends into a region known to be important for GEF, GAP and effector protein recognition and binding *(16),(53),(131).* To explore the possibility that acetylation of K5 is capable of altering Ras activity *in vitro*, we generated KRas protein containing acetyl-lysine at position K5 using an unnatural amino acid approach. Here, a cognate pair of $tRNA_{CUA}$/tRNA synthase was used to direct the installation of Nε-acetyl-lysine into KRas in response to an amber codon at the genetic level, in a manner similar to as described previously *(68),(132),(133).* Incorporation of acetyl-lysine was verified by mass spectrometry to be greater than 95% (**Figure 2.5A,B**).

Cellular studies conducted by the Sers lab demonstrate an equal increase in Ras-GTP levels as identified by Raf RBD pulldowns independent of mutational status due to MS-275 treatment and therefore Ras acetylation (**Figure 2.3A**). This suggests that regulation of Ras activation due to K5 acetylation likely occurs via a similar mechanism in wild-type and oncogenic KRas *G12V*. This would hold true despite the propensity of oncogenic KRas *G12V* to remain in an activated phenotype due to significantly impaired GAP-mediated hydrolysis *(4),(5),(27),(33).* In order to assess the activation of Ras proteins *in vitro* we evaluated intrinsic and regulator-mediated nucleotide cycling and hydrolysis rates using fluorescence-based methods *(134),(135).* Alterations in the ability of Ras proteins to cycle their nucleotides could lead to the activated phenotype of acetylated Ras proteins in cells. We were able to identify no significant defects in the ability of KRas *WT* or KRas K5 acetylated proteins to intrinsically cycle GDP ($4.23\pm1.07 \times 10^{-4}$ s^{-1} vs. $3.67\pm0.691 \times 10^{-4}$ s^{-1} for KRas *WT* and acetylated protein, respectively) or GMPPCP, a GTP analogue ($40.7\pm0.278 \times 10^{-4}$ s^{-1} vs. $42.3\pm0.404 \times 10^{-4}$ s^{-1} for KRas *WT* and acetylated protein, respectively). We also demonstrated similar rates of intrinsic GTP hydrolysis in KRas *WT* and KRas K5 acetylated proteins ($2.94\pm0.219 \times 10^{-4}$ s^{-1} vs.

2.85±0.326 x 10^{-4} s^{-1} for KRas *WT* and acetylated protein, respectively) (**Figure 2.7, A-D**). Interestingly, we were able to identify mild defects in the ability of acetylated KRas protein to undergo regulator-mediated nucleotide exchange and hydrolysis, with larger defects observed in the activated form of Ras proteins. Slower GMPPCP nucleotide exchange (348±6.97 x 10^{-4} s^{-1} vs. 182±1.83 x 10^{-4} s^{-1} for KRas *WT* and acetylated protein, respectively) and GTP hydrolysis rates (24.3±0.277 x 10^{-4} s^{-1} vs. 9.96±0.178 x 10^{-4} s^{-1} for KRas *WT* and acetylated protein, respectively) in the presence of GEFs and GAPs may demonstrate a propensity for acetylated Ras proteins to remain in the active, GTP-bound form (**Figure 2.6, A-D**), although the noted defects are small in nature. Compiled nucleotide exchange and hydrolysis rates can be seen in **Table 2.1**. SOS is known to coordinate nearly every sidechain of the SWII region of Ras proteins. At the core of these interactions is a hydrophobic network in Ras proteins containing Y71 *(54)*. K5 is noted to pack against Y71 particularly in the GDP-bound form *(128)*. Acetylation could lead to alteration of Y71 and further disruption of the critical hydrophobic network in Ras that is responsible for placing SWII in the proper conformation for SOS binding. A similar disruption of SWII could lead to altered ability of acetylated Ras protein to undergo GAP-mediated hydrolysis *(136)*. However, as the identified defects are small in nature, this suggests that SWII is largely unperturbed. K5 acetylation may therefore impact SWII very minimally, consistent with the small defects identified.

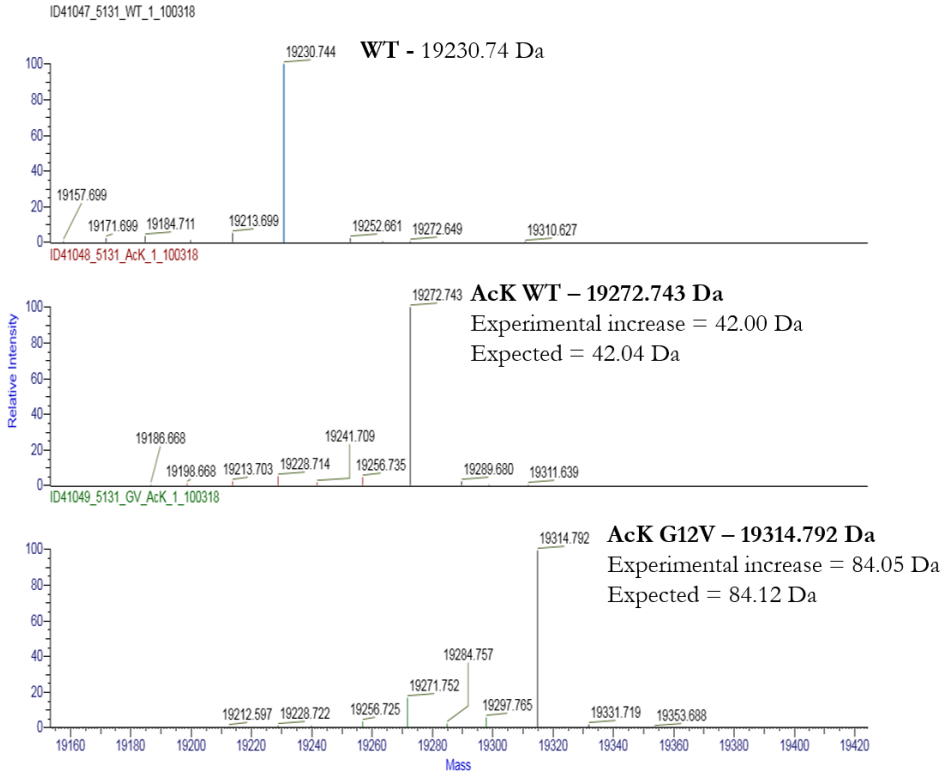

Figure 2.5. Mass spectrometry identification and characterization of acetylated KRas

Full-MS spectra of intact KRas protein verifies acetylation. Unmodified wild-type Ras (top panel, 19230.74 Da), acetylated wild-type Ras (middle panel, 19272.743 Da) and acetylated G12V Ras (bottom panel, 19314.792 Da) are verified. The acetylated KRas population was determined to be >95%, relative to wild-type protein.

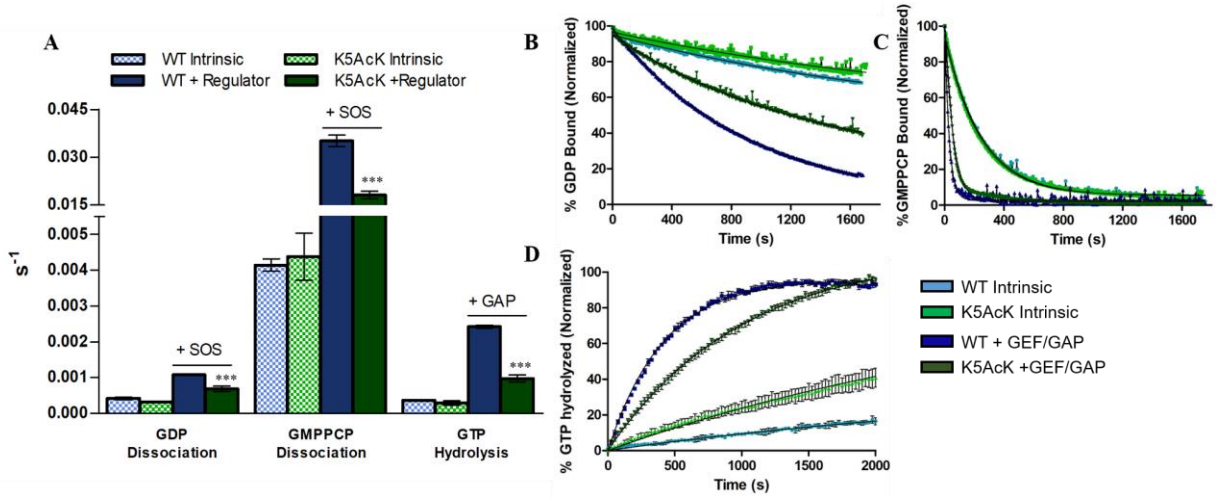

Figure 2.6. GEF and GAP-mediated defects identified in acetylated KRas

A. Fluorescence-based assays were used to determine the rates of nucleotide exchange and hydrolysis in the presence and absence of regulatory proteins. KRas *WT* and KRas K5 acetylaed proteins were loaded with Mant-GDP or Mant-GMPPCP and the rate of nucleotide dissociation was measured over time by the addition of excess non-labelled nucleotide in the absence or presence of a the catalytic domain of human SOS (Ras:SOS^{cat} = 1:1 molar ratio). Data were fit to an exponential dissociation curve using GraphPad Prism 5. Rates are reported as the mean ± S.E. (*n* = 3). Statistical analysis was conducted using the built-in one-way ANOVA analysis in GraphPad Prism 5 ($p<0.0001$) followed by a post hoc Tukey comparison to determine statistical significance. Results of Mant-GDP and Mant-GMPPCP dissociation can be seen in B and C, respectively. D. Intrinsic and p120 GAP^{cat}-mediated (GAP^{cat}/Ras = 1:200 molar ratio) GTP hydrolysis was determined using single-turnover hydrolysis assays for KRas *WT* and acetylated proteins. Ras proteins were loaded with GTP, and the addition Mg^{2+} stimulated GTP hydrolysis. The production of free phosphate was measured over time using the phosphate binding protein, Flippi 5U. Data was fit to a phosphate standard curve and GTP hydrolysis rates were calculated using the GraphPad Prism 5 one-phase exponential association equation. Results are the mean ± S.E.of three independent replicates (N=3).

Ras Protein	Nucleotide	Intrinsic (x 10^{-4}, s^{-1})	GEF/GAP-Mediated (x 10^{-4}, s^{-1})
Nucleotide Exchange			
KRas WT	GDP	4.23±1.07	10.8±0.075
KRas K5AcK	GDP	3.67±0.691	7.22±0.527
KRas WT	GMPPCP	40.7±0.278	348±6.97
KRas K5AcK	GMPPCP	42.3±0.404	182±1.83
Nucleotide Hydrolysis			
KRas WT	GTP	2.94±0.219	24.3±0.277
K5AcK	GTP	2.85±0.326	9.96±0.178

Table 2.1. KRas *WT* and KRas *K5AcK* rates of nucleotide exchange and hydrolysis

Determination of thermal melting temperatures can also provide insight into the structural role of K5 acetylation in contributing to overall protein stability. Using circular dichroism, we were able to identify alterations in the thermal stability of GDP-bound acetylated KRas protein, where melting temperature is defined as the temperature at which 50% of the protein is unfolded (**Figure 2.7, A-C**). Slightly more than a 4°C defect in the melting temperature of acetylated Ras protein was observed in the GDP-bound form relative to wild-type protein (63.5±0.055°C vs. 59.4±0.217°C for KRas *WT* and acetylated protein, respectively). This defect was not observed in the GMPPCP-bound form of the acetylated protein, indicating that K5 may play a structural role in stabilizing the GDP-bound form of the protein more extensively. Compiled results of thermal analysis of Ras proteins can be seen in **Table 2.2**. Taken together, the results of GEF- and GAP-mediated nucleotide exchange defects in the GMPPCP bound form and decreased thermal stability of acetylated protein in the GDP-bound form suggest that acetylation is likely to activate Ras, consistent will the observed cellular phenomena.

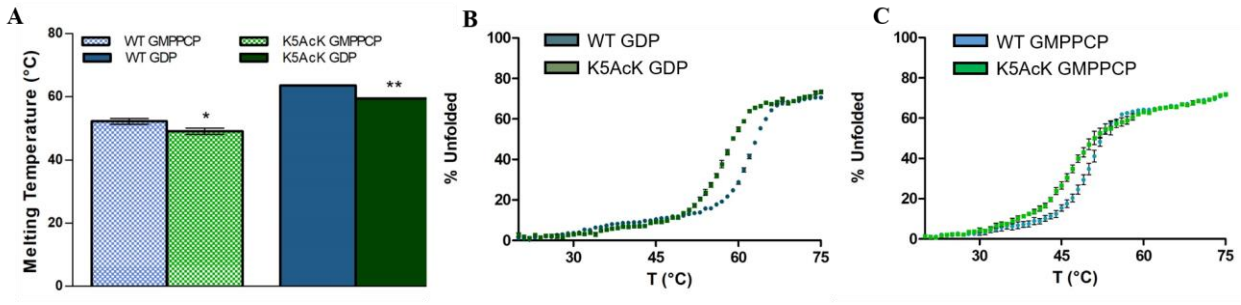

Figure 2.7. Minor alterations in thermal melting temperature due to KRas acetylation

A. Thermal melting temperature was determined using circular dichroism measurements for GDP- and GMPPCP-bound KRas *WT* and acetylated proteins. Protein unfolding was measured as a function of increasing temperature over time (20–95°C, 2°C per minute) at 222 nm of 30 μM Ras protein. The thermal melting temperature was determined by fitting the curve to a Boltzmann's sigmoidal equation in GraphPad Prism 5, where the V50 is indicative of the protein melting temperature. Results are reported as the mean ± S.E. (*n* = 3). Statistical analysis was conducted using the built-in one-way ANOVA analysis in GraphPad Prism 5 ($p<0.0001$) followed by a post hoc Tukey comparison to determine statistical significance. Results of GDP- and GMPPCP-bound thermal melts can be seen in B and C, respectively.

Ras Protein	Nucleotide	T_M (°C)
KRas WT	GDP	63.5±0.055
KRas K5AcK	GDP	59.4±0.217
KRas WT	GMPPCP	51.4±0.928
KRas K5AcK	GMPPCP	49.9±1.03

Table 2.2. Thermal melting temperature for KRas *WT* and KRas acetylated protein

Acetylation of KRas at K5 alters the binding affinity of Ras to the Raf RBDs

Ras proteins are highly dynamic and display distinct conformations in both their GDP- and GTP-bound forms dictated by the positioning of two highly flexible regions, namely switches I and II (SWI, SWII) *(9),(41)*. In their GTP-bound form, SWI and SWII form additional contacts with the guanine nucleotide, stabilizing the active form of Ras proteins *(41)*. Ras proteins display significantly tighter affinities to their downstream effector proteins in their GTP-bound form, promoting signaling through downstream cell signaling cascades *(15),(16)*. Cellular

and biochemical analyses of Ras proteins demonstrate that K5 acetylation leads to an increased GTP-bound population of protein as identified in Raf RBD pulldowns and enhanced signaling through the MAPK cascade. As the structural role of K5 in regulating Ras activity is unclear, we sought to determine if enhanced MAPK signaling was due to changes in the affinity of acetylated Ras protein to the Raf kinase RBD (Ras binding domain) or due solely to the increase in the GTP-bound population of the acetylated protein. Raf RBDs primarily interact with Ras proteins through SWI, whereas other effector proteins such as PI3K interact with Ras proteins using both SWI and SWII *(16),(50),(55)*. To assess whether K5 acetylation is capable of altering interactions with downstream effector proteins, we used isothermal titration calorimetry (ITC) to determine the binding affinity of Ras proteins to the RBDs of Raf and PI3Kα. Consistent with literature *(17)*, we were able to observe a weakened binding affinity of KRas *G12V* to both BRaf and CRaf RBD. Interestingly, acetylation at K5 was able to restore the weakened binding affinity of KRas *G12V* to wild-type values for both BRaf and CRaf (**Figures 2.8, 2.9, 2.10**). This would suggest that the increased MAPK signaling observed in cells as a result of MS-275 treatment and Ras acetylation is at least due in part to altered interactions with the Raf RBDs. Cellular analysis also indicated no change in PI3K-mediated signaling as a result of mutation or acetylation (data not shown). This was verified in further binding studies, where ITC analysis indicated no statistical differences in the binding affinities for KRas *WT,* KRas *G12V* or K5 acetylated KRas *G12V* for the PI3Kα RBD (**Figures 2.8, 2.11**). Combined results of ITC analyses are provided in **Table 2.3**.

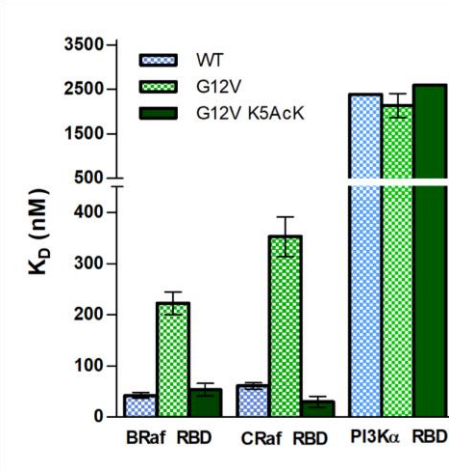

Figure 2.8. KRas *G12V-K5AcK* displays altered affinity to Raf-RBD

Binding affinities of KRas *WT* (blue), KRas *G12V* (light green) and K5 acetylated (K5AcK) KRas *G12V* (dark green) were determined to BRaf, CRaf and PI3Kα RBDs using isothermal titration calorimetry (ITC). Ras proteins at either 150 or 200 μM were titrated into effector proteins at molar ratios of 1:10 or 1:15 for Raf and PI3K RBDs, respectively. Heat of binding was measured at 25°C. A controlled subtraction was used to normalize the isotherm to the heat of saturation. Data was analyzed using a nonlinear least square algorithm and fit to a one-site model provided in the MicroCal PEAQ-ITC Origin Software. Calculated affinities were plotted in GraphPad Prism 5. Data are shown in replicate (N=3 for Raf RBDs, N=1 or 2 for PI3K RBD) ± S.E.

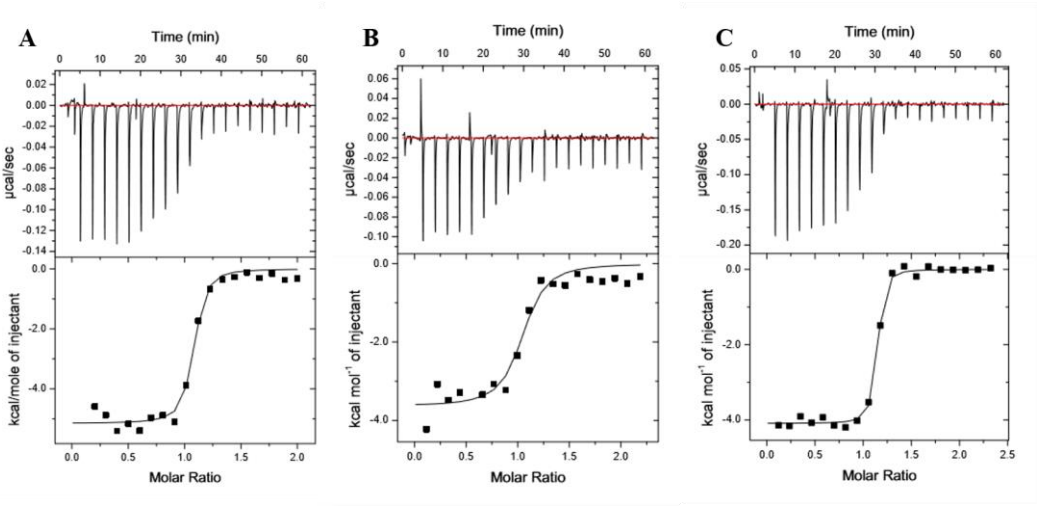

Figure 2.9. ITC binding analysis of KRas *WT*, KRas *G12V* and KRas *G12V-K5AcK* to BRaf RBD displays altered affinities

Representative isotherms of Ras:BRaf RBD binding experiments conducted using isothermal titration calorimetry (ITC). Either 150 µM or 200 µM Ras proteins were titrated into Raf RBDs at a starting molar ratio of 1:10. Isotherms are shown for A. KRas *WT*, B. KRas *G12V* and C. K5 acetylated KRas *G12V* binding to BRaf RBD. Experiments were conducted as described in Figure 2.8. Calculated affinities of 37.3 ± 5.7 nM, 223 ± 21.94 nM and 49.2 ± 12.62 nM correspond to A. KRas *WT*, B. KRas *G12V* and C. K5 acetylated KRas *G12V* binding to BRaf RBD, respectively. Compiled data can be seen in Table 2.3 where data is represented in replicate ± standard error (N=3).

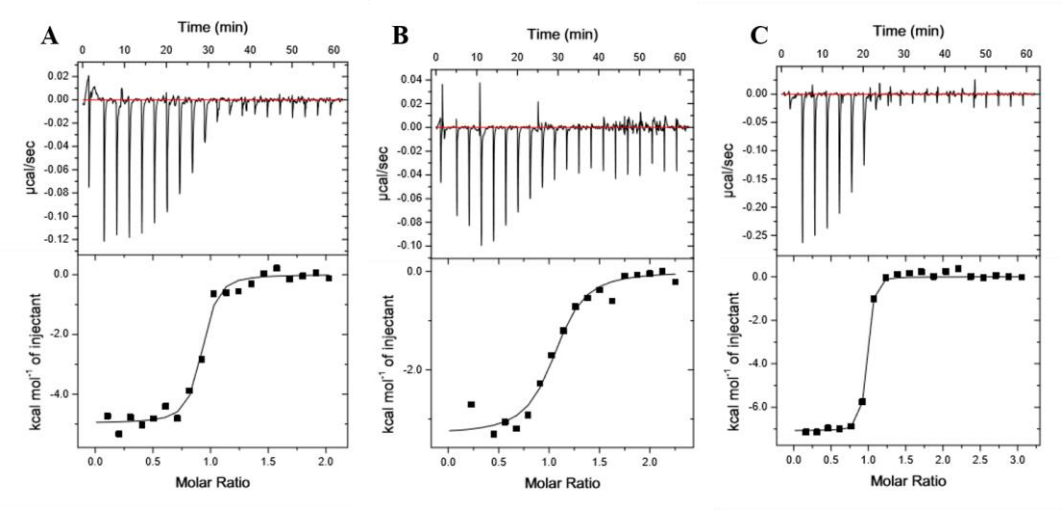

Figure 2.10. ITC binding analysis of KRas *WT*, KRas *G12V* and KRas *G12V-K5AcK* to CRaf RBD displays altered affinities

Representative isotherms of Ras:CRaf RBD binding experiments conducted using isothermal titration calorimetry (ITC). Either 150 µM or 200 µM Ras proteins were titrated into Raf RBDs at a starting molar ratio of 1:10. Isotherms are shown for A. KRas *WT*, B. KRas *G12V* and C. K5 acetylated KRas *G12V* binding to CRaf RBD. Experiments were conducted as described in Figure 2.8. Calculated affinities of 60.6 ± 6 nM, 344 ± 38.58 nM and 21.75 ± 10.71 nM correspond to A. KRas *WT*, B. KRas *G12V* and C. K5 acetylated KRas *G12V* binding to CRaf RBD, respectively. Compiled data can be seen in Table 2.3 where data is represented in replicate ± standard error (N=3).

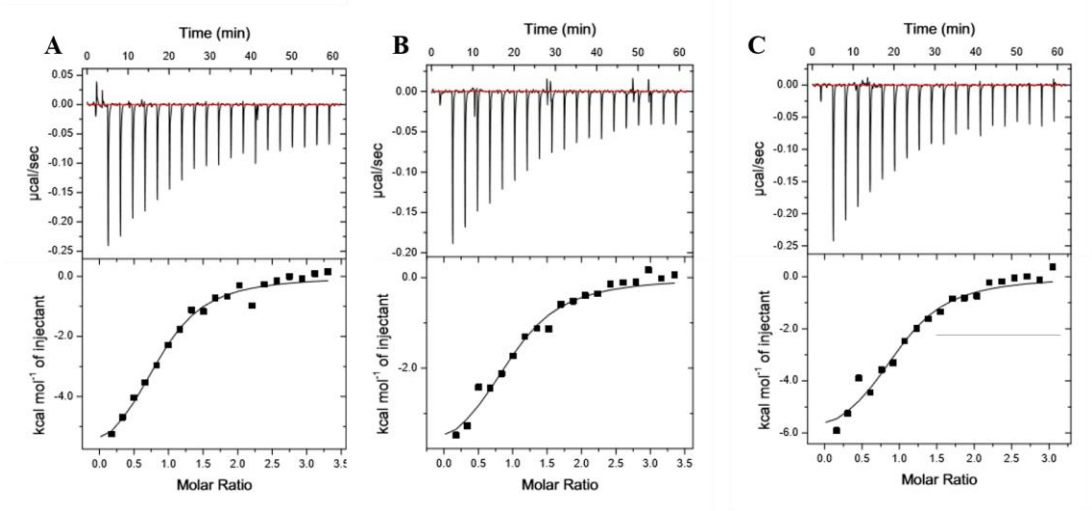

Figure 2.11. ITC binding analysis of KRas *WT*, KRas *G12V* and KRas *G12V-K5AcK* displays no difference in affinity to PI3Kα RBD

Representative isotherms of Ras:PI3Kα RBD binding experiments conducted using isothermal titration calorimetry (ITC). Either 150 µM or 200 µM Ras proteins were titrated into Raf RBDs at a starting molar ratio of 1:15. Isotherms are shown for A. KRas *WT*, B. KRas *G12V* and C. K5 acetylated KRas *G12V* binding to PI3Kα RBD. Experiments were conducted as described in Figure 2.8. Calculated affinities of 2.39 ± 0.010 µM, 2.0 ± 0.271 µM and 2.6 µM correspond to A. KRas *WT*, B. KRas *G12V* and C. K5 acetylated KRas *G12V* binding to PI3Kα RBD, respectively. Compiled data can be seen in Table 2.3 where data is represented in replicate ± standard error (N=2 for Ras *WT* and Ras *G12V*, acetylated protein is N=1).

Ras Protein	Effector RBD	KD (nM)
KRas *WT*	BRaf	37.3 ± 5.73
KRas *G12V*	BRaf	223 ± 21.9
KRas *G12V-K5AcK*	BRaf	49.2 ± 12.6
KRas *WT*	CRaf	60.6 ± 6.00
KRas *G12V*	CRaf	344 ± 38.6
KRas *G12V-K5AcK*	CRaf	21.8 ± 10.7
KRas *WT*	PI3Kα	2390 ± 10.00
KRas *G12V*	PI3Kα	2000 ± 271.4
KRas *G12V-K5AcK*	PI3Kα	2600

Table 2.3. Calculated binding affinities of KRas *WT*, KRas *G12V* and KRas *G12V-K5AcK* to BRaf RBD, CRaf RBD and PI3Kα RBD

Acetylation of K5 causes sidechain reorientation and altered dynamics in GDP- and GTP-bound protein

While K5 of Ras extends into the binding interface for regulatory and effector proteins, it is not noted to make any direct contacts *(128)*. In the GDP-bound form, the K5 sidechain has been suggested to interact with SWII residues T74 and Y71 *(128)*. Acetylation of K5 would likely disrupt these contacts, as is indicated by the mild change in thermal stability identified in **Figure 2.7**. In order to understand how acetylation alters intrinsic Ras protein activity, we conducted 200 ns Molecular Dynamic (MD) simulations of Mg^{+2}-GDP bound Ras proteins and Mg^{+2}-GTP bound Ras *WT*, Ras *G12V* and K5 acetylated (K5AcK) Ras *G12V*. Trajectories were subjected to clustering analysis using Gromacs *(137)*, and the centroids of the most populated, lowest energy clusters for each was examined using PyMol 2.1 (Schrödinger, LLC). Results from this analysis (**Figure 2.12**) indicate that acetylation causes reorientation of K5, altering contacts with residues in SWII and β2. Throughout the simulations, the lysine 5 backbone carboxyl oxygen and amide can be seen forming polar contacts with the backbone amides of Gly77 and Glu76 and the Cδ oxygen of Glu76. Acetylation of Ras wild type results in the formation of a polar contact with Asp54 in both the GDP- and GTP- bound forms (**Figure 2.12B,F**), where the Asp54 contact is only identified for Ras *WT* bound to GTP (**Figure 2.12E**). Similar to Ras wild type protein, lysine 5 in Ras *G12V* forms backbone contacts with the backbone amides of Gly77 and Glu76 in both GDP- and GTP-bound forms (**Figure 2.12C,G**). No contact is noted with Asp54 in Ras *G12V*. In acetylated Ras *G12V* protein, an additional polar contact is noted with Y71 in the GDP-bound form (**Figure 2.12D**). In the GTP-bound form, acetylated RasG12V only forms contacts with the backbone amide of E76 and the Cδ oxygen (**Figure2.12H**). Contrary to previous speculations *(128)*, no contacts are noted between

the lysine 5 sidechain and Thr74 in any models (polar contact distance cutoff of 3.6Å). Since the backbone of lysine 5 forms several contacts with the highly dynamic switch II region, it is possible that acetylation may result in altered protein dynamics.

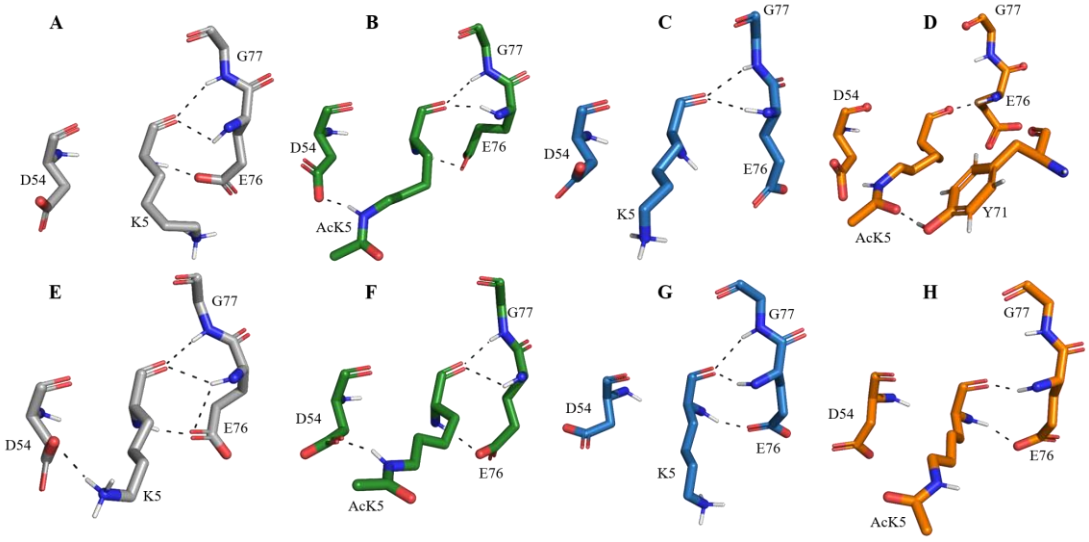

Figure 2.12 Lysine 5 acetylation causes reorientation of switch II and β2 contacts.

Lysine 5 contacts as identified from the lowest energy structure resulting from MD simulations and clustering analysis. Sidechains are shown as sticks. Ras wild type K5 (grey), wild type acetylated K5 (green), Ras *G12V* K5 (blue) and acetylated Ras *G12V* K5 (orange) models are shown in both GDP-bound (A-D) and GTP-bound (E-H) states. The backbone carboxyl oxygen and amide from backbone contacts with the switch II residues Gly77 and Glu76. Sidechain contacts are also note with Asp54 of β2. Mutation or acetylation results in reorientation of these contacts.

As Ras proteins are highly dynamic in nature, we also calculated the Cα residue RMSD fluctuations over time upon mutation or acetylation. By calculating the Cα residue RMSD throughout the MD simulations, we can gain insight into protein backbone dynamics. Results of these analyses for wild type and G12V Ras proteins are seen in **Figure 2.13**. In the GDP-bound form, acetylation in wild type protein greatly reduces the dynamic fluctuations in both SWI and SWII (**Figure 2.13B,D**). Ras *G12V* overall is more stable relative to wild type protein (**Figure**

2.13 E-H). In GDP-bound Ras *G12V*, increased dynamic fluctuations are identified immediately preceding SWI, in α1 helix. Acetylation dampened these fluctuations but increases were noted in the N-terminal portion of the α1 helix. The GTP-bound form of Ras *G12V* proteins display largely unchanged dynamics due to acetylation at K5, with only mild decreases of SWII fluctuations noted (**Figure 2.13G,H**). As we do not see large defects in protein stability, nucleotide binding or exchange (**Figure 2.6, 2.7**), it is likely that the slightly altered residue orientations and dynamics do not significantly impact innate functions of Ras proteins.

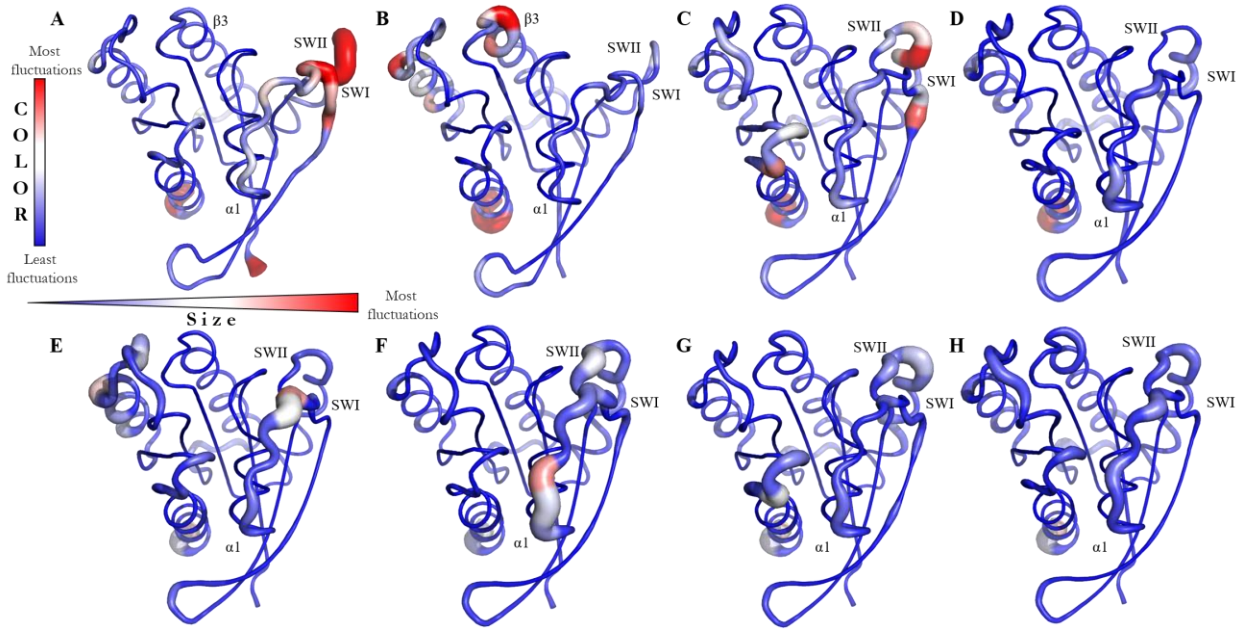

Figure 2.13 Cα backbone fluctuations calculated throughout the MD simulation demonstrate that acetylation stabilizes the Ras *WT* GDP- and GTP-bound structures

Cα backbone fluctuations throughout the course of the MD trajectory are mapped onto the structure of GDP- or GTP-bound Ras proteins. Fluctuations are labeled from least to most severe by color and size. Ras wild type and Ras wild type acetylated K5 GDP-bound are show in A and B respectively. Ras *G12V* and Ras *G12V* acetylated K5 GDP-bound are show in C and D respectively. Ras wild type and Ras wild type acetylated K5 GTP-bound are show in E and F respectively. Ras *G12V* and Ras *G12V* acetylated K5 GTP-bound are show in G and H respectively. In wild type Ras, acetylation (B and D vs A and C) appears to minimize dynamic fluctuations of SWII in particular. RasG12V proteins display less dynamic fluctuations as a whole and changes due to acetylation are minimal (E-H).

Acetylation of K5 in KRas fosters enhancement of the electrostatic network between Ras and Raf RBD

In Raf RBD pulldown experiments an increased GTP-bound population of protein was identified post MS-275 treatment (**Figure 2.3**). As no significant changes were identified in the innate functionality of Ras proteins but an increased binding affinity of acetylated proteins to the Raf RBDs was identified (**Figure 2.8**), it is likely that acetylation alters the ability of Ras

proteins to interact with the Raf RBD. As Raf RBDs interact with Ras proteins primarily through SWI *(16),(56)*, it is not immediately clear how acetylation could impact Raf RBD binding. The interaction interface between Ras and Raf is highly electrostatic in nature *(16),(42),(51)*, and mutation to any of the critical binding residues significantly alters or ablates binding *(43)*. To understand how acetylation at K5 is capable of altering the affinity of Ras proteins to Raf RBDs, we conducted 500 ns Molecular Dynamic (MD) simulations of Mg^{+2}-GTP bound Ras *WT*, Ras *G12V*, K5 acetylated (K5AcK) Ras *WT* and K5 acetylated (K5AcK) Ras *G12V* in complex with CRaf RBD. Analysis of these simulations was completed as described previously. Initial findings demonstrated that the acetyl sidechain of K5 reorients toward the effector interface (**Figure 2.14**), forming a novel electrostatic contact between the sidechain acetyl oxygen of K5AcK and the CRaf R67 guanidino NH sidechain. Mutation to either alanine or leucine at this site (R67) in the CRaf RBD dramatically alters binding to Ras proteins, indicating the importance of these electrostatic interactions in Ras:Raf RBD binding *(43)*. Based on the analysis of all centroids, the distance (CRaf R67 NH to Ras K5 acetyl oxygen) is in the range of ~3 Å, which is indicative of an energetically favorable electrostatic interaction *(138)–(140)*. The relative distance for Ras wild type is longer (~9 Å), possibly resulting from the repulsive nature of the positively charged lysine and arginine sidechains. This finding led us to further investigate the electrostatic network of binding interactions between Ras and the Raf RBD. Strikingly, we were able to identify a reordering and increased electrostatic network formation in Ras due to acetylation at K5 (**Figure 2.15A-D**). Several new electrostatic contacts were able to be identified due to acetylation involving Ras residues AcK5, Glu31, Glu37 and Asp54, which appear to be largely interconnected (**Figure 2.15**). Acetylation of lysine 5 appears to indirectly stabilize the Ras:Raf complex through the favorable reorganization of the electrostatic network. In Ras *G12V*, a

similar trend is also observed (data not shown). Taken together, the formation of novel electrostatic contacts and larger electrostatic networks are consistent with the increased binding affinity of acetylated proteins to the Raf RBDs (**Figure 2.10**) and also the increased GTP-bound population identified using Raf RBD pulldowns (**Figure 2.3**). Consistent with this, we are also able to observe the reorganization of the critical Ras:Raf binding interface elements α1, SWI and β3 in Ras and β2 and α1 in the Raf RBD (**Figure 2.16A,B**). In acetylated protein, an increased number of hydrogen bonds is noted between the β-strand interaction interface between Ras and the Raf RBD. Further, we can see that SWI in Ras and α1 in the Raf RBD reorient to position the polar, electrostatic C-terminal of α1 helix closer to the interface (**Figure 2.16B**).

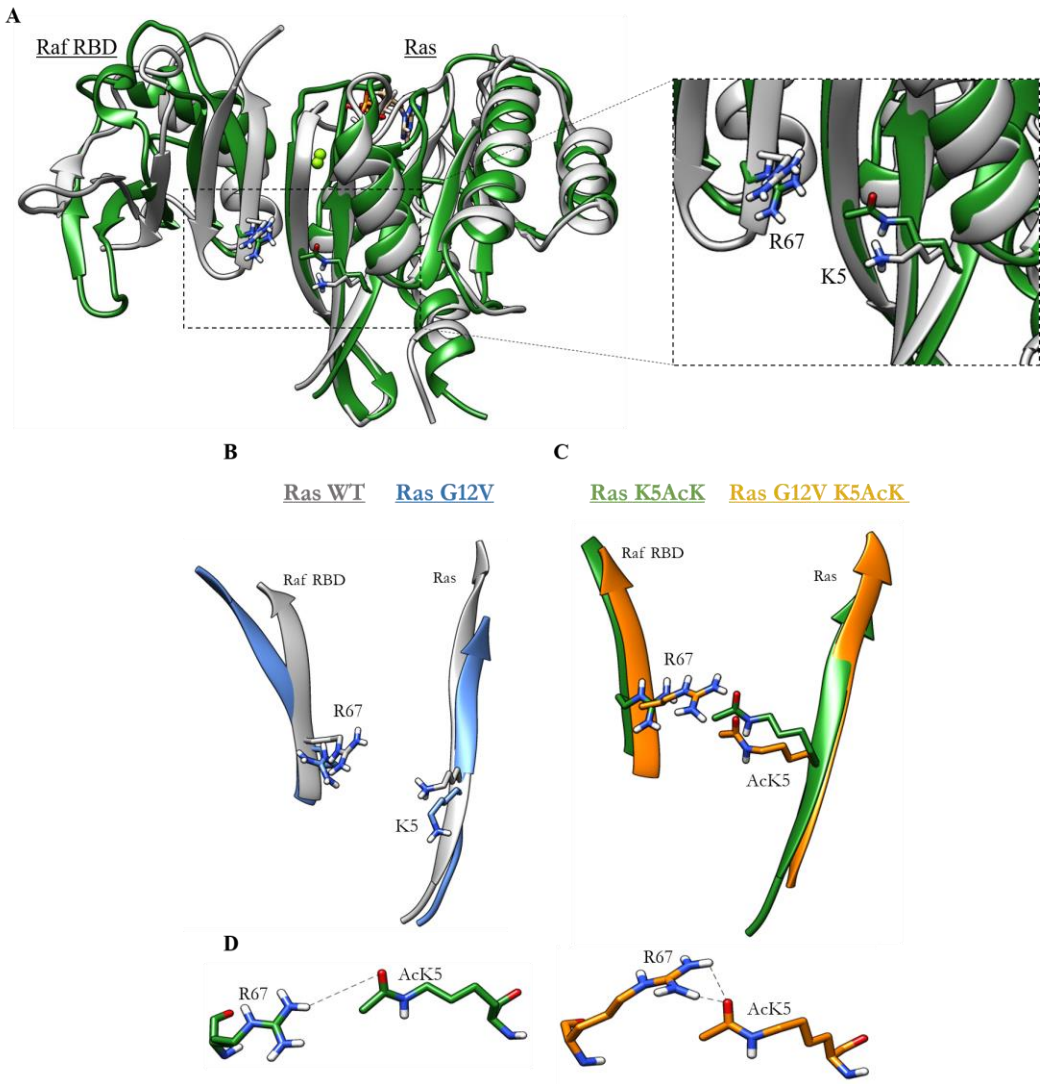

Figure 2.14. Representative models of MD simulations of Ras *WT* ,Ras *G12V*and K5 acetylated Ras proteins in complex with Raf RBD demonstrating overall reorientation of the K5 sidechain in response to acetylation. A. Ribbon diagram representation of Ras *WT* (grey) and K5 acetylated Ras (green) in complex with CRaf RBD obtained from MD simulations highlights differences in the positioning of Ras K5. In both Ras *WT* and Ras *G12V* (grey and blue, respectively), the K5 sidechain tucks inward and away from the solvent exposed interface, B. In K5 acetylated simulations, the acetyl-lysine sidechain reorients itself into the effector interface (Ras *WT* and Ras *G12V* on green and orange, respectively) We can see concurrent reorientation of the R67 sidechain in the Raf RBD, C. The lysine 5 acetyl oxygen forms an electrostatic contact with the guanidino NH sidechain of R67 in the CRaf RBD measuring ~ 3Å in the lowest energy clusters in Ras *WT* and Ras *G12V*, D.

A

Electrostatic contribution to binding		
Ras WT (res #)	Raf RBD (res #)	Distance (Å)
Glu 3	Lys 65	3.0
Glu 31	Lys 84	2.8
Glu 31	Lys 87	2.9
Asp 33	Arg 89	4.8
Glu 37	Arg 67	3.4
Asp 38	Arg 89	4.4
Asp 54	Arg 67	3.6
***Glu 62**	***Arg 73**	3.6
***Glu 63**	***Arg 73**	3.8

B

Electrostatic contribution to binding		
Ras WT-AcK (res #)	Raf RBD (res #)	Distance (Å)
Glu 3	Lys 65	3.0
***Lys-AcK 5**	***Arg 67**	3.0
***Glu 31**	***Arg 73**	4.9
Glu 31	Lys 84	3.7
Glu 31	Lys 87	2.7
Asp 33	Arg 89	4.9
Glu 37	*Arg 59*	3.7
Glu 37	Arg 67	3.4
Asp 38	Arg 89	4.6
***Asp 54**	***Lys 65**	3.0
Asp 54	Arg 67	4.1

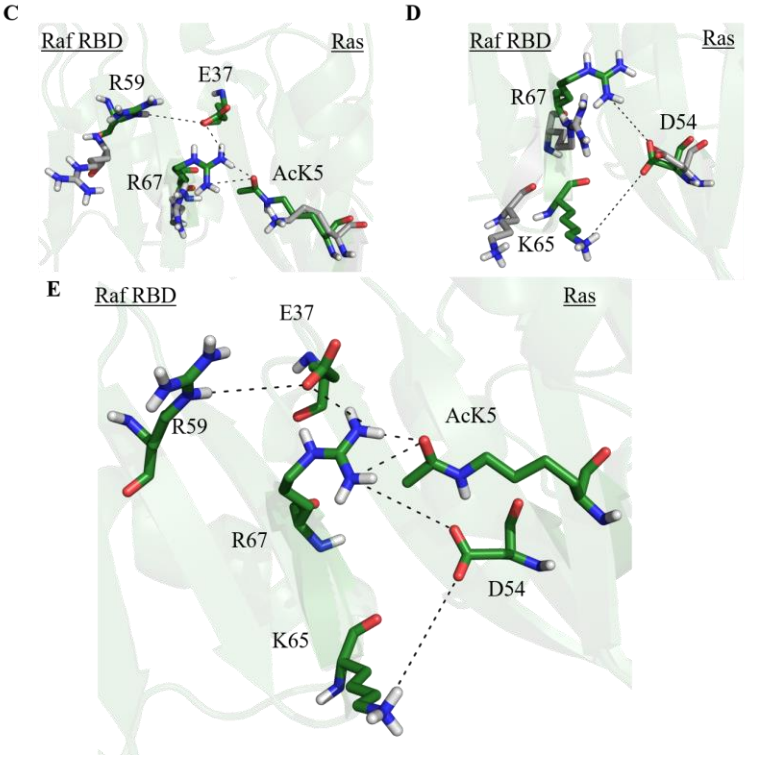

Figure 2.15 Reordering and strengthening of the electrostatic network of the Ras:Raf binding interface due to lysine 5 acetylation.

Novel electrostatic contacts and networks are identified due to acetylation at K5. Identified residues for Ras *WT* and acetylated Ras *WT* are noted in A and B, respectively. Distances noted are the minimum distance through the trajectory as calculated using VMD Software *(141)*. Representative reorientation of residues is shown in C and D. The electrostatic network in acetylated protein is much more interconnected as is seen in E, relative to wild type protein.

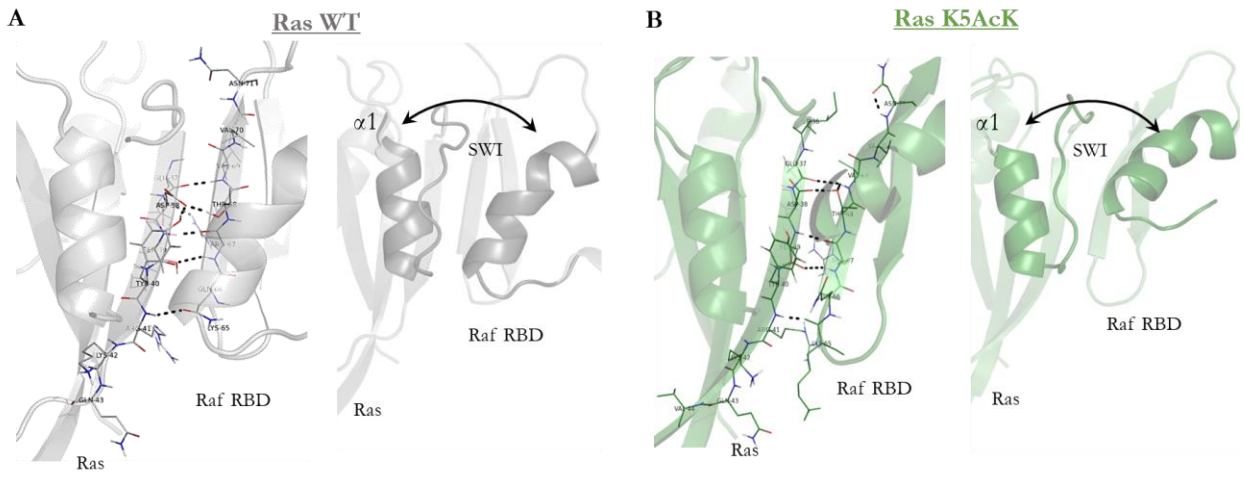

Figure 2.16 Reorientation of critical α-helical and β-strand pairing binding interfaces due to mutation or acetylation are identified in Molecular Dynamic simulations

In final structural models of Ras:Raf RBD complexes, large structural rearrangements can be identified due to K5 acetylation. Relative to Ras *WT* protein (A, grey), K5 acetylation alters critical α-helical and β-strand pairing networks for Ras binding to the Raf RBD (B).

Dramatic rearrangement of the binding interface between Ras and the Raf RBD have been identified in our MD simulations. However, as these are static structures and Ras proteins are known to be highly dynamic in nature, we calculated the RMSF fluctuations of each Cα backbone carbon throughout each trajectory. This will provide insight into how protein dynamics may play a role in Raf RBD binding. Consistent with the structural perturbations identified in **Figure 2.15**, we can also observe alterations in protein dynamics due to acetylation and G12 mutation. Ras *G12V* mutation increases the backbone conformational dynamics of α1, SWI, SWII and critical α-helical binding residues in the CRaf RBD (**Figure 2.16B**). Most striking are the overall dampening of backbone dynamics observed upon acetylation of Ras *G12V* (**Figure 2.16D**). Here, we can see translated onto the complex structure an overall decrease in the number and intensity of Cα backbone fluctuations, likely due to the stabilization of the binding network

between Ras and Raf RBD. This is consistent with the formation of a very stable Ras:Raf RBD complex and is reflected in the increased binding affinity of acetylated Ras *G12V* to the Raf RBDs (**Figure 2.8**). Here, we have identified the formation of a larger and more interconnected electrostatic binding network due to protein acetylation, which would support the increased affinity observed for acetylated protein to the Raf RBDs and increased MAPK cellular signaling.

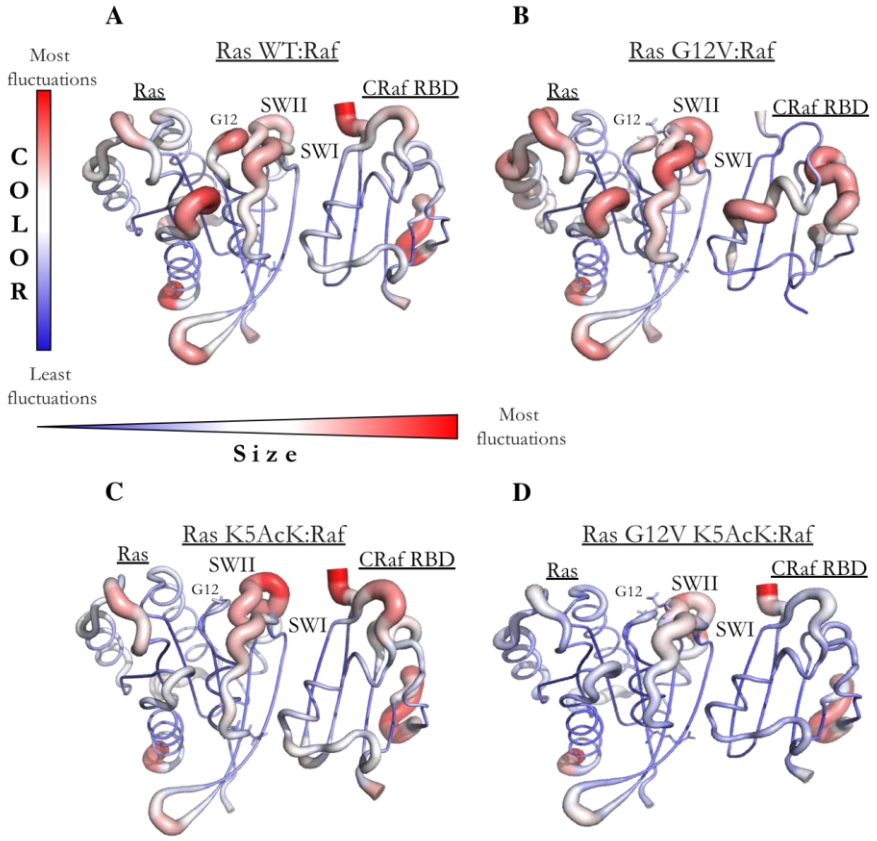

Figure 2.17. Altered conformational dynamics in the Ras:Raf RBD complex due to mutation or acetylation identified in molecular dynamics simulations.

Cα backbone fluctuations throughout the course of the MD trajectory are mapped onto the structure of Ras proteins in complex with the Raf RBD. Fluctuations are labeled from least to most severe by color and size. Relative to Ras *WT* protein (A), acetylation does not significantly affect the dynamics of critical α1, SWI and SWII regions (B). Ras *G12V* displays increased fluctuations in the Raf RBD, specifically in regions critical for binding, C. Acetylation of Ras *G12V* dampens dynamic fluctuations of the entire complex, consistent with the formation of a highly stable complex, D.

Discussion

Ras proteins have remained elusive drug targets for more than 30 years *(24)*. However, small molecules that target the mutational status of Ras proteins are currently in clinical trials for the treatment of Ras G12C specific cancers (clinical trial identifier: NCT03785249 and NCT03600883). As direct targeting strategies have been largely ineffective, new approaches to target Ras in cancers focus on using indirect strategies including inhibiting Ras association with effector proteins and inhibiting the ability of Ras proteins to associate with the cellular membrane *(83)*. Drugs that target post-translational modifications are gaining much interest as novel anti-cancer therapeutics. Histone deacetylase inhibitors (HDACi) have demonstrated success in the treatment of many non-solid tumors *(96),(110)–(112)*. However, as the class I HDACi, Entinostat and other pan-HDAC inhibitors have been primarily studied in the context of hematologic (blood) cancers *(142)*, it is unclear why HDACi have not proven to be clinically viable monotherapies in Ras-driven solid tumors *(106),(115)*.

The class I HDACi Entinostat is known to disrupt cell cycle progression through the induction of $p21^{WAF1/CIP1}$ transcriptional activation *(143)*. $p21^{WAF1/CIP1}$ binds and inhibits the activity of cyclin-dependent kinase complexes responsible for leading cells through cell cycle, a process that is often dysregulated in cancers *(144)*. While the overexpression of HDACs has been linked to increased cancer cell proliferation in a $p21^{WAF1/CIP1}$ dependent manner *(145)*, HDAC overexpression is not linked to a poor prognosis in all cancer types *(146)*. This is not the case for the Ras-driven colorectal cancer. Ras proteins are mutated in ~50% of colorectal cancers *(5)*. High levels of HDAC2 expression have been identified in colorectal cancers *(96),(119)–(122)* and HDAC2 specifically has been linked with poor patient survival *(121)*. As HDAC2 is a target of the class I HDACi Entinostat, it is reasonable that Entinostat may present a novel

therapeutic strategy in Ras-driven CRC. Surprisingly, we were able to determine that Ras is a direct target of Entinostat treatment. In CRC cells Entinostat caused Ras acetylation and fostered protein hyper-activation and preferential signaling through the Ras/MAPK mediated pathway.

We were able to discover that Ras proteins are acetylated in colorectal cancer (CRC) cells at a novel location, K5 due to treatment with the class I HDACi, Entinostat (**Figure 2.2**). This data represents a novel finding that Ras is acetylated at a never-before described location, K5, due to HDACi treatment. Using a genetic code expansion technique to generate acetylated Ras proteins, we were able to determine that acetylation does not severely impact the innate functions of Ras proteins. The ability of Ras proteins to bind and cycle nucleotides intrinsically or in the presence of modulatory proteins was not significantly altered due to acetylation (**Figure 2.6**). This is not surprising as K5 is not noted to play any role in binding or coordinating nucleotides, nor is it noted to interact with the Ras modulatory proteins, GEFs and GAPs. However, in Raf RBD pulldown assays using colorectal cancer (CRC) cells, HDACi treatment led to an increase in the GTP-bound population of cells (**Figure 2.3**). Consistent with this, HDACi treatment in wild type and G12V oncogenic CRC cells caused increased MAPK signaling (**Figure 2.4**), while no changes in PI3K signaling were observed. This was supported by our findings of increased binding affinity of acetylated proteins to the Raf RBDs most striking in the case of oncogenic G12V, where complete restoration to wild-type affinity was observed (**Figure 2.8**). Mutation nor acetylation resulted in alterations in binding affinity to the PI3Kα RBD (**Figure 2.8**).

Computational molecular dynamic simulations provided further confirmation of our biochemical and cellular findings. The Raf RBD interacts with Ras primarily through SWI *(16)*, and as such it is not immediately clear how acetylation at K5 could alter Raf binding. Most importantly, the interface between Ras and Raf is highly electrostatic in nature and mutations in

critical binding residues have been demonstrated to significantly alter or even ablate binding of Ras to the Raf RBD *(43),(51)*. Upon acetylation the acetyl-oxygen of the K5 sidechain forms a novel contact with Arg67 of the Raf RBD (**Figure 2.14**). Concurrent with this we also identified a complete rearrangement of the critical binding interface between Ras and the Raf RBD (**Figure 2.15**) and a further enhancement of a strongly interconnected electrostatic network between Ras proteins and the Raf RBD in response to acetylation (**Figure 2.15**). A dampening of protein dynamics was also identified in acetylated proteins in complex with the Raf RBD, consistent with the formation of a very stable complex, most notably identified in the Ras *G12V-K5AcK*:Raf RBD model (**Figure 2.17**).

We present for the first time the direct regulation of Ras proteins by the class I HDACi Entinostat. Entinostat was granted 'Breakthrough Therapy' designation by the United States FDA in 2013 after promising clinical results were described in breast cancer *(147)*. Since then, several clinical trials have been initiated using Entinostat as a monotherapy or part of a combination therapy strategy in a host of solid and hematologic cancers (clinicaltrials.gov). Recent studies have demonstrated that combination strategies using MEKi+HDACi and MEKi+HDACi+PI3Ki have resulted in favorable synergistic drug activities and increased cellular death in Ras-driven pancreatic cancer cells and murine lung cancer xenograft models *(100)–(102)*. Therapeutic targeting of Ras-driven cancers is notoriously difficult in part because of the dramatic pathway cross-talk and paradoxical activation of Ras-specific signaling cascades observed upon drug treatment *(83)*. Our data may initially seem to contradict these findings as acetylation led to more robust Raf RBD binding and increased MAPK-specific signaling. However, it may be possible that HDACi serve to alleviate the extensive pathway crosstalk in Ras CRC, and thereby allow for more efficient MAPK therapeutic targeting. Increased MAPK

signaling is known to upregulate the transcription of key cell cycle regulatory proteins (CDK4/6, cyclin D) crucial in G1/S cell cycle transition *(148),(149)*. Specifically, activation of the Ras/Mek/Erk pathway has been demonstrated to induce cyclin D transcription *(148)*. The cyclin dependent kinase inhibitor, p21 disrupts CDK4/6-cyclin D complex formation, and can serve as a negative regulator of cell cycle progression *(148),(150)*. Given that Entinostat is known to induce cell cycle arrest through upregulation of p21 *(143)*, HDACi may present a method to mitigate oncogenic cancer cell proliferation. Further, the Ras/MAPK transcription factor myc has also been suggested to play a role in p21 regulation both upstream and downstream of the critical G1 cell cycle checkpoint *(148),(149)*, further linking the Ras/MAPK pathway to cell cycle control. Future work should focus on determining the underlying mechanism of Ras-specific cell cycle regulation by HDACi. Further, determining the underlying mechanism of therapeutic combinations with HDACi in regulating Ras-specific signaling and cell death will be crucial in understanding the clinical utility of HDACi as combination therapies in Ras-driven cancers.

Materials and Methods

Cell Culture

The CRC cell lines were maintained in the appropriate cell culture medium supplemented with serum and antibiotics as specified by the suppliers. In the case of the CaCO-2, DLD-1 and SW837 cell lines containing conditional gene expression systems, cells were additionally cultured 72 hrs prior to experiment and further maintained for the full duration of the experiment in the presence of doxycycline (2 μg/ml). HEK-ER cells were additionally cultured 48 hrs prior to the experiment and further maintained for the full duration of the experiment in the presence of 4-Hydrotamoxifen (20 nM). All the cell lines were authenticated by short tandem repeat (STR) analysis (CLC Cell Line Service GmbH) and routinely checked for mycoplasma.

Retroviral and Lentiviral Constructs

All CRC cell lines in which conditional expression of either RAS isoforms, BRAF or c-MYC was induced, were generated by initially infecting the cells with the lentiviral vector *pRRL-SFFV-rtTA3- IRES-EcoRec-PGK-Puro,* kindly gifted by Johannes Zuber (IMP, Vienna) in order to make the cells ecotropic and thereby allow transfection with the retrovirus produced by the ecotropic packaging cell line. The retroviral vectors in question are *pSIN-TRE3G-KRASG12V-IRES_BFP-PGK-Hygro, pSINTRE3G-KRASG12V-K5A-IRES_BFP-PGK-Hygro, pSIN-TRE3G-KRASG12V-K5R-IRES_BFP-PGK-Hygro, pSIN-TRE3G-KRASWT-IRES_BFP-PGK-Hygro, pSIN-TRE3G-KRAS-WT-K5A-IRES_BFP-PGK-Hygro, pSIN-TRE3G-KRAS-WT-K5R-IRES_BFP-PGK-Hygro, pSIN-TRE3G-NRASQ61K-IRES_BFP-PGKHygro, pSIN-TRE3G-NRASWT-IRES_BFP-PGK-Hygro, pSIN-TRE3G-MYCWT-IRES_BFP-PGKHygro, pSIN-TRE3G-MYCT58A-IRES_BFP-PGK-Hygro* and *pSIN-TRE3G-MYCT58A/S62A-IRES_BFPPGK-Hygro*.

The retroviral vectors *pSIN-TRE3G-KRASG12V-IRES_BFP-PGK-Hygro, pSIN-TRE3GNRASQ61K- IRES_BFP-PGK-Hygro* and *pSIN-TRE3G-NRASWT-IRES_BFP-PGK-Hygro* were kindly provided by K.K-N, B.G and N.K.

The cells already containing *pSIN-TRE3G-KRASG12V-IRES_BFP-PGK-Hygro* retroviral vector were in addition infected with the lentivirus *pCDH-ELK-GFP* for ELK-1 reporter expression.

To generate *pSIN-TRE3G-KRASWT-IRES_BFP-PGK-Hygro,* KRASWT cDNA sequence was PCR amplified from *pDONR221-KRASWT-KanR* vector kindly provided by Lange B. (MPI für Molekulare Genetik, Germany), restriction digested with NotI and XhoI and ligated into the

pSINTRE3G -IRES_BFP-PGK-Hygro vector backbone. The following primers were used: forward, 5'- TGGATCCGCGGCCGCATGACTGAATATAAACTTGTGGT-3' and reverse, 5'-GTTAACCTCGAGAGATCCGTCGACTCACATAATTACACACTTTGTCT-3'. Vector was sequenced to confirm its sequence accuracy.

To create *pSIN-TRE3G-MYCWT-IRES_BFP-PGK-Hygro, pSIN-TRE3G-MYCT58AIRES_BFP-PGK-Hygro* and *pSIN-TRE3G-MYCT58A/S62A-IRES_BFP-PGK-Hygro, MYCWT, MYCT58A* and *MYCT58A/S62A* cDNA was PCR-amplified from vectors kindly provided by Martin Eilers (University of Würzburg, Germany), namely *pBABE-MYCWT-Puro, pBABE-MYCT58A-Puro,* and *pBABEMYCT58A/S62A-Puro,* respectively. The resultant PCR products were restriction digested with NotI and XhoI, then ligated into the *pSIN-TRE3G -IRES_BFP-PGK-Hygro* vector backbone. The following primers were used to clone both *MYCWT, MYCT58A* and *MYCT58A/S62A*: forward, 5'-TAAGCAGCGGCCGCATGCCCCTCAACGTTAGCTTC-3' and reverse, 5'-TGCTTACTCGAGTTACGCACAAGAGTTCCGTAG-3'. All vectors were sequenced to confirm their sequence accuracy.

To generate the *pSIN-TRE3G-KRASG12V-K5A-IRES_BFP-PGK-Hygro* and *pSIN-TRE3GKRASG12V-K5R-IRES_BFP-PGK-Hygro, pSIN-TRE3G-KRAS-WT-K5A-IRES_BFP-PGK-Hygro, pSINTRE3G-KRAS-WT-K5R-IRES_BFP-PGK-Hygro* retroviral vectors, KRASG12V and KRASWT cDNA sequences were PCR-amplified to contain either K5A or K5R substitution mutations from the *pSINTRE3G-KRASG12V-IRES_BFP-PGK-Hygro* vector and the *pSIN-TRE3G-KRASWT-IRES_BFP-PGKHygro* vector respectively. The PCR product was restriction digested with NotI and XhoI, and subsequently ligated to the same *pSIN-TRE3G-IRES_BFP-PGK-Hygro* vector backbone. The

following primers were used to clone *KRASG12V-K5A* and *KRASWT-K5A*:
forward, 5'- TAAGCAGCGGCCGCATGACTGAATATGCACTTGTGGTAGTTGGAGCT-3', reverse, 5'-TGCTTACTCGAGAGATCCGTCGACTTACATAATTACACACTTTGTC-3', and to clone *KRASG12V-K5R* and *KRASWT-K5R*:
forward, 5'-TAAGCAGCGGCCGCATGACTGAATATAGACTTGTGGTAGTTGGAGCT-3', reverse, 5'- TGCTTACTCGAGAGATCCGTCGACTTACATAATTACACACTTTGTC-3'. All vectors were sequenced to confirm their sequence accuracy.

Inhibitors

All inhibitors used were dissolved in DMSO and further diluted to the indicated final concentration in cell culture medium at the time of treatment.

Cell Apoptosis Assay

Cells were plated and treated for a total of 72 hrs with the indicated agents. Cells were harvested for analysis by trypsinization and fixed in formaldehyde (2%) for 10 min at room temperature. Following a further incubation step on ice for 1min, the fixation solution was removed by centrifugation and cells were subsequently permeabilized in 90% ice-cold methanol and incubated again on ice for 30 min. Cells were thereafter washed by centrifugation with incubation buffer (PBS, 0.5% BSA) and probed with cleaved Caspase-3 Alexa Fluor® 647 conjugated antibody according to manufacturer's specification (Cell Signaling Tech., Cat# 9602). Following additional washing by centrifugation, $1x10^4$ cells per sample were analyzed with a BD AccuriTM C6 (BD Bioscience) Flow Cytometer.

Immunoblot Analysis

For fresh protein extraction, cells were washed twice with ice-cold PBS and subsequently lysed in MPER™ Mammalian Protein Extraction Reagent (ThermoFischer Scientific, Cat#

78501) supplemented with a protease and phosphatase inhibitor cocktail (Roche, Cat# 04693132001, 04906837001) for 30 min on ice. Lysates were cleared by centrifugation at 13,000 rpm for 15 min at 4°C, and protein concentrations were determined using Pierce™ BCA Protein Assay Kit (Thermo Scientific, Cat# 23225). Equal amounts of proteins were resolved on SDS-PAGE with appropriate acrylamide percentage and transferred onto nitrocellulose membranes (Amersham™, GE Healthcare Life Sciences). The membranes were blocked with 5% non-fat dry milk in TBS-T (25 mM Tris, 150 mM NaCl, 2 mM KCl, pH 7.4 containing 0.1% Tween-20) for 1 hr at room temperature and thereafter incubated overnight at 4°C with the indicated primary antibodies diluted in 5% non-fat dry milk with TBS-T. A washing step with TBS-T followed, and membranes were subsequently probed with secondary antibodies conjugated to either horseradish peroxidase (anti-rabbit/-mouse HRP-linked IgG antibody) (Cell Signaling Tech., Cat# 7074, 7076) or to a fluorophore (IRDye® 680RD anti-rabbit/- mouse IgG antibody) (Li-Cor Bioscience, Cat# 925-68071, 925-68071) for 1 hr at room temperature. The membranes were washed again as described above, and chemiluminescence was detected using GE Healthcare ECL (Ammersham ECL) western blotting detection reagents and imaged by Protein Simple FluorChem System, while fluorescence was detected using the Li-Cor Odyssey Infrared System.

Cell Viability Assay

Cells were seeded at densities between 1500-3000 cells/well (depending on pre-determined growth properties) in a 96-well plate and allowed to adhere overnight. The cells were subsequently treated with the indicated drugs for a total of 72 hrs before XTT cell proliferation assay (Roche) was performed. The absorbance read-out (optical density, OD) was measured at a wavelength of 450- 500nm with a reference wavelength at 650nm using an ELISA plate reader (Synergy|2 Microplate Reader, BioTek). Negative control was subtracted from the OD values

and cell viability rate (%) was calculated according to the following formula: (ODTREATED/ODCONTROL) ´ 100. Untreated cells served as the indicator of 100% cell viability. Drug-response curves of single compounds and combinations were generated by Graphpad Prism 6 software (GraphPad Software, inc., La Jolla, CA). The IC_{50} values were calculated by concentration response curve non-linear fitting (log(inhibitor) vs response).

LC/MS/MS Analysis

Proteins eluted from the IP beads were digested using an automated sample-preparation workflow (Axel-Semrau Proteome Digest-O-r 140). Briefly, the samples were reduced by 1mM tris (2- carboxyethyl) phosphine (TCEP, Merck) and free sulfhydryl groups carbamidomethylated using 5.5 mM chloroacetamide (Sigma-Aldrich). Proteins were digested with 0.5 µg sequencing grade endopeptidase LysC (Wako) overnight at room temperature. The reaction was terminated by adding trifluoroacetic acid (TFA, Merck) to a final concentration of 1% resulting in a final pH of 2. The peptides were purified using C18 stage-tips (Empore SPE disks, 3 M) 141 and measured on a QExactive plus mass spectrometer (Thermo-Fisher, Germany) coupled to a nano-LC system (easy-nLC, Thermo-Fisher, Germany). 2 µg of the peptide sample were injected and separated using a 3h gradient (4 to 76 % acetonitrile and 0.1 % formic acid in water) at a flow rate of 0.25 µl/min on an in-house prepared nano-LC column (0.075 mm x 250 mm, 3 µm Reprosil C18, Dr. Maisch GmbH). The separated peptides were ionized on a proxeon ion source and directly sprayed into the mass spectrometer (Q-Exactive Plus, Thermo Scientific). The MS1 acquisition was performed at a resolution of 70,000 in the scan range from 300 to 1700 m/z. The top 10 intense masses were selected for MS2 analysis. MS2 scans were carried out at a resolution of 15,500 with the isolation window of 2.0 m/z. Dynamic exclusion was set to 30 s and the normalized collision energy to 26 eV. For the

automatic interpretation of the recorded spectral data, the MaxQuant software package version 1.6.016 was used 142. Carbamidomethylation was set as a fixed modification while oxidized methionine and acetylated lysine were set as variable modifications. An FDR of 1% was applied to peptide and protein level, and an Andromeda-based search was performed using a human Uniprot database (uniprot.HUMAN.2016-08.fasta, downloaded August 2016).

Ras-GTP Pull-Down Assay

The Ras-GTP bound level was studied on the basis of Ras-Ras interaction using the RBD agarose beads as per manufacturer's specifications (Millipore Sigma, Cat# 17-218). Cells were washed twice with ice-cold PBS and subsequently lysed in MLB (25 mM HEPES, pH 7.5, 150 nM NaCl, 1% IGEPAL CA-630, 10 mM MgCL2, 1 mM EDTA) for 30 min on ice. The protein lysates were additionally sonicated for 10 sec and debris was removed by centrifugation at 13,000 rpm for 15 min at 4°C. The cleared lysates were incubated with RBD agarose beads for 45min and thereafter washed twice with MLB by centrifugation prior to the following immunoblotting analysis. Ras pulled down by RBD agarose beads indicates the presence of active GTP-bound Ras capable of interacting with Raf1.

Immunoprecipitation (IP)

Cells were washed twice with ice-cold PBS and fresh protein extraction was prepared by lysis of cells in M-PER™ Mammalian Protein Extraction Reagent supplemented with a protease and phosphatase inhibitor cocktail for 30 min on ice. Debris were removed by centrifugation at 13,000 rpm for 15 min at 4°C and protein concentrations were determined using Pierce™ BCA Protein Assay Kit. Lysates were pre-cleared with Dynabeads® Protein A/G (Invitrogen, Cat# 10002D, 10004D) for 1 hr at 4°C and subsequently incubated with the appropriate isotype control or the indicate antibody overnight at 4°C under gentle agitation. The immune complexes

were then precipitated with the Dynabeads® Protein A/G for 4hrs at 4°C under gentle agitation, washed with M-PER™ lysis buffer and resuspended in sample loading buffer. Following SDS-PAGE separation, proteins were transferred onto nitrocellulose membranes for immunoblot analysis.

Protein Purification

Acetylated KRAS-4B protein was generated and expressed using a duel vector system. The pUltra vector containing the coding regions for *Methanosarcina mazei* tRNACUA (MmtRNACUA) and the acetyl-lysyl-tRNA synthetase (AcKRS-3) *(132)* was co-expressed with a pET52 vector harboring a Nterminal 6-histidine tagged KRAS-4B (C118S, 1-169) with the amber stop codon at the desired site of acetyl-lysine incorporation and a TEV protease cleavage site. As described previously, acetyl-lysine incorporation is directed by the acetyl-lysyl synthetase and the cognate amber suppressor *M. mazei* tRNACUA in response to the amber codon in KRAS *(133),(151)*. Briefly, *E. coli* BL21-Gold (DE3) cells (Novagen) were transformed with both pUltra and pET52 vectors harboring the MmtRNACUA, AcKRS-3 and KRAS-4B (C118S) with an amber codon at position 5, respectively. Cells were grown at 37°C in Luria-Bertani (LB) medium supplemented with ampicillin and spectinomycin. At A_{600} of ~0.5 the culture media was supplemented with 10 mM N-ε-acetyl-lysine (Sigma, Cat# A4021) and 20 mM nicotinamide (Acros Organics, CAS 98-92-0) to inhibit the *E. coli* deacetylase, CobB *(152),(153)*. The temperature was reduced to 18°C, and RAS expression was induced after 30 min upon addition of 500 μM Isopropyl β-D-1-thiogalactopyranoside (IPTG). The culture was allowed to grow for 16 hrs at 18°C. The cells were harvested and pelleted at 4,000 rpm, resuspended in a lysis buffer containing 20 mM HEPES, 300 mM NaCl, 1 mM $MgCl_2$, and 20 mM imidazole (pH 7.75) and sonicated. The cell lysate was centrifuged at 15,000 rpm, and the

supernatant isolated. Acetylated KRAS-4B protein was purified using nickel-nitrilotriacetic acid-agarose (Ni-NTA agarose) affinity chromatography (Qiagen). Cells were washed with a buffer containing 20 mM HEPES, 500 mM NaCl, 5 mM $MgCl_2$, 40 mM imidazole, 5% glycerol, pH 7.75. Proteins were eluted in the wash buffer with lower salt and higher imidazole, 50 mM NaCl and 250 mM imidazole, respectively. The histidine tag was cleaved during overnight dialysis into 10 mM HEPES, 50 mM NaCl, 5 mM MgCl2, 10 μM GDP (pH 7.75) using TEV protease. Acetylated K5 KRAS-4B was further purified by size exclusion chromatography using a Sephadex G-75 column. Acetylated protein was then submitted for mass spectrometric analysis to ensure acetyl-lysine incorporation >95%. KRAS-4B (C118S) wild type protein was expressed and purified as noted above. KRas *G12V* and the amber codon containing *G12V* constructs were generated using standard mutagenesis strategies. They were grown and purified as described above.

The isolated RBD of human BRaf (residues 149-232) was subcloned into the pET28a bacterial expression vector encoding a N-terminal 6-histidine tag and TEV cleavage site *(28).* Briefly, BRaf RBD was expressed in BL21 (DE3) cells and were grown at 37°C in Luria-Bertani (LB) medium. At A_{600} of ~0.5 the temperature was reduced to 18°C, and BRaf RBD expression was induced after 30 min upon addition of 500 μM Isopropyl β-D-1-thiogalactopyranoside (IPTG). The culture was allowed to grow for 16 hrs at 18°C. The cells were harvested and pelleted at 4,000 x g, resuspended in a lysis buffer containing 20 mM HEPES, 300 mM NaCl, 1 mM MgCl2, 20 mM imidazole, and 5% glycerol (pH 7.75) and sonicated. The cell lysate was centrifuged at 15,000 x g, and the supernatant was isolated and purified using nickel-nitrilotriacetic acid-agarose affinity (Ni-NTA agarose) chromatography (Qiagen). Briefly, the supernatant was added to the column and washed with buffer containing higher salt (500 mM

NaCl and 40 mM imidazole) and then again with the lysis buffer. The protein was eluted using a buffer containing 15 mM HEPES, 50 mM NaCl, 5 mM MgCl2, 250 mM imidazole, pH 7.75. The histidine tag was cleaved during overnight dialysis into 10 mM HEPES, 50 mM NaCl and 5 mM MgCl2, pH 7.75 using TEV protease. BRaf RBD was further purified by size exclusion chromatography using a Sephadex G-75 column. Greater than 95% purity was achieved using size exclusion chromatography and verified using SDS-PAGE analysis.

The isolated RBD of human CRaf (residues 54-131) was subcloned into a pQlinkH bacterial expression vector, harboring a N-terminal 6-histidine tag with TEV protease cleavage site and purified as described previously *(64)*. CRaf RBD was expressed in BL21 (DE3) cells and were grown at 37°C in Luria-Bertani (LB) medium. At A_{600} of ~0.5 the temperature was reduced to 18°C, and CRaf RBD expression was induced after 30 minutes upon addition of 500 μM Isopropyl β-D-1-thiogalactopyranoside (IPTG). The culture was allowed to grow for 16hrs at 18°C. CRaf RBD was purified as described previously *(64)*. CRaf RBD was further purified by size exclusion chromatography and > 95% purity verified using SDS-PAGE analysis.

The catalytic domain of SOS^{cat} (residues 566 -1049) was purified as previously described *(131)*. Briefly, SOS^{cat} was transformed into BL21 (DE3) RIPL *E. coli* cells and was grown at 37 °C in Luria-Bertani (LB) medium until an A_{600} of ~0.5. The temperature was then lowered to 18 °C and the cells were induced with 0.5 mM isopropyl-β-D-1-thiogalactopyranoside (IPTG). Cells were allowed to continue expression for 16 hours. Cells were pelleted by centrifugation at 4000 x g and resuspended in wash buffer (25 mM Tris-Cl, 500 mM NaCl, 20 mM imidazole (pH 7.5) with the protease inhibitor phenylmethanesulfonyl fluoride (ACROS Organics)). Cells were sonicated and then centrifuged at 14,000 x g for 30 minutes. The supernatant was isolated and purified using standard Qiagen nickel affinity purification procedures. Proteins were washed

with 10 column volumes of wash buffer and eluted in wash buffer with 500 mM imidazole. Tobacco Etch Virus was used to cleave the N-terminal histidine tag on SOS^{cat} through overnight dialysis. SOS^{cat} protein was further purified by size exclusion chromatography using a Sephadex G-100 column. Protein purity of >95% was obtained and verified by SDS-PAGE analysis

The catalytic domain of p120GAP (GAP-334, residues 764-981) *(13)* in pQlinkH was expressed and purified as described for Ras proteins.

The Ras binding domain (RBD) of human PI3Kα (residues 157-297) was synthesized and cloned by Twist Bioscience into the pCDB24 bacterial expression vector, which encodes for an N-terminal 10-histidine tag and a SUMO cleavage site. The PI3K RBD was expressed in BL21 (DE3) RIPL cells and was grown at 37°C in Luria-Bertani (LB) medium. The cells were grown to an A_{600} of ~ 0.5, the temperature was then reduced to 18°C for 30 minutes and the cells were induced with 500 μM Isopropyl β-D-1-thiogalactopyranoside (IPTG). Following growth for 16 hours at 18°C, the cells were centrifuged at 4,000 x g, the pellet was resuspended in lysis buffer containing 50 mM HEPES, 500 mM NaCl, 20 mM imidazole, and 10% glycerol (pH 8.0) and then sonicated. The cell lysate was subsequently centrifuged at 15,000 x g for 25 minutes. The supernatant was purified using nickel-nitrotriacetic acid-agarose affinity (Ni-NTA agarose) chromatography. Briefly, the supernatant was applied to the Ni-NTA agarose column, washed with 5 column volumes (CV) lysis buffer, 5 CV buffer containing 1 M NaCl, 50 mM HEPES, 30 mM imidazole and 10% glycerol (pH 8.0), again with 5 CV lysis buffer, and lastly with 2 CV buffer containing 50 mM HEPES, 500 mM NaCl, 100 mM imidazole and 10% glycerol (pH 8.0). The protein was eluted with buffer containing 50 mM HEPES, 500 mM NaCl, 500 mM imdiazole, and 10% glycerol (pH 8.0). The 10-histidine tag was cleaved with ULP1 protease during overnight dialysis into a buffer containing 50 mM HEPES, 500 mM NaCl, and 5 mM β-

mercaptoethanol (BME) at 4°C. The PI3Kα RBD was further purified by size exclusion chromatography (SEC) using a Sephadex G-100 column. More than 95% purity was achieved using SEC and verified using SDS-PAGE analysis.

Mass Spectrometry of Unmodified KRas and KRas K5AcK

The ZipChip Interface (908 Devices) was coupled to an Orbitrap Fusion Lumos high resolution accurate mass tandem mass spectrometer (Thermo). A ZipChip HR microfluidic chip was used for the separations. Data was acquired at a resolution of 120K with an AGC target of 4e5 ions or 50 ms max injection time, a scan range set at 200-2000, and a cycle time of 3 sec. The total run time was 5 min. Spectra were visualized using Freestyle 1.3 (Thermo Scientific) and deconvoluted using BioPharma Finder 3.0 (Thermo Scientific). Wild-type Ras, acetylated wild-type Ras and acetylated G12V Ras were identified as >95% purity in samples analyzed.

Nucleotide exchange assays

The rate of nucleotide dissociation was measured by using a well-established fluorescence-based assay *(134),(135)*. Exchange assays were completed in both GDP and GMPPCP-bound forms. Proteins were loaded with Mant-labeled nucleotide using previously described methods *(154)* and loading was verified via HPLC. Nucleotide loaded Ras proteins were added to 1 ml of assay buffer (20 mM HEPES, 50 mM NaCl, 5 mM $MgCl_2$, pH 7.4) to a final concentration of 1 μM and nucleotide exchange was initiated by the addition of 1 mM unlabeled nucleotide. The rate of Mant-labeled nucleotide dissociation was measured as a change in fluorescence intensity over time (excitation, 365 nm; emission, 435 nm) (LS50B PerkinElmer Life Sciences luminescence spectrometer). Fluorescence data were fit using GraphPad Prism 5 software to a one-phase exponential decay curve. The minimal catalytic

domain of the Ras GEF, SOS^{cat} *(131)* was used to determine GEF-mediated nucleotide dissociation rates. For GEF-mediated dissociation, a 1:1 molar ratio of Ras to GEF was used.

Hydrolysis Assay

Single turnover GTP hydrolysis assays were performed as previously described *(154)*. Intrinsic and GAP-mediated GTP hydrolysis rates were determined by monitoring the production of phosphate upon GTP hydrolysis using the phosphate binding protein Flippi 5U *(155)*. Flippi 5U expression and purification have been previously reported *(155)*. Briefly, all assays used 5 μM FlipPi with 5 μM GTP-loaded Ras. GTP loading was performed as previously described *(154)* with desalting and removal of excess GTP completed using Zeba spin columns (ThermoFisher). Ras hydrolysis buffer consisted of 20 mM HEPES, 50 mM NaCl, 0.1 mM EDTA, 100 μM DTPA (diethylenetriaminepentaacetic acid), 0.5 mM inosine, pH 7.4. All buffers were made phosphate free using a 'phosphate mop' *(156)*. The rate of GTP hydrolysis was measured using a SpectraMax 5M fluorimeter by taking the ratio of the 535- and 485- nm emission wavelengths (excitation: 435 nm; 25˚C) of kinetic runs. Hydrolysis was stimulated by the addition of 1 mM Mg. GAP-mediated hydrolysis assays included the addition of the minimal catalytic domain of p120GAP (Scheffzek et al., 1997) at a 1:200 molar ratio. Using GraphPad Prism 5, the data was fit to a one phase exponential association curve and normalized to a phosphate standard curve. Data is reported as percentage of GTP hydrolyzed and the GTP hydrolysis rate.

Isothermal Titration Calorimetry (ITC)

The binding affinities of KRas-4B (C118S) wild type, KRas-4B (C118S) K5-acetylated, KRas-4B (C118S) *G12V*, and KRas-4B (C118S) K5-acetylated *G12V* to effector proteins were determined using a MicroCal PEAQ-ITC (Malvern Paranalytical). All ITC experiments were

performed in buffer containing 20 mM HEPES, 50 mM NaCl, 5 mM $MgCl_2$, 1 mM 2-mercaptoethanol (B-ME). Ras proteins at either 150 μM or 200 μM were titrated into effector proteins (BRaf RBD, CRaf RBD, PLCε, Ral GDS and PI3K-α). Starting effector to Ras molar ratios were 1:10 or 1:15. Heat of the binding event was measured at 25°C for 19 2-uL injections with a stirring speed of 650 rpm and an initial delay of 120 seconds. Injections were spaced at 180 seconds. Heats released during the last few injections (when saturation had occurred) were averaged and subtracted from all the heat peaks (control subtraction). Data were analyzed using a nonlinear least square algorithm and fit to a one-site model provided in the MicroCal PEAQ-ITC software.

Molecular Dynamic Simulations

United-atom Molecular Dynamics (MD) simulations of Mg^{+2}-GDP bound Ras proteins and Mg^{+2}-GTP bound Ras *WT*, Ras *G12V* and K5 acetylated (K5AcK) Ras *G12V* alone (200 ns) or in complex with the Raf RBD (500 ns). The Ras:Raf RBD complex was constructed using two high resolution X-ray structures from the protein data bank (PDB 4G0N *(55)* and 2C5L *(157)*. Missing fragments of the 4G0N structures were constructed using corresponding fragments of the 2C5L structure, and mutations were corrected to wild type protein. Amino acid substitutions of the residues G12 using PyMol 2.1 (Schrödinger, LLC). Acetylation at position K5 was generated using Vienna-PTM 2.0 server *(158)–(160)*. The structure of GTP was optimized using Maestro LigPrep tool (Schrödinger, LLC). Vienna-PTM and the Automated Topology Builder v 3.0 (ATP) were used to generate system topology and parameter files for the GROMOS 54a7 force field *(158)–(162)*. Each protein or complex (Ras *WT*:Raf, Ras *WT-K5AcK*:Raf, Ras *G12V*:Raf and Ras *G12V-K5AcK*:Raf) was solvated using TIP3P water model with and sodium ions were added to neutralize the system. All MD simulations were performed using GROMACS

2018 package with the GROMOS 54a7 force field *(163),(164)* at a constant pressure and temperature of 1 atm and 298 K for 200 ns for single proteins and 500 ns for protein complexes. Trajectories were subjected to clustering analysis using Gromacs *(137),* and the centroids of the most populated, lowest energy clusters for each was examined using PyMol 2.1 (Schrödinger, LLC).

Particle mesh Ewald (PME) *(165),(166)* was used for long-range electrostatic interactions, 10-Å cutoff were used for non-bonded interactions. Based on the analysis of the root-mean-square deviation (RMSD) of backbone Cα positions first 10 ns of the simulations were omitted for further analysis as to get simulations to reach equilibrium. To select representative models of the complex, clustering analysis was performed using a GROMACS clustering algorithm *(137)* on the simulation trajectories. The distance cut-off for clustering was chosen to be 1.5 Å, to correlate with distances from high-resolution of X-ray structure. The structures of the centroids representing the most populated clusters for each protein-protein complex were examined using PyMol 2.1 (Schrödinger, LLC).

To study relative difference in binding between different complexes we used g_mmpbsa tool for the GROMACS *(167),(168)*. Molecular mechanics Poisson–Boltzmann surface area (MM-PBSA) calculations are often used to estimate free energy of interaction between biological molecules as well as to provide energy-based scoring in computational drug discovery. Based on MD trajectory MM-PBSA calculations allow to estimate the following contributions to the binding energy: standard bonded interactions (bond, angle and dihedral), van der Waals and electrostatic interactions, polar and non-polar contributions to the energy of solvation. The polar contribution to the solvation energy is computed by solving the Poisson–Boltzmann equation, whereas the non-polar term is calculated using linear approximation to the solvent accessible

surface area (SASA). As some recent studies suggest *(169)* that the method not always provide an reliable value on absolute binding affinities we will use it only to estimate a relative difference in the Ras:Raf binning affinities depending on the mutations.

Chapter 3. The 'Ras-opathy' mutant KRas K5N potentiates protein activation through destabilization of the GDP-bound state

Introduction

Ras proteins are small GTPases that are critical for normal cellular function. Three Ras genes encode for four Ras proteins (H-, N- KRas-4A and KRas-4B). They utilize a molecular switching mechanism to cycle between active, GTP-bound and inactive, GDP-bound states. This process is further regulated by interactions with modulatory proteins (GEFs, guanine nucleotide exchange factors and GAPs, GTPase activating proteins) *(41).* In their active forms, Ras proteins bind to downstream effector proteins, mediating pathways that regulate cellular growth, differentiation and apoptosis *(17),(33).* Oncogenic, activated Ras proteins are mutated in approximately 30% of all human cancers, and they are known to be oncogenic drivers of some of the most aggressive cancers, such as lung, pancreatic and colorectal cancers *(5).*

Mutant Ras proteins have also been identified in a subset of genetic diseases. 'Ras-opathies' are rare genetic disorders that are known to be driven by the dysregulation of the Ras/Mitogen-activated protein kinase (MAPK) pathway *(128),(170),(171).* These diseases include Noonan's syndrome (NS), cardio-facio cutaneous syndrome (CFC) and Costello syndrome (CS). The clinical features of CS, NS and CFC overlap greatly *(130),(171).* Interestingly, HRas has been reported to be mutated in high percentages (82.5-92%) in CS patients *(130),* whereas KRas germline mutations are identified in NS *(128).* This suggests that while Ras-opathies may all be characterized by overall defects in Ras/MAPK signaling, their mechanisms may be unique. Interestingly, the germline KRas mutations identified in NS are at

residues unique from those implicated as driving forces in human cancer *(128)*, and are located within both the highly conserved effector domain and the sequence divergent allosteric lobe *(46),(128),(172)–(177)*. Genetic analysis revealed that the major mutations identified in NS were those of KRas, SOS1 and PTPN11 *(130),(178)*. These genes all play roles in fine-tuning the overall activation status of Ras in cells. PTPN11 is the gene responsible for the production of SHP-2 protein, which plays an essential role in the recruitment of the SOS protein (SOS1 gene) to the cellular membrane where it serves to activate Ras proteins *(172),(179)*. While data quantifying actual disease prevalence is not available, NS is estimated to occur between 1 in 1,000-2,500 births each year *(178)*. As NS is a genetic disorder, treatment options focus on managing symptomatology. However, recent Ras-related drug approaches are being examined *(180)*.

Ras proteins have distinct conformations and dynamics as determined by their nucleotide-bound state *(41)*. In NS patients, several KRas germline mutations have been identified at amino acid positions K5, V14, Q22, P34, I36, T58, G60, V152, D153 and F156 *(46),(128),(172)–(177)*. However, the functional role of these mutations in regulating Ras activity is not well understood. Residues that coordinate the guanine nucleotides or that are located in the dynamic 'switch regions' are highly conserved among the Ras isoforms and include V14, Q22, P34, I36, T58, G60 *(4)*. Several of these residues also form contacts with the Ras modulatory proteins, GEFs *(16),(53),(128),(131)*. Further, these mutations are located in the effector lobe of Ras, which is 100% conserved between the Ras isoforms *(5)*, suggesting that these residues play important roles in Ras structure or activity. Although located within the allosteric lobe of Ras, V152, D153 are noted to further stabilize the guanine nucleotide binding pocket primarily through hydrophobic interactions *(172)*. Since these mutations are located in

regions of Ras proteins that play crucial roles in binding guanine nucleotides and are at the interface of interactions with GAPs, GEFs or effector proteins *(16),(53),* it is not surprising that mutations at these residues would alter Ras activity.

K5N is the one mutation that does not seem to have a clear role in mediating any of these processes. K5 is not noted to play a role in effector or modulatory protein recognition or binding, nor is it reported that K5 plays any role in nucleotide binding or exchange. It is therefore probable that the K5N mutation displays a unique mechanism to potentiate enhanced protein activation and MAPK signaling. Previous biochemical and cellular analysis of the K5N mutation revealed a modest increase in the GTP-bound population of Ras and a dramatically lowered GTP association rate as compared to wild type protein *(128).* However, a comprehensive mechanism of Ras regulation through K5N mutation was not able to be determined. As noted previously, K5 may play an indirect role in stabilizing nucleotide binding in the GDP-bound form of the protein *(128)*. It is suggested that mutation to asparagine would disrupt these contacts, leading to destabilization of GDP-bound Ras, which may serve to activate the protein *(128)*. Further, K5R/E/N mutations are found in pancreatic, stomach, lung, and colon cancers and leukemia *(181)–(185),* but the mechanism by which they elicit an oncogenic role is unclear. In decades of research, Ras has remained an elusive target for therapeutic generation and is commonly considered undruggable *(24).* Here we report the results of biochemical, structural and computational analysis confirming that KRas K5N mutation destabilizes the inactive form of Ras proteins, while not significantly impacting the active form. This may lead to a mechanism in cells where Ras proteins are more likely to be GTP-bound and activated, leading to the increased cellular signaling characteristic of ‘Ras-opathies’. We provide further discussion as to how these mutations could represent novel mechanisms of Ras activation in genetic disorders and cancers.

Results

KRas K5N mutation disrupts overall protein stability and alters nucleotide association and exchange in primarily the GDP-bound form

Ras proteins are GTPases (guanosine triphosphatases), meaning that they cycle the guanine nucleotides, GDP and GTP for their activity. In their inactive form, Ras proteins are bound to GDP, while their active form is characterized by a distinct conformational change upon GTP binding *(4)*. Germline mutations have been identified in KRas at lysine (K) 5 in the Ras-driven genetic disorder, Noonan syndrome (NS). These diseases are largely characterized by dysregulated Ras/MAPK downstream signaling and cellular hyper-activation *(46),(128),(172)–(177)*. Lysine 5 is highly conserved in the Ras superfamily *(5)*, but the role of K5 mutation in regulating Ras activity is currently unknown. As described by Gremer et al, the lysine 5 sidechain forms interactions with switch II, a highly dynamic region of the Ras protein, primarily in the GDP-bound form. It is suggested that the K5 sidechain directly interacts with T74 and packs against Y71 *(128)*. These sidechain interactions are lost in the GTP-bound form of the protein. It is therefore reasonable that K5 mutations could activate Ras proteins in an indirect manner, stemming from a destabilization of the inactive, GDP-bound form of the protein. In order to investigate the role of K5 mutations in regulating Ras activity in NS, we mutated K5 to asparagine and first determined if mutation alone altered protein stability. As shown in **Figure 3.1** mutation to asparagine at lysine 5 caused a decrease in thermal stability of KRas in both GDP-bound and GTP-bound forms. A drop in the thermal melting temperature of approximately 5 °C is observed due to K5N mutation in both GDP- and GMPPCP-bound protein (**Figure 3.1 and Table 3.1**) compared to KRas WT protein (60.64 ± 0.18 °C for GDP-bound KRas and 49.26

± 0.12 °C for GMPPCP-bound KRas protein). This data demonstrates that lysine 5 likely plays an essential role in contributing protein stability in both active and inactive forms of the protein.

Lysine 5 has been implicated in contributing to the structural regulation of the critical switch II region in GDP-bound Ras. Ras proteins display distinct conformations in the highly dynamic switch I (SWI) and switch II (SWII) regions upon nucleotide binding *(41)*. Disruption of the ability of Ras proteins to adopt these distinct conformations due to mutation could be one possible mechanism of Ras activation. In order to investigate the ability of the K5N mutation to regulate nucleotide-dependent Ras activity, we can first investigate the ability of Ras proteins to load and exchange GDP and GMPPCP. K5N mutation in GDP- nor GMPPCP-bound Ras protein was able to significantly alter intrinsic rates of nucleotide exchange (WT- GDP: 2.39±0.42 x 10^{-4}, s^{-1}, WT GMPPCP: 10.23±0.62 x 10^{-4}, s^{-1} vs. K5N-GDP: 3.92±0.32 x 10^{-4}, s^{-1}, K5N-GMPPCP: 11.40±0.51 x 10^{-4}, s^{-1}) (**Figure 3.2 and Table 3.2**). However, an impaired SOS-mediated nucleotide exchange rate was identified in the GDP-bound K5N mutant. Here, we observe approximately a 2-fold increase in the rate of GDP-bound nucleotide exchange in the presence of the catalytic domain of the GEF, SOS^{cat} (WT- GDP: 37.3±0.63 x 10^{-4}, s^{-1}vs. K5N-GDP: 59.2±0.88 x 10^{-4}, s^{-1}). This trend was not observed in GMPPCP-bound Ras proteins (**Figure 3.2 and Table 3.2**). SOS is known to form several direct contacts with the Ras SWII region. At the core of these interactions is a hydrophobic network in Ras proteins containing Y71. The proper positioning of the hydrophobic core leads to the coordination of nearly every SWII sidechain by SOS upon complex formation *(54)*. As K5 is noted to pack against Y71 in the GDP-bound form *(128)*, mutation could lead to alteration of Y71 and further disruption of the critical hydrophobic network in Ras that is responsible for placing SWII in the proper conformation for SOS binding. K5 is not noted to make contacts with Y71 in the active form of the protein, consistent with the

lack of observed differences in SOS-mediated nucleotide exchange in WT and K5N Ras proteins (**Figure 3.2 and Table 3.2**). The highly dynamic switch regions in Ras proteins are also recognized by GAP proteins, which facilitate the hydrolysis of GTP to GDP, thereby inactivating Ras proteins *(136)*. Intrinsic nor GAP-mediated defects in hydrolysis rates were able to be identified in KRas K5N proteins *(128)*. We further investigated the ability of Ras proteins to associate or load GDP and GMPPCP. Results from this analysis demonstrated that mutation to asparagine resulted in an increased rate of GDP association. An approximate 2-fold increase in GDP association was identified due to K5N mutation (WT- GDP: $8.17 \pm 0.09 \times 10^{-4}$, s^{-1} vs. K5N-GDP: $18.9 \pm 0.31 \times 10^{-4}$, s^{-1}) (**Figure 3.3 and Table 3.3**). Taken together, the faster off-rate in SOS-mediated GDP exchange and faster on-rate for GDP in the asparagine mutant suggests a possible instability in the GDP-bound form of the protein. This could be due to a structural defect as is described by loss and re-orientation of SWII residues upon K5 mutation. As GTP is in significant excess in the cellular milieu *(186)*, K5N mutation may potentiate GTP loading and protein activation.

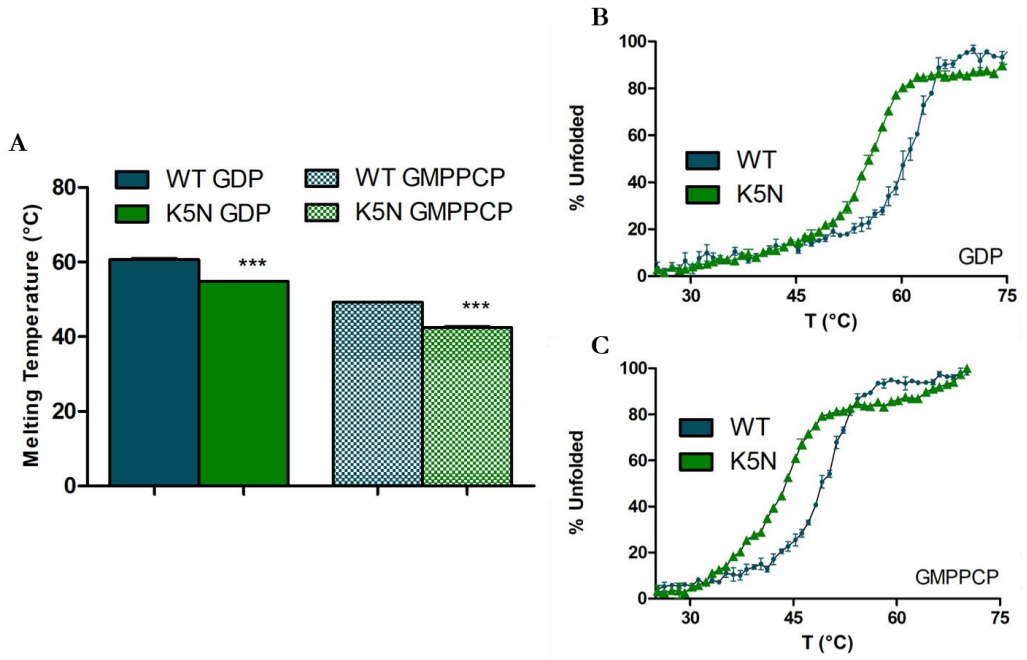

Figure 3.1. KRas *K5N* mutant is less thermostable in both active and inactive forms.

A. Circular Dichroism measurements were used to determine thermal melting temperatures of KRas *WT* and KRas *K5N* proteins in GDP- and GMPPCP-bound forms. Protein unfolding was measured as a function of increasing temperature (20–95°C, 2°C per minute) at 222 nm of 15 μM Ras protein. Data was fit to a Boltzmann's sigmoidal equation in GraphPad Prism 5, where the V50 is indicative of the thermal melting temperature. Results are reported as the mean ± S.E. (*n* = 3). One-way ANOVA statistical analysis was conducted using GraphPad Prism 5 ($p<0.0001$) followed by a post hoc Tukey comparison test to determine statistical significance. Results of GDP- and GMPPCP-bound thermal melts can be seen in B and C, respectively. Thermal melting temperatures are noted in Table 5.1.

Ras Protein	Nucleotide	T_m (°C)
KRas WT	GDP	60.64 ± 0.18
KRas K5N	GDP	54.84 ± 0.14
KRas WT	GMPPCP	49.26 ± 0.12
KRas K5N	GMPPCP	43.02 ± 0.16

Table 3.1. Melting temperature of KRas *K5N* and wild-type protein.

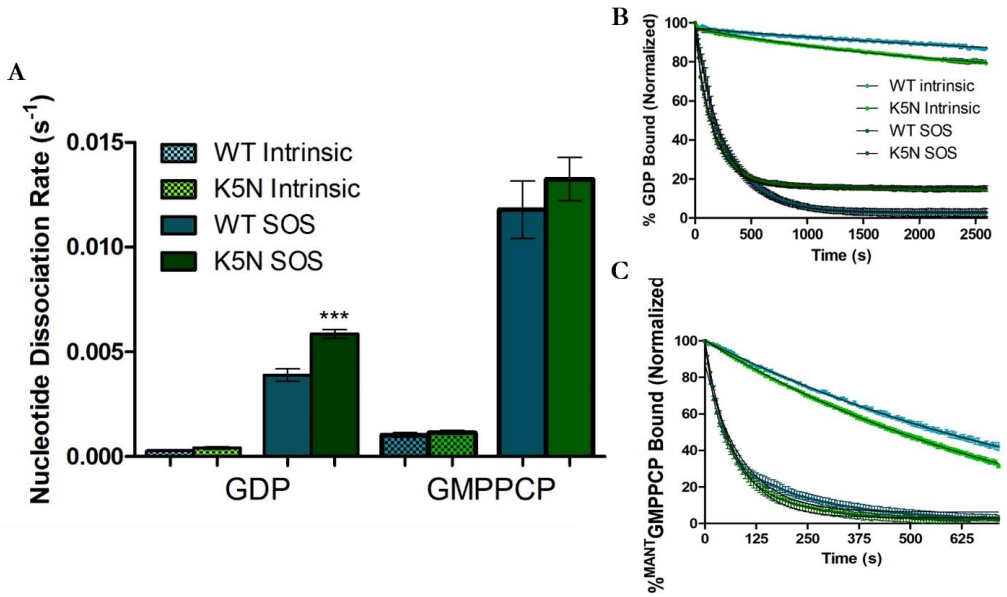

Figure 3.2. KRas *K5N* has a GEF defect in the GDP-bound form.

A. Nucleotide dissociation rates for GDP- and GMPPCP- bound KRas *WT* and KRas *K5N* were determined using fluorescence-based assays. Ras proteins were loaded with either Mant-GDP or Mant-GMPPCP and nucleotide dissociation was stimulated by the addition of excess non-labeled nucleotide in the absence or presence of a the catalytic domain of human SOS (Ras:SOS^{cat} = 1:1 molar ratio). Data was fit to an exponential dissociation curve using GraphPad Prism 5 to determine the nucleotide dissociation rate. Rates are reported as the mean ± S.E. (*n* = 3). One-way ANOVA statistical analysis was conducted using GraphPad Prism 5 ($p<0.0001$) followed by a post hoc Tukey comparison test to determine statistical significance. Results of Mant-GDP and Mant-GMPPCP dissociation can be seen in B and C, respectively. Nucleotide dissociation rates are noted in Table 5.2.

Ras Protein	Nucleotide	Intrinsic (x 10^{-4}, s^{-1})	GEF-Mediated (x 10^{-4}, s^{-1})
Nucleotide Exchange			
KRas WT	GDP	2.39±0.42	37.3±0.63
KRas K5N	GDP	3.92±0.32	59.2±0.88
KRas WT	GMPPCP	10.23±0.62	113.7±3.1
KRas K5N	GMPPCP	11.40±0.51	132.6±2.4

Table 3.2. Nucleotide exchange properties of KRas K5N and KRas WT proteins.

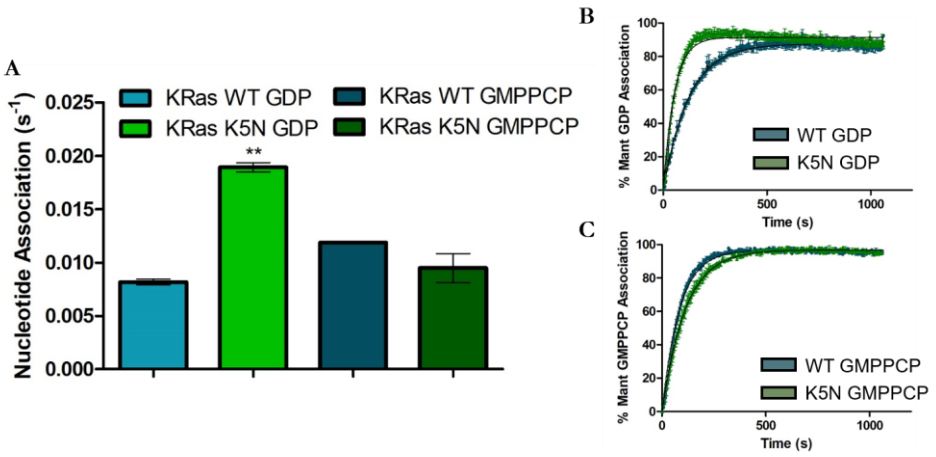

Figure 3.3. KRas *K5N* mutant displays alterations in the ability to associate GDP

A. The rates of GDP and GMPPCP nucleotide association were determined using fluorescence-based methods for KRas *WT* and KRas *K5N* proteins. Ras proteins were loaded with either GDP or GMPPCP and nucleotide association was stimulated by the addition of Mant-nucleotide in the presence of 1.25 molar excess EDTA to $MgCl_2$, B and C. Data was fit to a one-phase exponential association curve using GraphPad Prism 5 software. Statistical analysis was conducted using the built-in one-way ANOVA in GraphPad Prism 5 ($p<0.0017$) followed by a post hoc Tukey comparison test to determine statistical significance. Data are reported as mean ± S.E. (*n* = 4 for GDP, n=3 for GMPPCP). Nucleotide association rates are noted in Table 5.3.

Ras Protein	Nucleotide	Association Rate ($x\ 10^{-3}, s^{-1}$)
KRas WT	GDP	8.17 ± 0.09
KRas K5N	GDP	18.9 ± 0.31
KRas WT	GMPPCP	11.9 ± 0.095
KRas K5N	GMPPCP	8.89 ± 0.066

Table 3.3. Nucleotide association rates for KRas *WT* and KRas *K5N*

K5N mutation does not alter protein binding to Raf RBDs

Noonan syndrome (NS) and the overarching class of the 'Ras-opathies' are rare genetic disorders known to be driven by the dysregulation of the Ras/Mitogen-activated kinase (MAPK) pathway *(128)*. While K5 is not noted to make direct contacts with any Ras-effector proteins *(16)*, it is possible that mutation may disrupt the ability of Ras proteins to bind or recognize their

effector proteins. In order to test this, we used isothermal titration calorimetry (ITC) to determine the binding affinity of Ras proteins to the Ras-binding domains (RBDs) of their effector proteins. As 'Ras-opathies' are primarily associated with defects in the MAPK pathway, binding analysis was conducted using the Raf-RBDs. Results from ITC analysis demonstrated that K5N mutation does not alter the binding affinity of Ras protein to the B- or CRaf RBD (KRas WT:BRaf RBD - 28.35 ± 4.15 nM, KRas WT:CRaf RBD - 52.65 ± 7.35 nM versus KRas K5N:BRaf RBD - 23.70 ± 3.70 nM, KRas K5N:CRaf RBD - 74.40 ± 4.90 nM) (**Figures 3.4 and 3.5, Table 3.4**). This is consistent with literature where K5N mutation did not disrupt Raf1 (CRaf RBD) binding as determined using a fluorescence polarization assay *(128)*. These results along with the GDP-exchange defects would suggest that increased signaling through the downstream MAPK-mediated pathway is likely due to an increase in the GTP-bound form of the protein potentiating increased signaling and not due to an increased preference to bind or signal through the Raf RBDs.

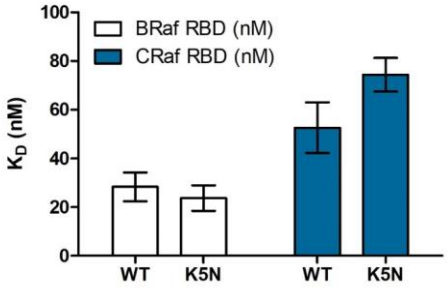

Figure 3.4. KRas *K5N* does not alter binding to the Raf RBDs.

Binding affinities of KRas *WT* and KRas *K5N* were determined to B- and CRaf RBDs (white and blue, respectively), using isothermal titration calorimetry (ITC). Ras proteins at either 150 μM were titrated into effector proteins at molar ratios of 1:10 Raf RBDs. Heat of binding was measured at 25°C. A controlled subtraction was used to normalize the isotherm to the heat of saturation. Data was analyzed using a nonlinear least square algorithm and fit to a one-site model provided in the MicroCal PEAQ-ITC Origin Software. Calculated affinities were plotted in GraphPad Prism 5. Data are shown in replicate n=2 ± S.E.

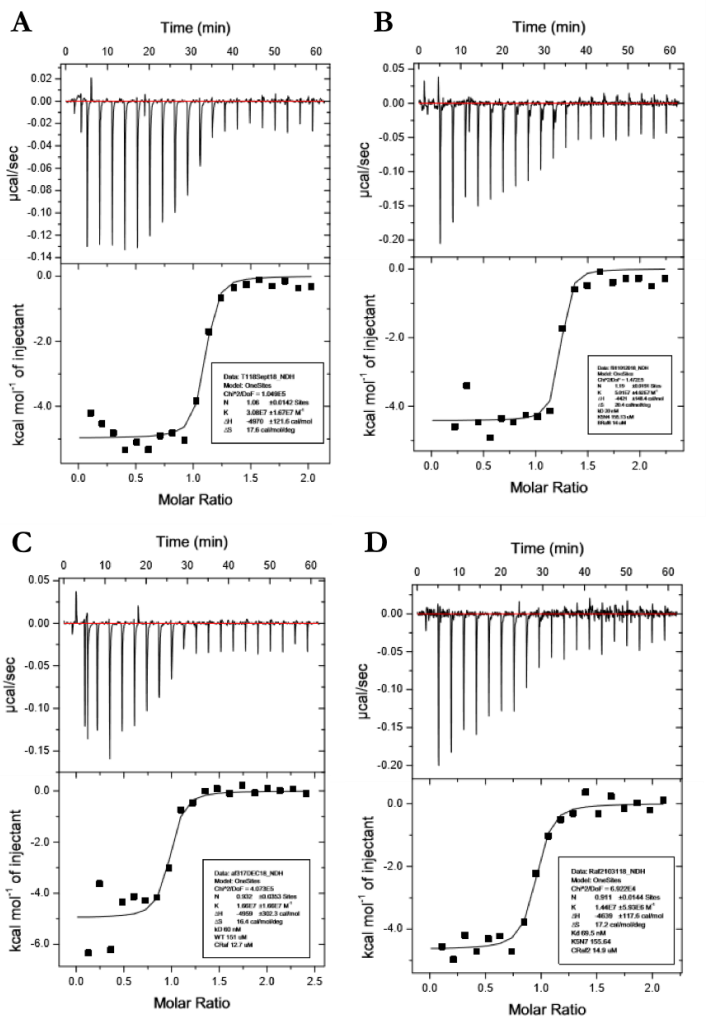

Figure 3.5. KRas *K5N* mutation does not disrupt binding to Raf RBDs

A. KRas *K5N* mutation does not alter binding to BRaf or CRaf RBDs as indicated by isothermal titration calorimetry ITC. Representative isotherms of Ras:Raf RBD binding experiments conducted using isothermal titration calorimetry (ITC). 150 µM Ras proteins were titrated into Raf RBDs at a starting molar ratio of 1:10. Isotherms are shown for KRas *WT* (A) and KRas *K5N* (B) binding to BRaf RBD and KRas *WT* (C) and KRas *K5N* (D) binding to CRaf RBD. No statistical differences in the affinity of the K5N mutant to BRaf or CRaf RBDs were observed. Data are reported as mean ± S.E. (*n* = 2). Compiled data can be seen in Table 5.4.

Ras Protein	Effector RBD	K_D (nM)
KRas *WT*	BRaf	28.35 ± 4.15
KRas *K5N*	BRaf	23.70 ± 3.70
KRas *WT*	CRaf	52.65 ± 7.35
KRas *K5N*	CRaf	74.40 ± 4.90

Table 3.4. Calculated binding affinities of KRas *WT* and KRas *K5N* to BRaf and CRaf RBDs

NMR structural analysis reveals large structural perturbations in GDP-bound Ras due to K5N mutation

Lysine 5 is noted to make contacts with critical SWII residues primarily in the GDP-bound form of Ras *(128)*. While NS is characterized by defects in MAPK-mediated signaling, our ITC binding analysis demonstrates that the increased signaling is not due to an increased affinity to the Raf RBDs. Our biochemical data demonstrates a significant decrease in thermal stability of K5N mutant protein in both GDP- and GMPPCP-bound forms, suggesting a structural perturbation due to mutation. However, our nucleotide loading and exchange data suggest that the K5N mutation may impact the GDP-bound form of the protein more severely, which could be explained by disruption of K5 contacts with critical SWII residues exclusively in the GDP-bound form. To investigate whether a structural defect due to K5N mutation could be the causative factor in modulating protein activity we employed the use of nuclear magnetic resonance (NMR) to gain structural insight. 2D ^{1}H-^{15}N heteronuclear single quantum coherence (HSQC) spectral overlays of KRas WT and KRas K5N bound to GDP and GMPPCP are shown in **Figure 3.6A** and **Figure 3.7A**, respectively. Backbone assignments for KRas protein were obtained previously *(69)*. ^{1}H-^{15}N HSQCs are capable of providing a 'fingerprint' of the protein backbone as NH resonances can be detected for every amino acid residue with the exception of proline *(69)*. 156 and 153 peaks were able to be assigned in the GDP-bound KRas WT and KRas K5N proteins, respectively. In the active form of the protein, the switch regions are in

intermediate exchange on the NMR timescale, making them invisible in the spectrum. In the GMPPCP-bound form, 96 KRas WT peaks and 95 KRas K5N peaks were able to be confidently assigned. Chemical shift perturbations (CSPs) were calculated for both nucleotide-bound forms of Ras proteins. CSP analyses revealed a significant number of peak shifts in the GDP-bound form of KRas K5N protein (**Figure 3.6B**). Approximately 22% of peaks shifted > 0.05 ppm, with the largest perturbations corresponding to residues surrounding K5 (β1), SWI, β3, SWII/α2 and α3. Results from the CSP analysis are mapped onto the structure of Ras (PDB 4OBE) (**Figure 3.6C**). These perturbations encompass nearly the entire effector lobe of Ras, suggesting a large change in the electrochemical environment in the GDP-bound form due to K5N mutation. This is largely consistent with the decreased thermal stability observed for GDP-bound KRas K5N (**Figure 3.1 and Table 3.1**) and may imply that K5N mutation destabilizes GDP-bound Ras. CSP analysis was additionally conducted for GMPPCP-bound proteins. Bearing in mind that several SWI and SWII residues are not visible in the NMR spectra in GMPPCP-bound KRas K5N, only approximately 4% of identifiable peaks demonstrated CSPs > 0.05 ppm (**Figure 3.7**). These changes are additionally mapped onto the GTP-bound Ras structure (PDB 5VQ6) (**Figure 3.7C**), with the most severe CSPs surrounding the K5N mutation site (β1). Results from this analysis indicate that K5N mutation may not severely impact the active form of the protein.

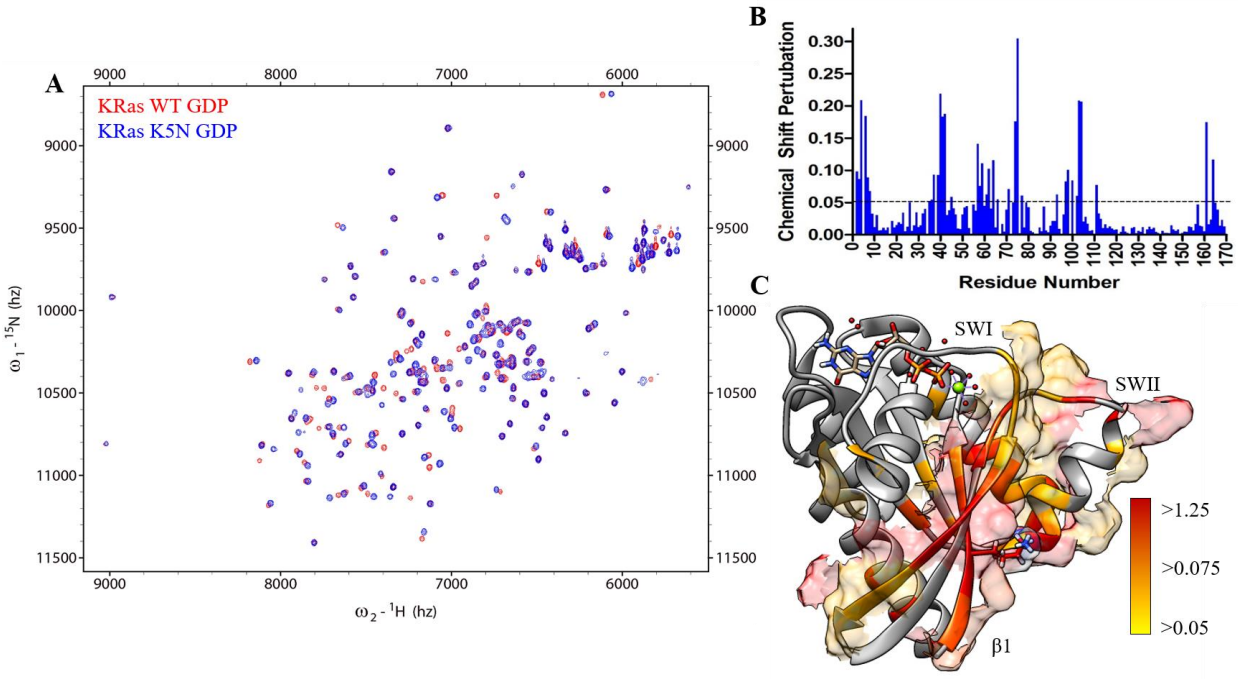

Figure 3.6. KRas K5N mutation significantly disrupts the Ras effector lobe in the GDP-bound state.

A. ^{1}H-^{15}N 2D HSQC NMR spectral overlay of ^{15}N-enriched KRas *K5N* (blue) and KRas *WT* (red). B. Chemical shift perturbation (CSP) resulting from the mutation reveal large chemical shift changes in β1- β3, switch I/II and α2- α3. C. CSPs resulting from the K5N mutation were mapped onto KRas *WT* structure (PDB 4OBE). Results from this analysis demonstrate that K5N mutation alters the electrochemical environment significantly throughout the effector interface, potentially leading to disruption of GTPase regulation or downstream signaling. All NMR spectra were recorded on KRas (1-169) GDP using a Bruker Avance III 850MHz. Data was processed using NMRFam Sparky *(187)*.

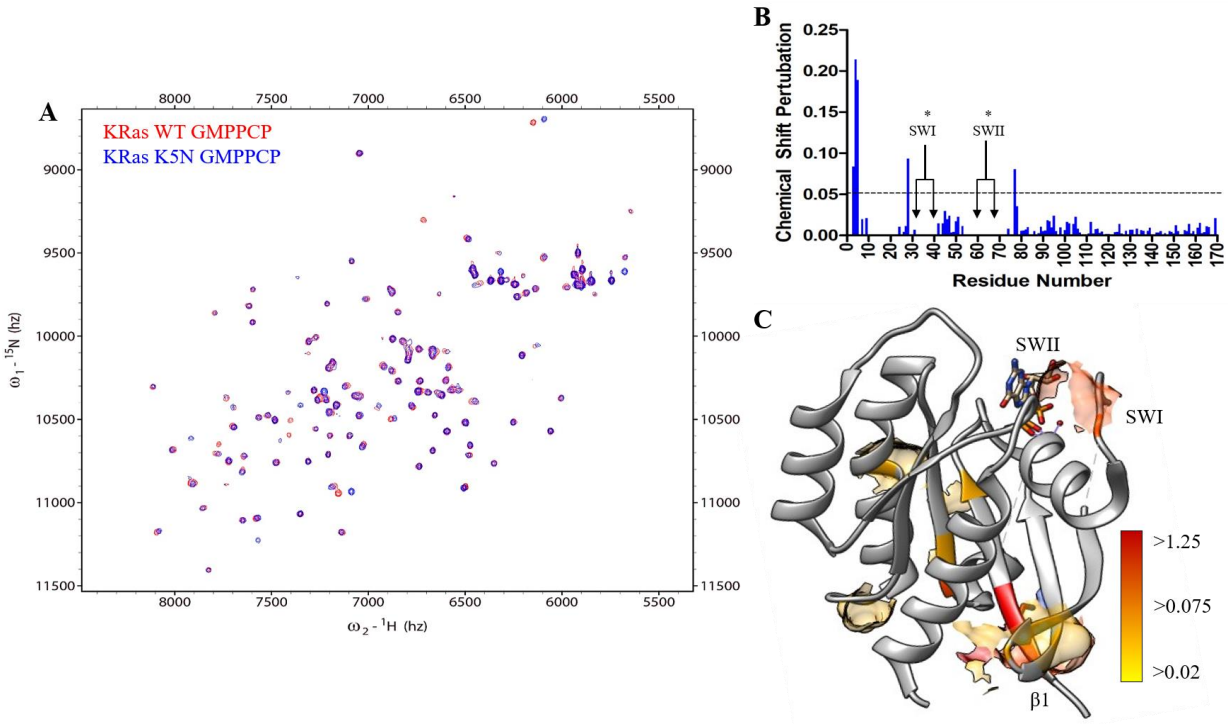

Figure 3.7. K5N mutation displays modest impact in GMPPCP-bound KRas.

A. ^{1}H-^{15}N 2D HSQC NMR spectral overlay of ^{15}N-enriched KRas *K5N* (blue) and KRas *WT* (red). B. Chemical shift perturbation (CSP) resulting from the mutation reveal modest changes throughout the protein, with prevalent shifts surrounding K5. Moderate shifts are identified near switch I and switch II regions. C. CSPs resulting from the K5N mutation were mapped onto KRas *WT* structure (PDB 5VQ6). Results from this analysis indicate minimal CSPs, primarily surrounding residue 5. This may indicate that K5N mutation may not severely impact the activity of GTP-Ras. NMR spectra were recorded on KRas (1-169) GDP using a Bruker Avance III 850MHz. Data was processed using NMRFam Sparky *(187)*. * Some switch I and switch II residues are not visible in the GMPPCP-bound form as they are in intermediate exchange on the NMR timescale.

Molecular Dynamic (MD) simulations indicate Ras K5N reorganizes SWI and SWII contacts and results in larger scale structural changes primarily within the effector lobe of Ras.

As the structural role of K5 is unclear, molecular dynamic (MD) simulations were conducted to provide insight into how K5N mutation could alter Ras activity. 100 ns MD

simulations of Mg^{2+} GDP-bound and GTP-bound Ras WT and Ras K5N were conducted (see Methods for details). The trajectories of the simulations were subjected to a clustering analysis *(137)*, and the centroids of the most populated, lowest energy clusters for each protein was examined using PyMol 2.1 (Schrödinger, LLC) and UCSF Chimera 1.13.1 *(188)*. K5 is noted to interact with the SWII region most extensively in the GDP-bound form of Ras *(128)*, and disruption of this region could serve as a potential mechanism of activation through destabilization of the GDP-bound form. MD simulations demonstrate that K5 makes several SWII contact in both the GDP- and GTP-bound forms.

The K5 backbone carboxyl oxygen and amide form contacts with the amide of G77 and the E76 Cδ oxygen, respectively in both nucleotide-bound states (**Figure 3.8A,C**). The K5-N_H sidechain forms a contact with T74-O_H in the GDP-bound state, but not in the GTP-bound state where the K5 sidechain repositions away from the switch regions (**Figure 3.8A,C**). In the GDP-bound form of the K5N mutant reorientation of the backbone contacts occur, where the N5 backbone carboxyl oxygen makes contacts with the amides of E76 and G77 and the N5- N_H sidechain amine creates an additional polar contact with the E76 Cδ oxygen (**Figure 3.8B**). We can also note that the packing around this region has become much more electrostatic in nature relative to GDP-bound WT Ras with potentially unfavorable electrostatic packing identified between Y71:N5:T74 and between T74:E76. In the GTP-bound form, the K5 carboxyl oxygen forms a contact with the amide of E76 in addition to those previously mentioned (**Figure 3.8C**). Also noted is packing of K5 against the β2 residue D54 in both nucleotide-bound forms. In GTP-bound Ras K5N, the backbone carboxyl oxygen and amide form contacts with the amide of E76 and the Cδ oxygen. We also note the formation of a β2 contact with the carboxyl oxygen of D54 (**Figure 3.8D**). Overall, K5N mutation in the GDP-bound form may result in unfavorable

electrostatic packing due to the mutation, which may result in destabilization in the GDP-bound form. In the GTP-bound form, K5N may be further stabilized by an additional contact with D54 in β2 and the relief of unfavorable residue packing.

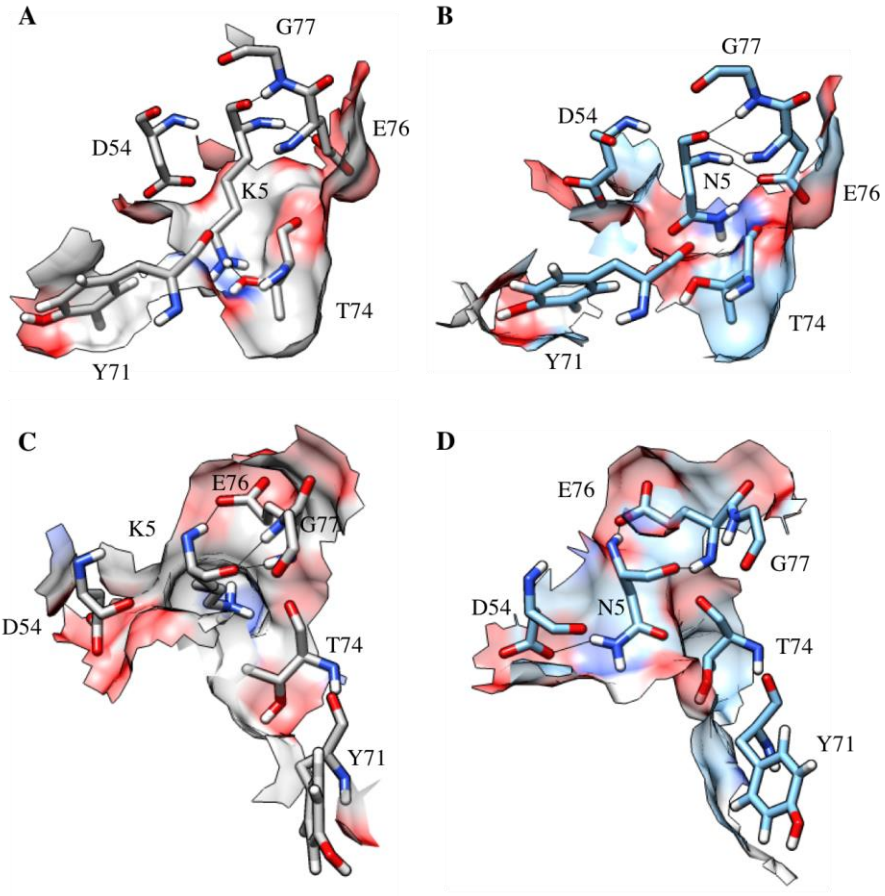

Figure 3.8. Molecular dynamics simulations identify altered contacts in SWI and SWII due to K5N mutation. **Results from molecular dynamic (MD) simulations identify several backbone and sidechain contacts made by K5 with Switch II residues in the GDP-bound (A) and GTP-bound (C) forms. The K5 carboxyl oxygen makes backbone contacts with the amides of E76 and G77 in both GDP and GTP-bound states. The backbone amide of K5 forms a polar contact with E76 Cδ oxygen. K5-N_H also creates an additional contact with T74-O_H in the GDP-bound state (A). This contact is lost in GTP-bound WT Ras and reorientation of the K5 sidechain can be observed (C). K5N mutation in the GDP-bound form creates an additional contact between N5- N_H sidechain amine and the E76 Cδ oxygen. Also identified is the loss of the T74 contact (B). In the GTP-bound form (D) the Ras K5N carboxyl oxygen and backbone amide form contacts with the backbone amide and Cδ oxygen of E76, respectively. Contact with G77 is lost relative to GTP-bound Ras WT protein. An additional contact is identified between the N5- N_H sidechain amine and the β2 D54 sidechain carboxyl oxygen.**

We can also identify larger structural rearrangements as a result of K5N mutation in GDP- and GTP-bound forms of the protein isolated largely to the effector lobe. Consistent with our NMR analysis (**Figure 3.6**), in GDP-bound K5N protein, alterations in the overall conformation and secondary structure are identified in β3, SWII and α2 (**Figure 3.9A**). The binding of SOS to SWII causes the reorientation of backbone residues in β3 and α2, which is a crucial part of the mechanism of nucleotide exclusion *(54)*. The large-scale disruptions in these regions as identified by MD simulations and NMR analysis could speak to the underlying mechanism behind the SOS-mediated defect in GDP exchange identified in **Figure 3.2**. In the GTP-bound form (**Figure 3.9B**), the K5N mutation appears to primarily disrupt the SWII/α2 helix of Ras. As SWII plays critical roles in binding and stabilizing the β- and γ- phosphates of GTP *(41)*, the disruption of SWII could lead to destabilization of the protein, consistent with the decreased thermal stability identified (**Figure 3.1A,C**). In the GMPPCP- bound NMR studies in **Figure 3.3**, K5N mutation did not significantly alter CPSs relative to WT protein. However, as the switch regions are in intermediate exchange in the active form, they are not visible in the NMR spectra.

Ras proteins are highly dynamic in nature, and their ability to act as 'molecular switches' is critical for their activity. By calculating the Cα residue RMSF throughout the MD simulations, we can gain insight into protein backbone dynamics which may provide further insight into how K5N mutation is capable of regulating Ras activity. Results from these analyses were mapped onto the protein structure for both GDP- and GTP-bound forms (**Figure 3.10**). Upon K5N mutation in the GDP-bound form of the protein, we can identify several areas of the protein that display significantly increased dynamic fluctuations relative to Ras WT (**Figure 3.10A,B**). Of particular interest, SWII (residues 61-65) and the critical nucleotide binding NKXD motif both

display dramatic increases in conformational sampling and dynamics. We can also identify a loss in the N-terminal portion of the α2 helix, potentially as a result of the increased dynamics of SWII. The NKXD motif is a highly conserved structural motif in Ras proteins that is essential in coordinating the binding of and providing specificity for the guanine-nucleotide base. Mutations at these residues greatly destabilize Ras nucleotide binding, resulting in increased protein activation *(1),(46),(47)*. In the GTP-bound form of the protein, no dramatic changes in the dynamic fluctuations are identifies as a result of K5N mutation (**Figure 3.10C,D**). Very modest fluctuations are noted in SWI, SWII and N-terminal portion of α3. Taken together, the analysis of the Cα backbone dynamics provides further evidence of mutation-induced instability in the GDP-bound form. This may potentiate GTP-binding which could lead to increased cellular signaling. We therefore propose that K5N mutation activates Ras in an indirect manner, by destabilizing the GDP-bound form of the protein.

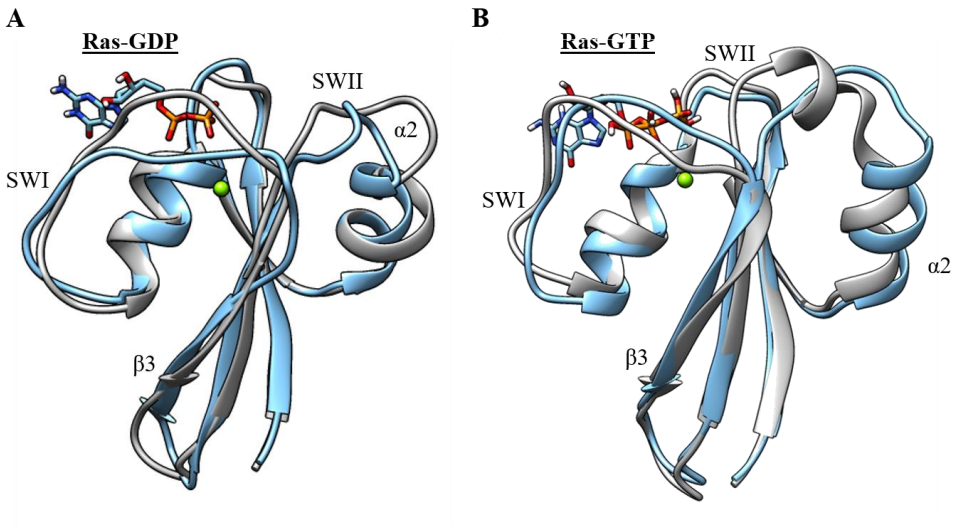

Figure 3.9. K5N mutation causes structural changes in the effector lobe of Ras.

A. The effector lobes of Ras WT-GDP (grey), Ras K5N-GDP (light cyan) and B Ras WT-GTP (grey), Ras K5N GTP (light cyan) are overlayed and represented as cartoons. Residue 5 is shown as sticks. Results from molecular dynamic (MD) simulations indicate significant structural changes in both GDP-bound and GTP-bound Ras K5N (teal and light cyan, respectively). There is loss in the secondary structure associated with β3 in GDP-bound Ras K5N relative to wild type protein. Additionally, we can see SWII/α2 helix shifts in the Ras K5N mutant (A). B. There is a significant loss of the α2 helix in GTP-bound K5N mutant Ras relative to WT protein. β3 and α2 regions are important regions in Ras proteins as they flank two highly dynamic switches in Ras, switch I (SWI) and switch II (SWII). As these regions are highly disrupted primarily in the GDP-bound state, it is likely that K5N mutation serves to disrupt the inactive form of the protein more severely.

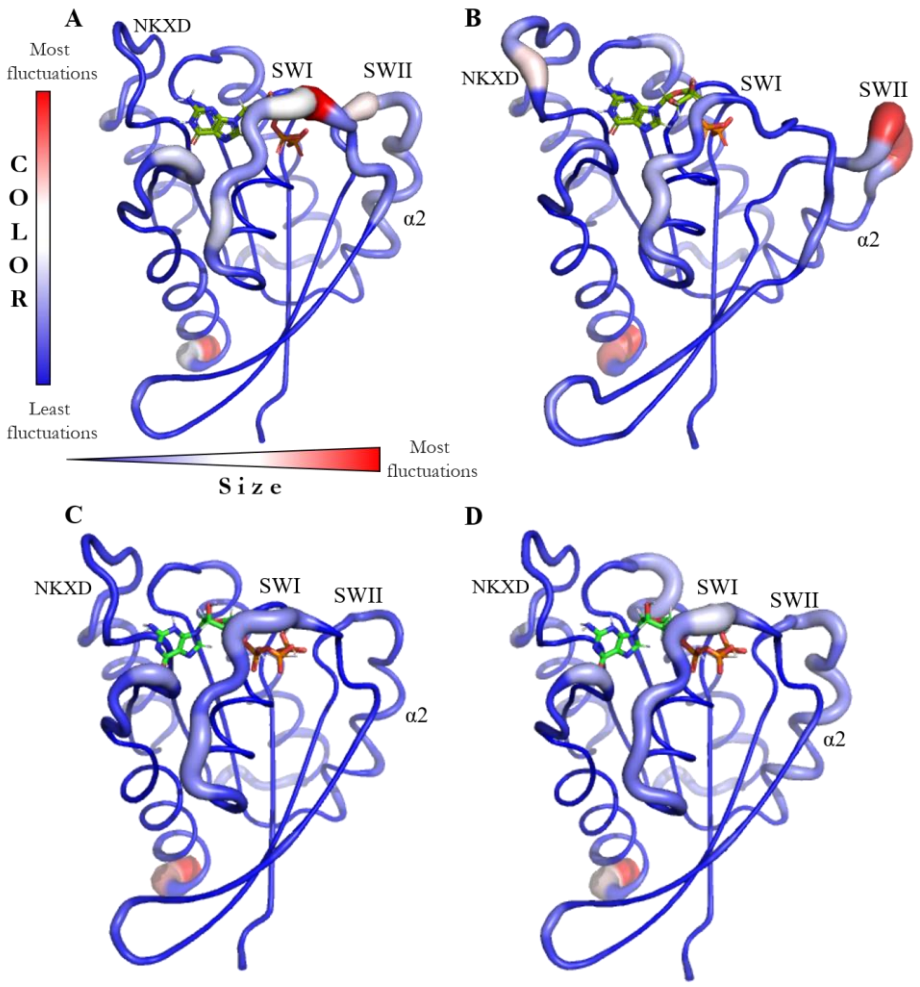

Figure 3.10 K5N mutant causes significant structural perturbations in GDP-bound form

RMSF fluctuations of backbone Cα residues plotted onto the cartoon representation of Ras proteins. Ras proteins can be seen in both GDP- and GTP- bound forms. Fluctuations are gradated based on least to most severe with color and size. Ras *WT* GDP-bound fluctuations are shown in A. Due to *K5N* mutation, in the GDP-bound form we calculate significant dynamic fluctuations of SWII (residues 61-65) and partial loss of the N-terminal portion of α2, B. Larger fluctuations are also calculated in the critical nucleotide binding NKXD motif. Disruptions in these regions would impact the ability of Ras *K5N* to properly coordinate nucleotide binding in the GDP-bound form and could lead to protein instability. Modest dynamic fluctuations also extend into the N-terminal portion of α3. Ras *WT* GTP-bound fluctuations are shown in C. Relative to *WT* protein, *K5N* mutation in the GTP-bound form displays modest fluctuations, with mild changes noted in SWI, SWII and N-terminal portion of α3, D.

Discussion

Germline mutations in KRas proteins have been identified in a subset of genetic diseases that are characterized by dysregulaton of the Ras/MAPK pathway *(128),(130).* Interestingly, these mutations are not at the common Ras 'hotspot' locations, which are known drivers of human cancers *(5),(26).* In Noonan's syndrome, KRas mutations are identified that spread throughout the highly conserved effector lobe and the more divergent allosteric lobe *(46),(128),(172)–(177).* While several of these mutations occur at locations known to play critical roles in regulating nucleotide binding or protein activity *(4),(16),(41),(53),(128),(131),* this is not the case for lysine (K) 5 mutations. The functional role of K5 in regulating Ras protein activity is not well understood. K5 has been implicated in playing an indirect role in stabilizing nucleotide binding in the inactive, GDP-bound form of the protein, but not in the active form *(128).* Further, K5R/E/N mutations have been identified in pancreatic, stomach, lung, and colon cancers and leukemia *(181)–(185).* As such, K5 mutations may present novel mechanisms of activation in genetic disorders and cancers.

Here, we show that K5N mutation causes a significant shift in the thermal stability of the protein in both GDP- and GTP-bound forms (~ 5 °C). This would likely be caused by a structural or conformation change in the protein due to mutation. Consistent with these findings, we are able to identify significant alterations in the NMR spectra of GDP-bound K5N protein, mapping predominately to the effector lobe. We identify significant CSPs in β1- β3, switch I/II and α2- α3 due to K5N mutation. While the switch regions are in intermediate exchange on the NMR timescale in the GTP-bound form of the protein and therefore not visible in the spectrum, K5N mutation in the active form displays very few alterations relative to WT protein. This would suggest that the K5N mutation may impact the GDP-bound form of the protein more severely. In

support of this, computational analysis identified potentially unfavorable electrostatic packing and altered SWII contacts in Ras K5N GDP-bound protein. Significantly altered dynamics and structure were also identified in SWII/α2 (residues 61-65) and the critical nucleotide binding NKXD motif in the GDP-bound form upon K5N mutation. The highly conserved NKXD motif is essential in coordinating the binding of and providing specificity for the guanine-nucleotide base. Mutations at these residues greatly destabilize Ras nucleotide binding, resulting in increased protein activation *(1),(46),(47)*. Taken together, these results may aid in providing support for the structural instability of GDP-bound Ras K5N.

While K5 is not noted to make direct contacts with SOS, it is located very close to SOS residues Asp910 and His 911 (~ 5 Å) *(36),(54)*. It is possible that the K5N plays a small role in disrupting these interactions. The switch regions are also critical locations for the interaction of Ras with SOS^{cat} *(36),(54)*. In particular residues, Tyr64, Met67 and Tyr71 in Ras provide a hydrophobic anchor in the binding interface with SOS. The proper orientation of this core allows for the coordination of several sets of charged interactions, resulting in the binding of nearly every SWII residue by SOS *(54)*. Gln61 forms interactions SOS^{cat} Thr935 in addition to packing against the Ras hydrophobic core residues. Glu62 in Ras forms a critical intra-molecular contact with the phosphate-binding (P-loop) lysine 16. Glu63 contacts Arg826 of SOS^{cat}. While Tyr64 is part of the hydrophobic core in the Ras:SOS interface, it also forms a contact with the SOS^{cat} residue 912. Structural changes are also noted in the Ras NKXD motif and extending through loop 8 in the Ras;SOS complex (residues 118-123) *(54)*. Moderate dynamic fluctuations were also identified in this region due to K5N mutation in the GDP-bound form. Large dynamic fluctuations primarily in the Ras SWII residues responsible for SOS^{cat} interactions and unfavorable electrostatic packing of K5N with SWII along with moderately increased

fluctuations of the residues of the NKXD motif may support the slight SOS-defect identified in the GDP-bound form. Residues 61–64 are also highly implicated in binding interactions with Ras GAPs *(13)*. However, K5N mutation displayed no defects in intrinsic or GAP-mediated hydrolysis *(128)*. Contrary to previous literature, we were able to identify a mild defect in the ability of Ras K5N to associate GDP but not GMPPCP. These differences could potentially stem from the different methodology used for data collection *(128)*.

'Ras-opathies' are characterized by defects in Ras/MAPK signaling *(128),(170),(171)*. We investigated whether this could be due to an altered affinity of the K5N mutant to bind BRaf or CRaf RBDs. As Raf RBDs interact with Ras primarily through the SWI region *(16)*, it was not surprising that binding analysis revealed no changes in affinity due to K5N mutation. In the GTP-bound form, Ras K5N mutation displays very mild perturbations as noted in our biochemical, NMR and computational studies. Previously, small increases in MAPK-mediated signaling were identified in Ras K5N cells *(128)*, but the overarching mechanism still remains unclear. Our data would suggest that K5N mutation causes protein instability in the GDP-bound form. This is demonstrated in the altered thermal stability of the protein and in NMR and computational studies. Given that physiologic levels of GTP are much higher in the cell, it is possible that K5N protein may be more GTP-bound. This may lead to increased signaling. Results from our analysis demonstrate that K5 plays an indirect role in stabilizing nucleotide binding, as noted previously *(128)*. N5 mutation causes unfavorable packing in the GDP-bound form against SWII, which is reflected in the large dynamic fluctuations and alterations identified in the GDP-bound forms of the protein in NMR and MD analyses. As the increase in cellular signaling identified was minimal *(128)*, it is possible that Ras K5N mutations would co-occur with either SOS1 or PTPN11 mutations that would further potentiate activation of the Ras-

mediated MAPK signaling cascade. K5N mutation presents a unique mechanism of activation, through destabilization of the inactive form of the protein. As K5N/E/R mutations have been identified in cancers *(181)–(185)*, our analysis may provide novel ways of K5 mutation-specific targeting.

Materials and Methods

Protein Purification

Human KRas-4B (C118S) (residues 1–169) was subcloned into a pET21 vector with an N-terminal 6-histidine tag and a TEV protease cleavage site for expression in *Escherichia coli* BL21 (DE3) cells (Novagen). Standard site-directed mutagenesis techniques were used to generate the KRas K5N mutant. Briefly, *E. coli* BL21 (DE3) cells were grown at 37 °C in Luria-Bertani (LB) medium supplemented with ampicillin and chloramphenicol until A_{600} of ~0.5. The temperature was then lowered to 18 °C, and KRas expression was induced with 0.5 mM isopropyl-β-D-1-thiogalactopyranoside (IPTG) after 30 min. The cells were grown 15 hours at 18 °C and were then harvested. The cells were pelleted at 4000 x g, resuspended in a lysis buffer (20 mM HEPES, 300 mM NaCl, 1 mM $MgCl_2$, 20 mM imidazole, 5% glycerol (pH 7.75) and sonicated. The cell lysate was centrifuged at 15,000 x g, and the supernatant was isolated. KRas proteins were purified using standard Qiagen nickel affinity purification procedures. Proteins were washed with a buffer containing 20 mM HEPES, 500 mM NaCl, 5 mM $MgCl_2$, 40 mM imidazole, 5% glycerol (pH 7.75). Proteins were then eluted in a buffer containing 20 mM HEPES, 50 mM NaCl, 5 mM $MgCl_2$, 250 mM imidazole (pH 7.75). The histidine tag was cleaved during overnight dialysis using TEV protease. Cleaved Ras proteins were further purified by size exclusion chromatography using a Sephadex G-75 column. Protein purity of

>95% was obtained and verified by SDS-PAGE analysis. Proteins were stored in a buffer containing 20 mM HEPES, 50 mM NaCl, 5 mM $MgCl_2$, pH 8.0.

The catalytic domain of SOS^{cat} (residues 566 -1049) was purified as previously described *(131)*. Briefly, SOS^{cat} was transformed into BL21 (DE3) RIPL *E. coli* cells. Cells were grown at 37 °C in Luria-Bertani (LB) medium supplemented with ampicillin and chloramphenicol until A_{600} of ~0.5. The temperature was then lowered to 18 °C and the cells were induced with 0.5 mM isopropyl-β-D-1-thiogalactopyranoside (IPTG). Expression was continued for 16 hours. Cells were then pelleted by centrifugation at 4000 x g and resuspended in a buffer containing 25 mM Tris-Cl, 500 mM NaCl, 20 mM imidazole (pH 7.5) and the protease inhibitor phenylmethanesulfonyl fluoride (ACROS Organics). Cells were sonicated followed by centrifugation at 14,000 x g. The supernatant was isolated and purified using standard Qiagen nickel affinity purification procedures. Proteins were washed with several column volumes of the buffer listed above and then eluted in this same buffer with 500 mM imidazole. SOS^{cat} was dialyzed overnight with Tobacco Etch Virus to cleave the N-terminal histidine tag. SOS^{cat} protein was further purified by size exclusion chromatography using a Sephadex G-100 column. Protein purity of >95% was obtained and verified by SDS-PAGE analysis

The RBD of human BRaf (residues 149-232) was subcloned into the pET28a bacterial expression vector encoding a N-terminal 6-histidine tag and TEV cleavage site and purified as described previously *(28)*. BRaf RBD was expressed in BL21 (DE3) RIPL *E. coli* cells and was grown at 37°C in Luria-Bertani (LB) medium. At A_{600} of ~0.5 the temperature was reduced to 18°C, and protein expression was induced after 30 minutes upon addition of 500 μM Isopropyl β-D-1-thiogalactopyranoside (IPTG). The culture was allowed to grow for 16 hours. The cells

were then harvested and pelleted at 4,000 x g, resuspended in a lysis buffer containing 20 mM HEPES, 300 mM NaCl, 1 mM MgCl2, 20 mM imidazole, and 5% glycerol (pH 7.75) and sonicated. The cell lysate was centrifuged at 15,000 x g, and the supernatant was isolated. Protein was purified using standard Qiagen nickel affinity procedures. The supernatant was added to the column and washed with buffer containing 20 mM HEPES, 500 mM NaCl, 1 mM $MgCl_2$ and 40 mM imidazole and then again with the lysis buffer. The protein was eluted using a buffer containing 15 mM HEPES, 50 mM NaCl, 5 mM MgCl2, 250 mM imidazole, pH 7.75. The N-terminal 6-histidine tag was cleaved during overnight dialysis into 10 mM HEPES, 50 mM NaCl and 5 mM MgCl2, pH 7.75 using Tobacco Etch Virus protease. BRaf RBD was further purified by size exclusion chromatography using a Sephadex G-75 column. Greater than 95% purity was achieved using size exclusion chromatography and verified using SDS-PAGE analysis.

The isolated RBD of human CRaf (residues 54-131) was subcloned into a pQlinkH bacterial expression vector, harboring a N-terminal 6-histidine tag with TEV protease cleavage site and purified as described previously *(64)*. CRaf RBD was expressed in BL21 (DE3) RIPL *E. Coli* cells and was grown at 37°C in Luria-Bertani (LB) medium. At A_{600} of ~0.5 the temperature was reduced to 18°C, and CRaf RBD expression was induced after 30 minutes upon addition of 500 μM Isopropyl β-D-1-thiogalactopyranoside (IPTG). The culture was allowed to grow for 16 hrs at 18°C. CRaf RBD was purified as described previously *(64)*. Further purification was completed by size exclusion chromatography and > 95% purity verified using SDS-PAGE analysis.

Nucleotide Dissociation Assay

Nucleotide dissociation was measured using a well-established fluorescence-based assay *(189)*. Briefly, Ras proteins were loaded with either MANT-GDP ((2'-(or-3')-O-(N-Methylanthraniloyl) Guanosine 5'-Diphosphate) or MANT-GMPPCP (2'/3'-O-(N-Methyl-anthraniloyl)-guanosine-5'-[(β,γ)-methyleno]triphosphate), and loading was verified via HPLC to be >95%. 2 μM of loaded Ras protein was added to a final volume of 60 uL in assay buffer (20 mM HEPES, 50 mM NaCl and 5 mM $MgCl_2$, pH 7.4) and nucleotide exchange was initiated by the addition of 2 mM GDP or GMPPCP. Nucleotide dissociation was measured as a change in fluorescence over time (excitation, 360 nm; emission, 440 nm) using a SpectraMax M2 plate reader at 25°C. Fluorescence data was fit to a one-phase exponential decay curve using GraphPad Prism 5.

Nucleotide Association Assay

Nucleotide association rates were determined using fluorescence-based assays *(189)*. Briefly, Ras proteins were loaded with either GDP or GMPPCP and loading was verified using HPLC. Ras proteins were added to 1 ml of assay buffer (20 mM HEPES, 50 mM NaCl, 5 mM $MgCl_2$, pH 7.4) to a final concentration of 5 μM for GDP-bound association assays. EDTA was added in slight molar excess to the $MgCl_2$ (1:1.25 molar ratio) to stimulate nucleotide loading. Mant-GDP was added to start the association reactions (0.25 μM). The rate of Mant-labeled nucleotide association was measured as a change in fluorescence intensity over time (excitation, 365 nm; emission, 435 nm) (LS50B PerkinElmer Life Sciences luminescence spectrometer). Fluorescence data were fit using GraphPad Prism 5 software to a one-phase exponential association curve. GMPPCP association assays were conducted in a similar manner as described above (2.5 μM protein, 0.125 μM Mant-GMPPCP and no EDTA).

Thermal Stability of Ras

CD (circular dichroism) data were collected on a Jasco J-815 CD spectrometer. UV CD scans were collected using a 1-mm cuvette at a concentration of 15 μM KRas protein and 15 uM nucleotide in a sparged buffer containing 10 mM $KH_2PO_4^{3-}/K_2HPO_4^{3-}$, 500 μM $MgSO_4$, pH 7.2, at 20 °C. Thermal melts were obtained over a temperature range of 20–95 °C using a temperature increment of 2 °C per min. The CD signal was measured at 222 nm. T_m values were calculated by fitting the mean residue ellipticity to a Boltzmann sigmoidal equation, where V50 is representative of the melting temperature. Data calculations were completed using GraphPad Prism 5.

NMR Analyses

For NMR measurements, ^{1}H-^{15}N-enriched Ras proteins were produced using standard methods in M9 minimal media *(190)*. Proteins were exchanged into NMR buffer (20 mM HEPES, 50 mM NaCl, 5 mM $MgCl_2$, 5% D_2O, 3% $_{d6}$-DMSO, (pH 6.8)) with 1:1 molar ratio of protein to nucleotide. NMR spectra were acquired at 25 °C on a Bruker Avance III 850 NMR spectrometer. 2D ^{1}H-^{15}N HSQC experiments were recorded for $KRas^{WT}$ and $KRas^{K5N}$ in both GDP- (50 μM) and GMPPCP-bound (40 μM) forms. Data was collected as 2048 and 128 complex points in the direct and indirect dimensions, respectively with 32 scans per increment. Spectral widths used were 11904.762 Hz (^{1}H) and 3102.058 (^{15}N) Hz. Spectra were processed using NMRFAM sparky *(187)*. ^{1}H-^{15}N chemical shift perturbations (CSPs) were calculated using the square root of $((\Delta\sigma\ ^{1}H)^2 + (\Delta\sigma\ ^{15}N)^2/25)$, where $\Delta\sigma\ ^{1}H$ and $\Delta\sigma\ ^{15}N$ are the observed changes in ^{1}H and ^{15}N chemical shifts.

Molecular Dynamic Simulations

United-atom Molecular Dynamics (MD) simulations of Mg^{2+}-GDP and GTP- bound Ras WT and Ras K5N were conducted in Gromacs 2018 using GROMOS 54a7 force field

parameters *(163)*. An initial structure of GDP- or GTP-bound Ras was constructed using high resolution X-ray structures from the protein data bank (PDB ID 1CRP *(48)* and 4G0N *(55)*). The coordinates for the missing Ras *WT* residues in 4G0N were reconstructed using the Ras structure 2C5L *(157)*. Mutations were corrected to generate Ras *WT* using PyMol 2.1 (Schrödinger, LLC). The Ras *K5N* mutation was constructed using PyMol 2.1 (Schrödinger, LLC). GTP topology and parameters files for GROMOS 54a7 force field were generated using the Automated Topology Builder version 2.2 *(161),(162)*. GTP charges were optimized using the Antechamber module from AmberTools package *(191)*. To begin the simulations, Ras- Mg^{2+}-GDP, Ras- Mg^{2+}-GTP was solvated using a TIP3P water box. The system was neutralized by the addition of sodium ions, and the system was allowed to equilibrate at 300K. All simulations were run at constant temperature for a total of 200 ns. We determined that the system reached equilibrium by 2 ns by analyzing the root-mean-square deviation (RMSD) of backbone Cα position distribution during the simulations. The initial 2 ns simulations were omitted from the trajectories for the analysis. To select representative models of GDP- or GTP-bound Ras *WT* and Ras *K5N*, clustering analysis was performed using a GROMACS clustering algorithm *(137)*. The distance cut-off for clustering was chosen to be 1.5 Å, to correlate with distances of high-resolution X-ray crystallographic structures. The structures of the lowest energy centroids associated with the most populated clusters for each protein or protein-protein complex were examined using PyMol 2.1 (Schrödinger, LLC). Final models were constructed using UCSF Chimera 1.13.1 *(188)*.

Isothermal Titration Calorimetry (ITC)

The binding affinities of KRas-4B (C118S) wild type, and KRas-4B (C118S) K5N to effector proteins were determined using a MicroCal PEAQ-ITC (Malvern Paranalytical). All ITC experiments were performed in a buffer containing 20 mM HEPES, 50 mM NaCl, 5 mM $MgCl_2$,

1 mM 2-mercaptoethanol. Ras proteins (150 μM or 200 μM) were titrated into effector proteins (BRaf RBD, CRaf RBD and PI3K-α). Starting effector to Ras molar ratios were roughly 1:10 or 1:15. The heat of the binding event was measured after an initial 120 second delay at 25°C for 19 2-uL injections with a stirring speed of 650 rpm. Injections were spaced at 180 seconds. Heats released during the last few injections (when saturation had occurred) were averaged and subtracted from all the heat peaks (control subtraction). Data were analyzed using a nonlinear least square algorithm and fit to a one-site model provided in the MicroCal PEAQ-ITC Origin software.

Chapter 4. A KRas GTPase K104Q Mutant Retains Downstream Signaling by Offsetting Defects in Regulation[2]

Introduction

RAS proteins function as molecular switches that cycle between active GTP- and inactive GDP-bound states to regulate signal transduction pathways that modulate cellular growth control. In the unstimulated cell, RAS proteins are populated in their inactive GDP-bound state. However, in response to growth-stimulatory signals, guanine nucleotide exchange factors (GEFs) *(8)* co-localize and up-regulate RAS by facilitating exchange of GDP for GTP. Inactivation of RAS is achieved through GTPase-activating proteins (GAPs) that bind to GTP-bound RAS and promote GTP hydrolysis *(8),(53).* Several point mutations in RAS have been identified that dysregulate RAS nucleotide exchange or hydrolysis, often leading to hyperactivation and promoting tumorigenesis. The most common RAS mutations identified in cancer occur at residues 12, 13, and 61 and render RAS GAP defective, thereby populating RAS in its active GTP-bound state *(82).* Constitutive hyperactivation of RAS promotes chronic stimulation of effector-mediated downstream pathways, causing deregulated growth and tumorigenic growth transformation.

RAS contains two dynamic regions termed switch I (SWI; residues 30–37) and switch II (SWII; residues 60–76 with 66–74 corresponding to helix 2 (H2)) that populate distinct conformations when the protein is bound to GDP *versus* GTP. Effectors and GAP proteins

[2] This chapter previously appeared as an article in the Journal of Biological Chemistry. This original citation is as follows: Yin, G.; Kistler, S.; George, S. D.; Kuhlmann, N.; Garvey, L.; Huynh, M.; Bagni, R. K.; Lammers, M.; Der, C. J.; Campbell, S. L. A KRAS GTPase K104Q Mutant Retains Downstream Signaling by Offsetting Defects in Regulation. *J. Biol. Chem.* 2017, *292* (11), 4446–4456. https://doi.org/10.1074/jbc.M116.762435.

recognize specific conformations of the switch regions and bind with preferential affinity to the active GTP- bound state. Activated GTP-bound RAS can interact with multiple effectors (*e.g.* RAF kinase, RAL exchange factors, phosphoinositol 3-kinase (PI3K), the RAC-selective GEF TIAM1, phospholipase C, NORE1) to promote downstream signaling pathways that control cell growth, differentiation, and apoptosis *(107).*

RAS proteins show high sequence conservation within their core guanine nucleotide binding domain (G domain) yet possess a hypervariable C terminus. The hypervariable region undergoes a variety of post-translational modifications (PTMs) that facilitate membrane association and drive differences in localization and activity *(61).* Additionally, several lysines within the core G domain of RAS undergo post-translational modifications, including acetylation, ubiquitylation, and methylation *(61),* but the role of these distinct modifications in regulating RAS function is still unclear. For example, KRAS monoubiquitylation at lysine 147 up-regulates RAS activity, signaling, and tumorigenesis *(62).* Additionally, lysine 104 has been shown to be a minor site of ubiquitylation, and we have previously shown that ubiquitylation of KRAS at this position does not alter the intrinsic biochemical properties or regulation by GEFs and GAPs *(65).* In contrast, lysine 104 acetylation was reported to down-regulate KRAS G12V-driven effector signaling and growth transformation in NIH 3T3 cells *(67),(126).* Whereas knockdown of two deacetylases, HDAC6 and SIRT2, reduced the viability of NIH 3T3 cells expressing the oncogenic KRAS G12V mutant *(126),* recent findings indicate that Ac-Lys^{104} is not a direct substrate for HDAC6 and SIRT2 under the conditions tested *(68).* A KRAS K104Q variant was used as an acetylation mimetic to evaluate how acetylation alters KRAS signaling. Molecular dynamics (MD) simulations indicated that the KRAS K104Q mutation completely disrupts the structural integrity of H2 *(67),* consistent with *in vitro* observations that SOS1-

stimulated nucleotide exchange was impaired by 75%. However, the ability of KRAS K104Q to undergo GAP-stimulated GTP hydrolysis was not assessed *(67)*. In NIH 3T3 cells, the K104Q mutation impaired KRAS G12V-driven effector signaling and growth transformation *(67)*.

To better understand how perturbations at position 104 of KRAS alter intrinsic biochemical properties, structure, and regulatory and effector interactions, we characterized mutations at this position, including a K104Q mutant that has previously been employed as an acetylation mimetic *(67)*. We find that the K104Q mutation perturbed both GEF- and GAP-stimulated guanine nucleotide exchange and GTP hydrolysis, respectively, yet did not alter either CRAF RAS binding domain (RBD) or PI3Kγ binding. However, in contrast to previous MD predictions, our NMR analyses indicated that KRAS K104Q does not fully disrupt SWII but rather causes a partial disruption of H2. Given these observations, we measured the thermal stability (melting temperature (T_m)) of WT, K104Q and Ac-Lys^{104} KRAS using circular dichroism (CD). We found that both K104Q and Ac-Lys^{104} show a modest decrease in T_m of 1.5 and 3.7 °C, respectively, relative to WT KRAS. Moreover, we found that K104Q did not significantly impair WT KRAS function, as measured by the ability to restore growth to Rasless mouse embryo fibroblasts (MEFs). In slight contrast to a previous study, we also found that K104Q did not significantly alter mutant KRAS G12V effector signaling and induction of morphologic transformation. Taken together, our data indicate that the KRAS K104Q impairs the structural integrity of H2 and RAS regulation by GEFs and GAPs *in vitro* but does not significantly alter the steady-state level of GTP-bound protein in NIH 3T3 cells. Consistent with our findings that KRAS K104Q retains effector engagement *in vitro* and GTP levels in cells, the K104Q substitution did not significantly alter either WT KRAS or G12V biological activity. We

postulate that the consequences of the K104Q substitution on GAP and GEF regulation probably offset each other to maintain the active GTP-bound state and effector signaling in cells.

Results

KRAS Lys^{104} Mutations Disrupt SOS^{cat}-mediated Nucleotide Exchange and p120 GAP^{cat}-mediated Hydrolysis

RAS proteins cycle between inactive GDP- and active GTP-bound states to coordinate downstream signaling and cellular growth. Lysine 104 in KRAS undergoes multiple PTMs, yet the role of this residue in intrinsic RAS function has not been well characterized. In the X-ray structure of KRAS bound to GDP (PDB code 4LPK), the side chain of lysine 104 interacts with the backbone carbonyl group of Arg73 and Gly75contained within SWII. Disruption of these interactions has been proposed to perturb the structural integrity of SWII and alter interactions with regulatory proteins and effectors that interact with SWII *(192),(193)*. Moreover, Arg102 and Val103, surrounding Lys104 in H3, interact directly with the SOS catalytic domain (PDB code INVW) *(36)*. Hence, mutations or PTMs that perturb these interactions may prevent proper SOS-mediated up-regulation of RAS. Consistent with these observations, it has been shown previously that KRAS K104Q disrupts SOS^{cat}-mediated nucleotide exchange *(67)*. KRAS K104Q has been dubbed an acetylation mimetic, yet how this mutation affects the structure of RAS, GAP-mediated GTP hydrolysis, and effector recognition has not been determined. To further investigate the role of non-conservative and conservative mutations at this key position, we mutated residue Lys104 to glutamine, arginine, and alanine and monitored the rate of MANT-GDP nucleotide dissociation in the absence and presence of SOS^{cat}. As shown in **Figure 4.1A**, all three mutations impaired SOS-mediated nucleotide exchange. In particular, a reduction

in the rate of GDP dissociation by 78% for K104Q, 75% for K104R, and 50% for K104A was observed in comparison with WT KRAS ($12.5 \pm 0.2 \times 10^{-4}$ s^{-1}) (**Figure 4.1A** and **Table 4.1**). All three mutations, even the K104R variant that retains the side chain positive charge, impaired SOS-mediated exchange. Although KRAS K104R has previously been reported to retain GEF activity *(67)*, we find that this conservative substitution (K104R) impaired SOS regulation of RAS nucleotide exchange. These findings indicate that Lys^{104} plays an essential role in SOS^{cat}-mediated nucleotide exchange of KRAS. Because the K104Q variant was predicted to impair the structural integrity of SWII *(67)*, which is also important for GAP-mediated down-regulation of RAS activity, we measured both the intrinsic and GAP-mediated rate of GTP hydrolysis (**Table 4.1**). Although the intrinsic rate of GTP hydrolysis for KRAS K104Q is similar to that of WT KRAS, we found a significant reduction (53%) in the p120 GAP^{cat}-stimulated rate of GTP hydrolysis (**Figure 4.1B**). Taken together, these data suggest that the K104Q mutation, which has been used as a RAS acetylation mimic, impairs regulation of GDP/GTP cycling by both GEFs and GAPs.

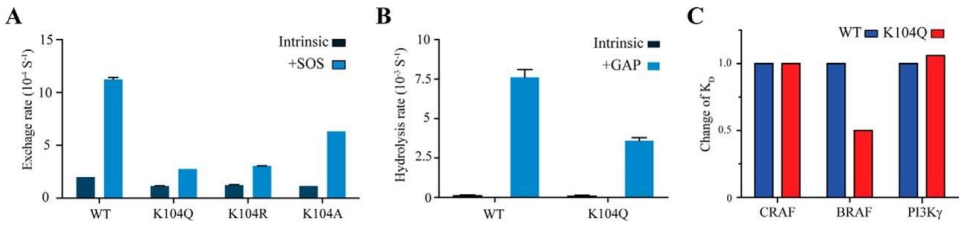

Figure 4.1. The KRAS K104Q mutation impairs regulation by GEFs and GAPs yet retains effector binding interactions with RAF and PI3K RAS binding domains.

A. *E. coli*-expressed and purified WT and mutant (K104Q, K104R, and K104A) were loaded with MANT-GDP, and the rate of GDP dissociation was determined by monitoring the decrease in MANT-GDP fluorescence emission over time in the absence and presence of an SOS (Ras/SOS = 1:1). Data were fit to an exponential dissociation curve. Rates are reported as the mean ± S.E. (*error bars*) (*n* = 2). B. p120 GAP-mediated GTP hydrolysis, as determined using single-turnover GTP hydrolysis for KRAS WT and K104Q in the absence or presence of p120 GAP (GAP/Ras = 1:200). Hydrolysis was initiated by the addition of Mg^{2+} and monitored by the change in fluorescence of the protein, Flippi, upon binding free phosphate. Data were converted to phosphate concentration using a standard curve. Results are the mean ± S.E. (*n* = 2). C. The binding affinity of KRAS WT and K104Q to CRAF RBD, BRAF RBD, and PI3Kγ K802T was determined by loading KRAS proteins with MANT-GMPPCP and measuring nucleotide release rates as a function of effector protein concentration. To determine the affinity (K_D) for the KRAS-effector complex, the data were fitted to a standard curve. Relative binding affinity to KRAS WT is shown with original values included in Table 1. Results are reported as the mean ± S.E. (*n* = 2). All of the original values are listed in Table 1.

TABLE 1
Biochemical properties of WT and KRas 104 mutants

Property	WT	K104Q	K104R	K104A
Nucleotide exchange rate (10^{-4} s^{-1})				
Intrinsic	2.0 ± 0.1	1.2 ± 0.1	1.4 ± 0.1	1.2 ± 0.1
SOS^{cat}	12.5 ± 0.2	2.8 ± 0.1	3.2 ± 0.1	6.3 ± 0.1
GTP hydrolysis rate (10^{-3} s^{-1})				
Intrinsic	0.1 ± 0.1	0.1 ± 0.1		
p120 GAP^{cat}	7.6 ± 0.5	3.6 ± 0.2		
Effector affinity (K_D) (μM)				
BRAF RBD	0.2 ± 0.1	0.1 ± 0.02		
CRAF RBD	0.2 ± 0.1	0.2 ± 0.1		
PI3Kγ (p110 subunit, K802T)	16.2 ± 6.1	17.2 ± 1.2		

Table 4.1. Biochemical Properties of KRas WT and K104 mutant proteins.

Upon GEF-mediated GDP exchange for GTP, RAS-GTP undergoes a conformational change in both the SWI and SWII regions. This in turn promotes binding to downstream effectors *(16)*. Although SWI is a primary binding site for a subset of RBDs (*i.e.* RAF and RALGEFs), some effectors (*i.e.* PI3K, PLCϵ, and NORE1) bind to RAS using both SWI and SWII regions *(16)*. To assess whether the K104Q mutation alters KRAS effector interactions, we determined the binding affinity of KRAS K104Q to the RAS RBDs of CRAF and BRAF as well as PI3Kγ, by monitoring the dissociation rate of MANT-GMPPCP as function of RAS effector concentration (**Table 4.1**). Results from these analyses indicate that KRAS K104Q retains binding to RAF RBDs and PI3Kγ relative to WT RAS (**Figure 4.1C**).

The KRAS K104Q and Ac-Lys^{104} Decrease Thermal Stability

To evaluate the effects of side chain modification at Lys^{104} on thermal stability, we measured the T_m for His$_6$-WT KRAS, K104Q, and Ac-Lys^{104} by CD, by monitoring the thermal transition as a function of temperature, as shown in **Figure 4.2A**. We found that K104Q and Ac-Lys^{104} KRAS showed similar cooperative unfolding transitions but possessed a lower T_m (K104Q (64.2 ± 0.1 °C), Ac-Lys^{104} (62.0 ± 0.5 °C)) in comparison with WT KRAS (65.8 ± 0.4 °C). The small T_m changes shown in **Figure 4.2B** indicate that acetylation or mutation of the Lys^{104} side chain alters protein stability.

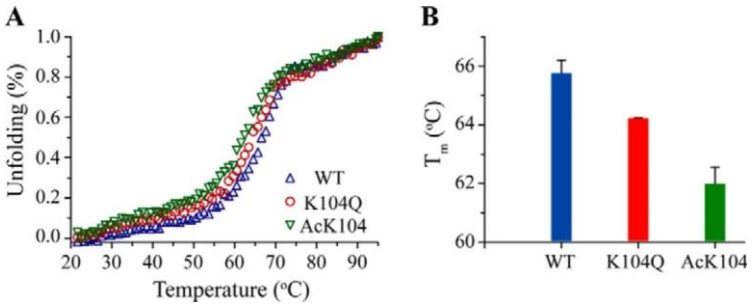

Figure 4.2. Ac-Lys^{104} and K104Q KRAS show decreased thermal stability relative to WT KRAS.

A. the CD signal at 222 nm was monitored as a function of temperature (20–95 °C) for His$_6$-WT KRAS, K104Q, and Ac-Lys^{104} (20 μM) bound to GDP. B. the midpoint of the thermal transition (T_m) was determined by fitting the temperature dependence in *A*. Results are reported as the mean ± S.E. (*error bars*) (*n* = 3).

The KRAS K104Q Mutation Perturbs the Conformation of Helix 2 and Helix 3

Given the decrease in protein stability observed for KRAS K104Q, we conducted NMR studies to investigate whether the mutation alters KRAS structure. The RAS switch regions undergo distinct conformations when bound to either GDP or GTP. These conformational changes are key to recognition of GAPs and effector proteins as well as GTP-dependent SOS allosteric regulation *(194)*. Based on the crystal structure of KRAS bound to GDP (PDB code 4LPK), the Lys^{104} amino side chain interacts with the backbone carbonyls of Arg-73 and Gly-75 located at the end of SWII (**Figure 4.5A**). These interactions were previously predicted to play a key role in the structural integrity of SWII, because MD simulations suggested that both the KRAS K104Q mutation and Lys^{104} acetylation cause complete disruption of H2 within SWII *(67)*. However, given our findings that KRAS K104Q retains the ability to hydrolyze GTP (**Figure 4.1B**), it is unlikely that helix 2 undergoes a full helix-coil transition upon mutation or acetylation. To better address this apparent discrepancy, we employed NMR spectroscopy to characterize structural and dynamic changes in KRAS upon mutation of lysine 104 to a glutamine. We first assigned the backbone resonances of WT and KRAS K104Q bound to

Mg^{2+} and GDP by acquiring a series of triple resonance NMR experiments on ^{13}C,^{15}N-enriched KRAS 1–169 *(195)*. We were able to assign 159 and 161 of 167 non-proline backbone NH, Cα, and Cβ resonances for WT and KRAS K104Q, respectively. A 2D ^{1}H-^{15}N heteronuclear single quantum coherence (HSQC) spectral overlay of K104Q and WT KRAS bound to GDP is shown in Fig. 3. ^{1}H-^{15}N HSQC spectra allow for the detection of protons directly bonded to a ^{15}N, including both backbone and side chain NH resonances. Because an NH resonance can be detected for every residue with the exception of proline, the spectrum contains a "fingerprint" of the protein backbone. Inspection of chemical shift differences between KRAS WT and K104Q bound to GDP show that ∼30% of the backbone NH peaks undergo changes in peak position. Using chemical shift perturbation (CSP) analyses (**Figure 4.4A**), we found that the largest CSPs (>0.2 ppm) corresponded to residues proximal to the site of the mutation (positions 102–110) and within SWII. Smaller (<0.2 ppm) CSPs were observed for residues within the first β-sheet. In contrast, residues in SWI do not show significant CSPs. These findings are consistent with perturbation of contacts between Lys^{104}, Arg^{73}, and Gly^{75}at the end of SWII due to mutation of Lys^{104} to glutamine.

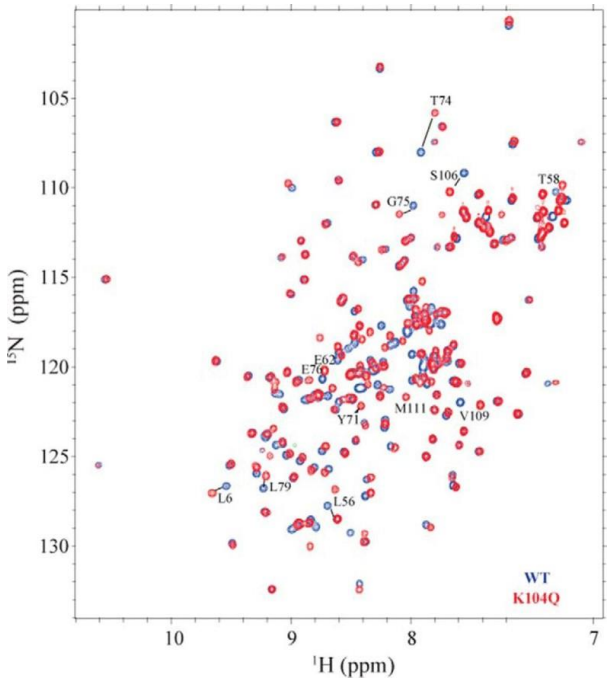

Figure 4.3. 2D ^{1}H-^{15}N HSQC NMR spectral overlay of ^{15}N-enriched KRAS K104Q (*red*) and WT (*blue*). Residues that show significant chemical shift perturbations (CSP > 0.15) are marked. Spectra were recorded on a Bruker Avance III 700 at 25 °C using 0.7 mM KRAS WT and KRAS K104Q bound to GDP.

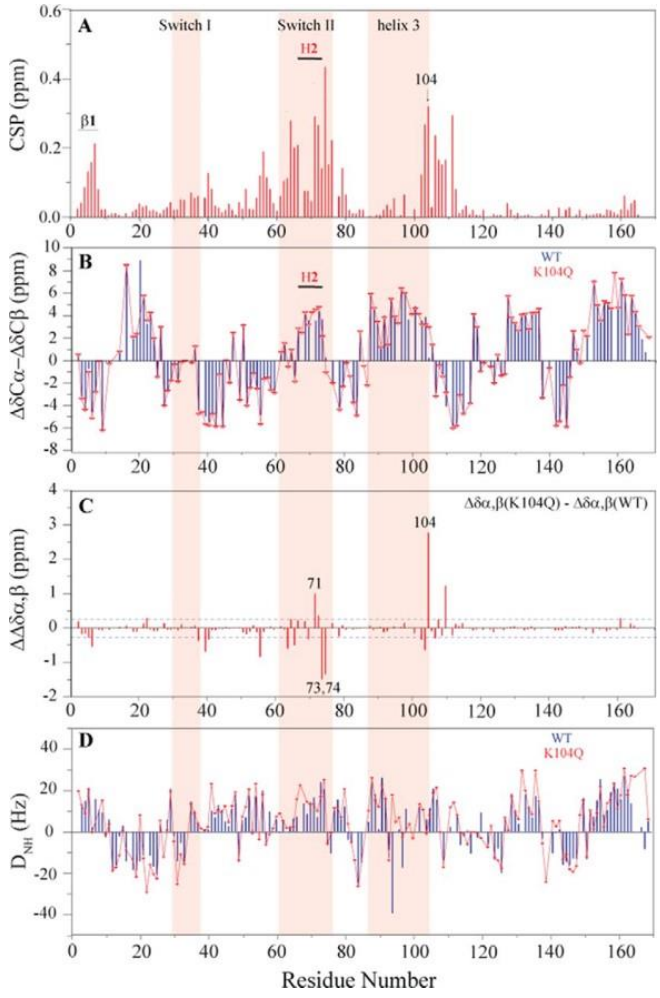

Figure 4.4. K104Q causes structural and dynamic perturbations primarily in helix 2 and helix 3.

A. NMR analyses of peak shifts reveal that the K104Q mutation causes large CSPs in switch II and residues 102–110 in helix 3 but minor changes in β1 and switch I. CSP was calculated based on weighted average chemical shift (square root of $((\Delta\sigma\ ^{1}H)^2 + (\Delta\sigma\ ^{15}N)^2/25)$) of WT and K104Q KRAS NH peaks in ^{1}H-^{15}N 2D HSQC NMR spectra. B. differences in secondary structure were determined from Cα and Cβ chemical shift indexing. C. the difference in chemical shift indexing between K104Q and WT KRAS indicates that the KRAS K104Q mutation perturbs the local conformation surrounding 104 in H3 and the later part of the α2 helix (residues 71–74) in switch II. *D*, NH RDCs were obtained from alignment in Pf1 bacteriophage with deuterium splitting of ~15 Hz. Switch I, switch II, and H3 are highlighted in *pink* (*ribbon*). NMR spectra were recorded at 25 °C on KRAS WT and K104Q (0.7 mm) bound to GDP using a Bruker Avance III 700 NMR spectrometer.

Because a comparison of Cα and Cβ chemical shifts can be used to evaluate differences in secondary structure *(196),* we employed chemical shift indexing (CSI) to compare secondary structural differences between K104Q and WT KRAS (**Figure 4.4B**). We found that overall, the secondary structure of WT KRAS is similar to K104Q with the exception of H2 and H3. In contrast to MD predictions that KRAS K104Q completely disrupts the structural integrity of the SWII region, CSI analyses (**Figure 4.4C**) indicate loss of secondary structure for residues 70–74 at the C-terminal end of H2 and loss of helical content for residues 102–103 in helix 3 (H3) near the mutation site (**Figure 4.4B**), which is consistent with the T_m decrease observed for K104Q. These secondary structural changes correlate with the large CSP observed for these residues (**Figure 4.4A**). The perturbed regions revealed by NMR are highlighted in the 3D structure (**Figure 4.5B**). Small distortions in secondary structure were also observed for the first half of SWII, β1, and the loop between SWI and SWII. However, SWI is unperturbed, consistent with our findings that binding of K104Q to effector RBDs is retained (**Figure 4.1C**). We also collected backbone NH residual dipolar coupling (RDC) data to generate long range distance constraints and evaluate changes in tertiary structure. As shown in Fig. 4D, comparison of the RDC profile for WT and KRAS K104Q indicates that the K104Q mutation does not significantly alter the overall tertiary structure of KRAS.

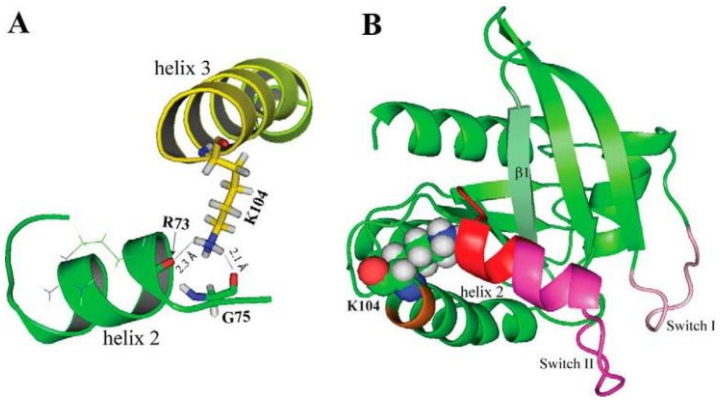

Figure 4.5. The side chain of Lys[104] in helix 3 interacts with helix 2 in switch II.

A. expanded region illustrating interactions between H3 and H2, derived from the X-ray structure of KRAS-GDP (PDB 4LPK, resolution 1.5 Å). Hydrogen atoms were added to structure using XLeap (Amber). The Lys[104] amino side chain is in close proximity to backbone carbonyl oxygens of Arg[73] (H2) and Gly[75] in switch II. B. structural perturbations revealed by NMR are mapped on the 3D structure (PDB code 4LPK). Switch I and switch II are *colored* with *pink* and *purple*, respectively. Lys[104] is represented by *spheres*. The perturbed regions, as determined by NMR-derived CSP and chemical indexing, are highlighted in *red* for the latter part of the H2 and the α2-β4 loop (residues 71–76) and *yellow* for residues 102–103 in H3.

The KRAS K104Q Shows Backbone Dynamics Similar to Those of WT KRAS

The switch regions of RAS have been shown to sample multiple conformations in both the GDP- and GTP-bound states, as revealed by NMR *(48),(197),(198)*. Conformational dynamic properties of these key regions are important for recognition of regulatory and effector proteins. Given the disruption in secondary structure within SWII, we evaluated whether the K104Q mutation alters backbone dynamic properties of KRAS, in the absence of regulatory proteins or effectors. We collected spin relaxation parameters R_1 (**Figure 4.6A**), R_2 (**Figure 4.6B**), and ^{15}N-(^{1}H) NOE (**Figure 4.6C**) and fit them to spectral density functions for obtaining order parameters *(199)*. The order parameter S^2provides a measure of restriction of motion over the picosecond to nanosecond range; whereas $S^2 = 1$ suggests that the NH vector is rigidly fixed in the molecular frame, $S^2 = 0$ is indicative of high mobility. Consistent with an increase in

backbone motion due to structural perturbations at residues proximal to the site of mutation and the C-terminal end of H2, reduced S^2 values were observed in the loop (positions 104–107) between H3 and β5 (**Figure 4.6D**) as well as for residues 72–73 in SWII. A smaller decrease in S^2 is observed for residues in SWI. We also observed that the K104Q mutation slightly enhances fast time scale backbone motions for the loop preceding H2 and residues 94–96 in H3. Taken together, these observations are consistent with our findings that H2 and H3 undergo small scale structural distortions and that the altered GEF and GAP activities observed for KRAS K104Q are probably due to changes in protein structure rather than the altered switch dynamics.

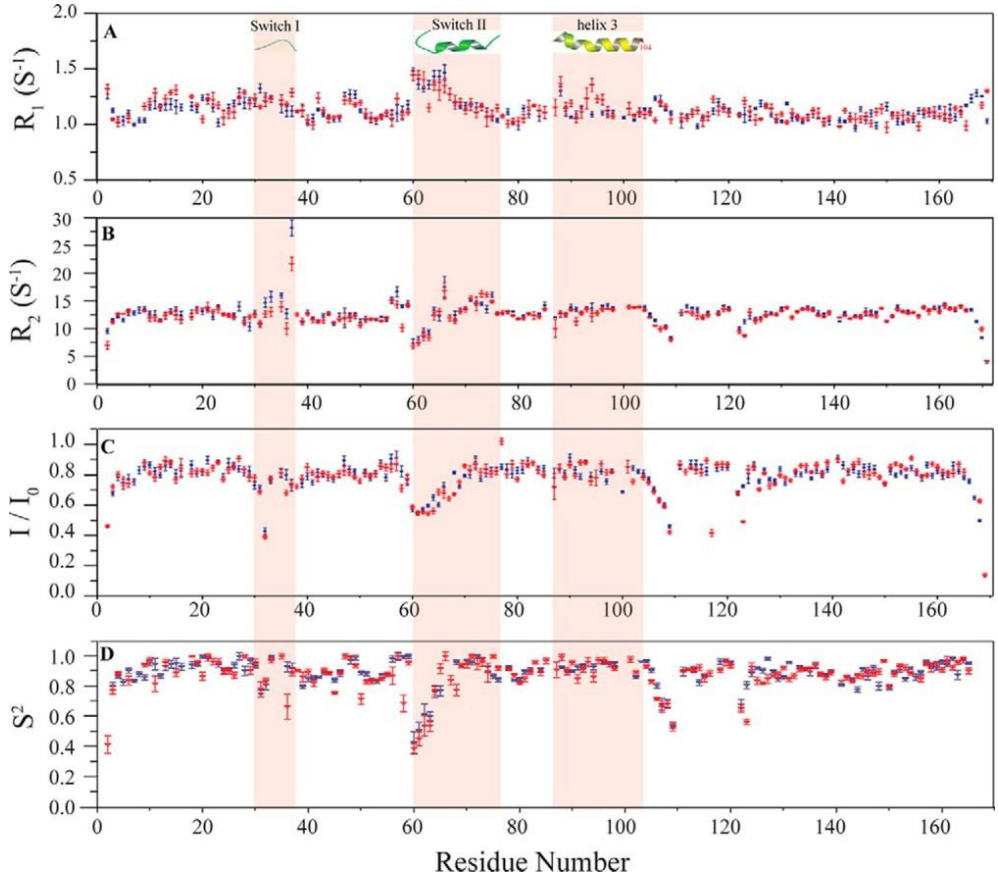

Figure 4.6. Backbone ^{15}N relaxation parameters for K104Q KRAS (*red*) and WT KRAS (*blue*). Shown from *top* to *bottom*, plotted against residue number, are longitudinal relaxation R_1 (A), transverse relaxation R_2 (B), (^{1}H)-^{15}N steady state heteronuclear NOE ($I_{saturated}/I_{unsaturated}$) (C), and order parameter S^2 (D). Switch I, switch II, and H3 are highlighted in *pink* (*ribbon*) with secondary structure content represented at the *top*. Residue 104 at the end of H3 is labeled in *red*. All measurements were performed on KRAS WT and K104Q bound to GDP. NMR data were collected at 25 °C on 0.2 mm KRAS WT and K104Q samples using a Bruker Avance III 700 NMR spectrometer.

KRAS K104Q Does Not Affect Growth in MEFs

Because the KRAS K104Q mutation is impaired in GEF/GAP-mediated nucleotide cycling yet retains the ability to bind the RAF RBDs and PI3Kγ, we conducted studies in cell culture to determine the role of the K104Q mutation in KRAS-driven cellular growth. For these studies, we employed the use of Rasless MEFs, which lack endogenous *Hras* and *Nras*, and a

conditional *Kras* allele that can be ablated by activation of a knocked-in 4-hydroxytamoxifen-inducible CreERT2 recombinase *(200)*. 4-Hydroxytamoxifen treatment was done to induce Cre-mediated disruption of the *Kras*allele with blotting analyses to verify loss of endogenous Kras protein expression (Fig. 7A). These viable but non-proliferating cells were then used to assess the ability of either WT KRAS or KRAS K104Q to rescue loss of endogenous Kras and restore proliferation. We found that both K104Q and WT KRAS were equally capable of promoting MEF proliferation, as assessed by 3-(4,5-dimethylthiazol-2-yl)-2,5-diphenyltetrazolium bromide (MTT) growth assays (**Figures 4.7, B and C**). These results suggest that KRAS acetylation may not impair the ability of KRAS to drive growth in a KRAS-dependent system. Based on our findings that K104Q is impaired in both GEF and GAP regulation, the disruption in GEF-mediated up-regulation by the K104Q mutation may be partially offset by a defect in GAP-mediated down-regulation of KRAS. Our findings that KRAS K104Q supports the growth of Rasless MEFs indicate that this mutant can still efficiently activate the RAF-MEK-ERK pathway, because this pathway is critical for the growth of Rasless MEFs *(200)*.

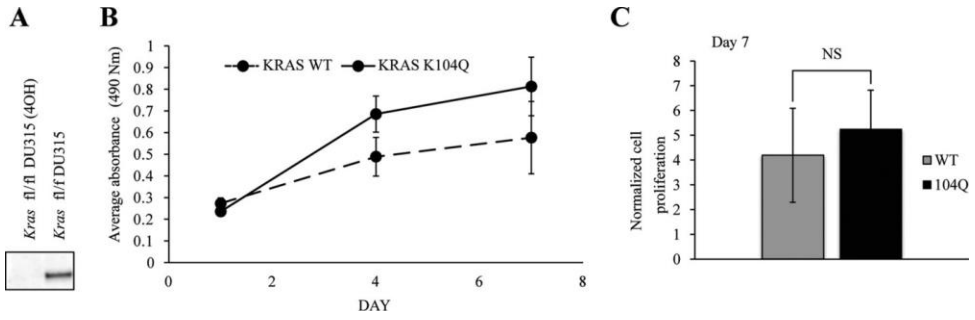

Figure 4.7. Exogenous KRAS K104Q expression supports the growth of Rasless MEFs.

A. the anchorage-dependent growth rate was determined for MEFs deficient for all *Ras* isoforms with ectopically expressed KRAS WT or K104Q. B. cells were plated, and growth was monitored at days 1, 4, and 7 using the MTT viability assay. Data shown are representative of two independent experiments. Data are the mean ± S.D. (*error bars*) (*n* = 48). Student's *t* test determined that the difference was not significant (*NS*). C. quantitation of the average ± S.D. of three independent experiments for day 7. Data shown are the average of three independent experiments.

The KRAS K104Q Variant Retains RAS Activity, Downstream Signaling to Critical KRAS Effectors, and KRAS-driven Transformation in NIH 3T3 Cells

We next assessed the consequences of the K104Q substitution for the cellular activity of WT and G12V KRAS when transiently expressed in NIH 3T3 mouse fibroblasts. First, we performed a RAF-RBD pull-down analysis to assess the relative steady-state levels of activated GTP-bound KRAS protein. The K104Q substitution did not significantly alter the low level of GTP-bound protein for WT KRAS or the elevated level for KRAS G12V (**Figure 4.8**). Similarly, KRAS G12V- and KRAS G12V/K104Q-expressing cells exhibited comparable levels of effector signaling, with equivalent levels of phosphorylated and activated ERK and AKT (**Figure 4.9**) and morphologic transformation (**Figure 4.10**). We conclude that mutation of Lys^{104} to glutamine (a putative acetylation mimetic) did not significantly alter KRAS function.

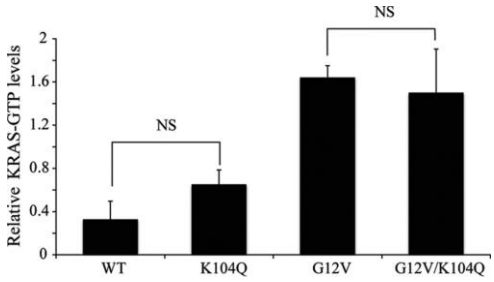

Figure 4.8. The K104Q mutation does not alter the levels of GTP-bound KRAS.

CRAF RBD pull-down analyses were done using cell lysates from NIH 3T3 cells transiently expressing (72 h post-infection) the indicated HA epitope-tagged KRAS WT or mutant proteins. GST-CRAF RBD was used to monitor the level of GTP-bound KRAS protein, with total expression determined by anti-HA blot of total cellular lysates. Data shown are representative of three independent experiments. Quantitation of three experiments done in *A* (*n* = 3), with KRAS-GTP levels normalized to total HA-tagged KRAS levels. *Error bars*, S.E. Student's *t* test determined that the difference was not significant (*NS*).

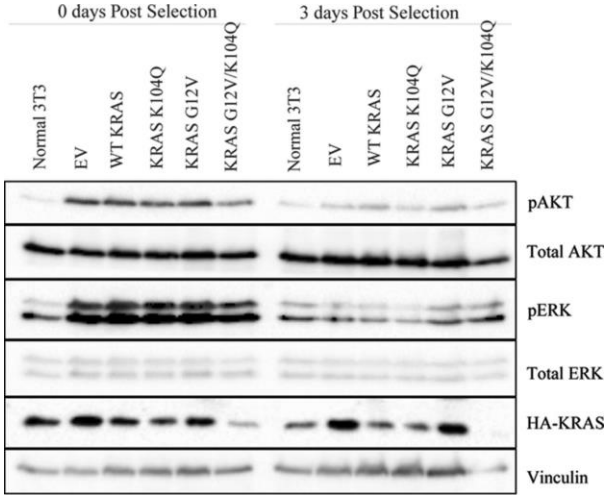

Figure 4.9. The K104Q mutation does not alter KRAS effector signaling in NIH 3T3 cells.

Shown is Western blotting analysis of total cell lysates from mass populations of NIH 3T3 cells transiently infected (72 h) with retrovirus expression vectors encoding the indicated KRAS proteins. Blotting analyses with antibodies for total or phosphorylated and activated AKT and ERK (*pAKT* and *pERK*, respectively) were done. Data shown are representative of three independent experiments.

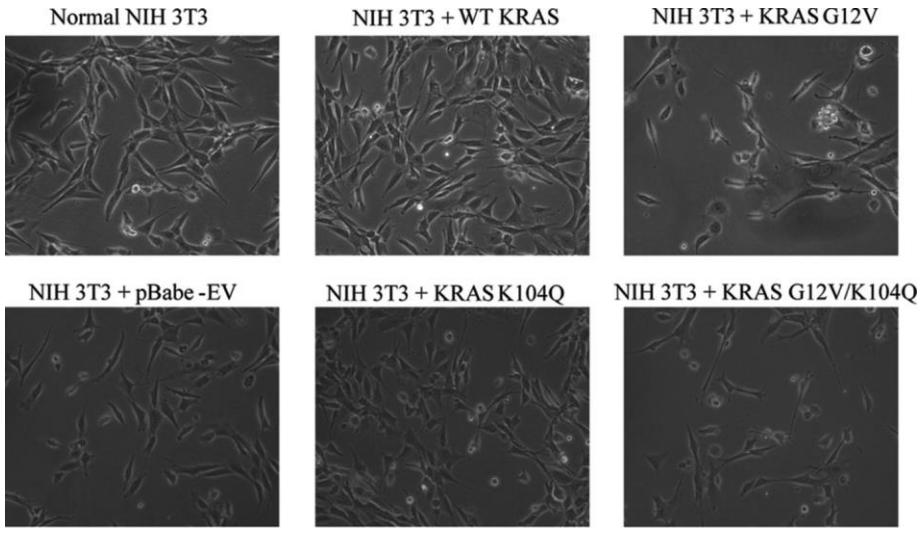

Figure 4.10. The K104Q mutation does not alter wild type or activated KRAS morphologic transforming activity.

Shown is a photomicrograph of mass populations of NIH 3T3 cells transiently (24 h) infected with pBabe-puro retrovirus expression vectors encoding the indicated KRAS proteins.

Discussion

Whereas GEF and GAP proteins play a critical role in regulating the activation state of RAS proteins, post-translational modifications within the G domain of RAS add another level of complexity. Lysine 104 in KRAS undergoes multiple PTMs, including acetylation *(67)* and ubiquitylation *(62)*. Because oncogenic mutations at this position have not been identified in H-, N-, or KRAS, the role of this key residue has not been well characterized. Here, we show that both conservative and non-conservative mutations at KRAS lysine 104 (Gln, Arg, and Ala) impair SOS^{cat}-mediated nucleotide exchange. The K104Q mutant also impairs p120 $RASGAP^{cat}$-mediated GTP hydrolysis. Consistent with these observations and our findings that KRAS K104Q shows a small decrease in thermal stability (1.5 °C), NMR structural analysis indicates that the K104Q mutation perturbs protein conformation proximal to the site of mutation in H3 as

well as the end of H2 in SWII. Both of these regions are part of the RAS/SOS^{cat} binding interface *(36)*. Residues 61–64 and 67 in SWII also form binding interactions with RAS GAP^{cat} *(13)*.

Residues within H2 and H3 of RAS form multiple interactions with SOS1^{cat} in crystal structures of RAS proteins bound to SOS1 (PDB codes iBKD, 1NVW, and 1XD2) *(36),(54),(131)*. In particular, Arg102 in H3, next to the mutation site, forms contacts with Phe1010and Asp1007 in SOS^{cat}. Valine 103 in H3 interacts with Ser881 in SOS^{cat}. Moreover, residues Gln70, Tyr71, and Arg73 at the end of H2 in RAS form multiple binding interactions with SOS^{cat} *(201)*. Specifically, Tyr71 forms a hydrogen bond with Tyr912 of SOS^{cat}. Additionally, the side chain of Arg73 forms a hydrogen bond with the carboxyl oxygen of Asn879, and its aliphatic side chain forms additional interactions with the aromatic ring of Tyr884 in SOS^{cat}. Thus, structural distortions due to either mutation or PTM in H2 could potentially impair binding interactions to SOS^{cat}. Given the structural distortions observed for residues in SWII and H3, it is not surprising that binding to and subsequent nucleotide exchange ability of SOS^{cat} is impaired by the K104Q mutation *(36),(201)*. In addition to SOS, residues in SWII, including Glu63 and Tyr64, make multiple contacts with RAS GAP proteins (PDB code1WQ1) *(13)*. Structural distortions at the end of SWII may cause more subtle changes in these key residues, resulting in the partial disruption of GAP-mediated GTP hydrolysis, observed for KRAS K104Q.

Consistent with our findings that the structure of the KRAS SWI region is not perturbed by the K104Q mutation, the KRAS K104Q mutant shows similar binding to isolated RAS effector RBDs, such as CRAF and BRAF, which bind exclusively through SWI (PDB code 4GON). A distinct effector, PI3Kγ, interacts with RAS primarily at SWI but also forms additional contacts with Tyr64 and Arg73 in SWII (PDB code 1HE8). Despite the structural

perturbations induced by the KRAS K104Q mutation in the SWII region, KRAS K104Q retains binding to PI3Kγ. Whereas RAS interacts with a number of downstream effectors to regulate cellular growth, our analyses in Rasless MEFs indicate that the K104Q substitution does not prevent KRAS WT from driving proliferation in this biological context. Furthermore, our analyses in NIH 3T3 cells indicate that K104Q did not significantly alter the steady-state GTP-bound state or effector signaling and activation of ERK or AKT. These studies also indicate that KRAS G12V/K104Q is equally capable of driving morphologic transformation in NIH 3T3 cells. Hence, if K104Q functions as an acetylation mimetic, our studies indicate that this PTM may not significantly impair mutant RAS oncogenic function in these cells. Our findings differ from those described previously *(67)*, where K104Q did reduce KRAS G12V stimulation of NIH 3T3 cell proliferation. Because these analyses evaluated morphologic and not growth transformation, our results cannot be directly compared with those of the previous study. One possible explanation for our different conclusions is that there exist multiple strains of NIH 3T3 cells and there are strain-specific differences in the mechanisms by which RAS drives growth transformation *(202)*.

In summary, we found that the K104Q mutation in KRAS impaired GEF and GAP regulation but retained interactions with RAF and PI3Kγ RBDs. Our observations that signaling and cellular growth properties of K104Q are similar to those of WT KRAS suggest that the partial defect in GEF is at least partially offset by a defect in GAP regulation to retain RAS signaling. It is unclear whether the K104Q mutation or acetylation at this position perturbs interactions with all RAS GEFs. Whereas the CDC25 domains associated with RASGRP and RASGRF proteins show high homology *(35),(203)*, allosteric regulation of these GEFs is quite

distinct from that of SOS1. Moreover, crystal structures of these GEFs in complex with RAS are lacking.

Given the difficulties in preparation of various protein PTMs, mutations are often used as reagents to either mimic the desired modification or prevent the PTM. Although K104Q has been employed as an acetylation mimetic, this has yet to be truly validated *(70)*. In fact, Lys^{104} acetylation has recently been reported to retain SOS activity *(68)*. Computational analysis of the Ku protein revealed that acetylation of the Ku may not alter DNA interaction, yet a K-to-Q mutation decreased the binding compared with the WT protein *(70)*. Indeed, the side chain of glutamine is quite distinct from an acetylated lysine in both size and composition, and it is unlikely that the K104Q mutant will be recognized by acetylation readers or deacetylases, such as SIRT2 and HDAC6, in a similar manner to native acetylated RAS *(117)*. Although emerging data indicate that Lys-to-Gln mutations may not fully mimic acetylation, our studies do indicate that Lys^{104}, a hot spot for RAS PTMs, plays a key role in maintaining the structural integrity of H3 and H2. Given the proposed role of H3 in RAS-mediated dimerization at the membrane, it is possible that KRAS acetylation may alter RAS dimerization *(204)*. It will be important to evaluate each PTM (acetylation, ubiquitylation) separately to determine how the PTM may directly alter RAS activity as well as protein-protein interactions.

Materials and Methods

Protein Expression and Purification

The human KRAS4B (C118S) cDNA sequence encoding the G domain (residues 1–169) was subcloned into a pET21 vector that adds an N-terminal 6-histidine tag and a TEV protease cleavage site for expression of recombinant protein in *Escherichia coli* BL21(DE3) cells (Novagen). Standard site-directed mutagenesis techniques were used to generate *KRAS* cDNA

sequences encoding K104Q, K104A, and K104R missense mutants. The mutations were subsequently verified by DNA sequencing. *E. coli* BL21 (DE3) cells were grown at 37 °C in Luria-Bertani (LB) medium supplemented with ampicillin and chloramphenicol until A_{600} of ~0.5. The temperature was then lowered to 18 °C, and KRAS expression was induced with 0.5 mM isopropyl-β-D-1-thiogalactopyranoside (IPTG) after 30 min. The cells were grown for an additional 15 h at 18 °C. The cells were then harvested and pelleted at 4000 rpm, resuspended in a lysis buffer (20 mM HEPES, 500 mM NaCl, 1 mM $MgCl_2$, 20 mM imidazole, 5% glycerol (pH 7.75), and protease inhibitor phenylmethanesulfonyl fluoride (ACROS Organics)), and sonicated. The cell lysate was centrifuged at 15,000 rpm, and the supernatant was isolated. KRAS proteins were purified using nickel-nitrilotriacetic acid-agarose affinity chromatography (Qiagen), and the histidine tag was cleaved during overnight dialysis using TEV protease. If needed, KRAS proteins were further purified by size exclusion chromatography using a Sephadex G-75 column. Protein purity of >95% was obtained and verified by SDS-PAGE analysis.

The catalytic domains of human SOS1 (SOS^{cat}, residues 566–1049) *(131)* and p120-RASGAP (GAP^{cat}, residues 764–981) were expressed in a pQlinkH vector (Addgene) and purified as described previously *(63)*. cDNA sequences encoding the isolated RBDs of human BRAF (amino acids 149–232) and CRAF (amino acids 51–132) were subcloned in a pET28a bacterial expression vector encoding an N-terminal 6-histidine tag and TEV cleavage sites and subsequently expressed in BL21 (DE3) cells. The RBDs were purified using nickel-nitrilotriacetic acid affinity chromatography. The N-terminal tags were cleaved overnight with TEV protease. The tagless BRAF RBD was further purified using size exclusion chromatography (Sephadex G-75) and verified to be >95% pure by SDS-PAGE analysis.

Purified PI3Kγ protein (amino acids 144–1102) containing a K802T substitution was kindly provided by Genentech.

Expression and Purification of His_6-WT KRAS, K104Q, and Ac-Lys^{104} Proteins

His_6-WT KRAS (residues 1–169, containing a 12-amino acid N-terminal non-cleavable His_6 tag) and K104Q were expressed in LB medium as His_6-tagged fusion proteins (pRSF-Duet, Merck Biosciences) in *E. coli* BL21 (DE3) cells as described *(68)*. The *E. coli*culture was grown to an A_{600} of 0.6 (37 °C; 160 rpm), and protein expression was subsequently induced by the addition of 300 μM IPTG and further incubated overnight for 16 h (18 °C, 160 rpm). KRAS containing an amber stop codon at Lys^{104}, was co-expressed with a pRSF-Duet-1 vector containing the synthetically evolved *Methanosarcina barkeri* MS $tRNA_{CUA}$ (*Mb*$tRNA_{CUA}$)/acetyl-lysyl-tRNA-synthetase (pAcKRS3) pair in Terrific broth medium. The *E. coli* BL21 (DE3) KRAS Ac-Lys^{104} culture was grown to an A_{600} of 0.6 at 37 °C at 160 rpm and then supplemented with 10 mM *N*-(ϵ)-acetyl-lysine (Chem-Impex International Inc.) and 20 mM nicotinamide to inhibit the *E. coli* deacetylase CobB. The temperature was then reduced to 18 °C. After 30 min, protein expression was induced by the addition of 300 μM IPTG. The cells were then grown for 16 h at 20 °C. After expression, the cells were harvested (4000 × *g*, 20 min) and resuspended in a buffer containing 50 mM Tris/HCl, pH 7.4, 100 mM NaCl, 5 mM $MgCl_2$, 2 mM β-mercaptoethanol, and 200 μM Pefabloc protease inhibitor mixture for His_6-WT KRAS and K104Q. For His_6-KRAS Ac-Lys^{104}, a buffer containing 50 mM K_2HPO_4/KH_2PO_4, pH 6.4, was used. The cells were lysed by sonication, and the soluble fraction (20,000 × *g*, 45 min) was applied to an equilibrated Ni^{2+}-nitrilotriacetic acid affinity chromatography column. The column was washed with a buffer containing 10 mMimidazole and 1 M NaCl, pH 6.4. The His_6-KRAS proteins were eluted with an imidazole gradient of ∼10

column volumes covering 10–500 mM imidazole. The protein was concentrated by ultrafiltration and applied to a HiLoad 16/600 Superdex 75 pg size exclusion chromatography column (GE Healthcare).

RAS Nucleotide Dissociation and Hydrolysis Assays

The rate of nucleotide dissociation was measured by a fluorescence-based assay using MANT-GDP (BioLog, San Diego, CA) as reported previously *(134),(135)*. Briefly, MANT-GDP-bound RAS was added to 1 ml of assay buffer (20 mM HEPES, 50 mM NaCl, 5 mM $MgCl_2$, and 100 μM diethylenetriaminepentaacetic acid (DTPA), pH 7.4) to a final concentration of 1 μM, and nucleotide exchange was initiated by the addition of 1 mM GDP. MANT-GDP dissociation was measured as a change in fluorescence intensity over time (excitation, 365 nm; emission, 435 nm) (LS50B PerkinElmer Life Sciences luminescence spectrometer). Fluorescence data were fit in GraphPad Prism (GraphPad Software, La Jolla, CA) to a one-phase exponential decay curve. For GEF-mediated dissociation, 1 μM RAS and 1 μM SOS^{cat} were used. Results are plotted as the mean ± S.E. (n = 3).

Single-turnover GTP hydrolysis assays were performed as described previously *(154)* using the phosphate-binding protein Flippi 5U (Addgene) to detect inorganic phosphate released upon GTP hydrolysis *(155)*. Flippi 5U was purified as described previously *(155)*. All buffers were made phosphate-free by dialysis with 1 unit of nucleoside phosphorylase (Sigma) and 2 mM inosine (Sigma). For GAP-mediated hydrolysis, 10 μM RAS was used with 0.05 μM p120-$RASGAP^{cat}$ (1:200). The ratio of fluorescence emission was measured at 485 and 530 nm with an excitation of 420 nm on a SpectraMax M5 microplate reader (Molecular Devices). Hydrolysis curves were fit in GraphPad Prism to a one-phase exponential association curve. Results are plotted as the mean ± S.E. (n = 2).

Effector Binding Assay

KRAS was preloaded with MANT-GMPPCP using methods described previously *(28)*. For quantitative binding to CRAF and BRAF RBDs and PI3Kγ (amino acids 144–1102, containing a K802T substitution), MANT-GMPPCP-bound KRAS was incubated with the desired effector at a range of concentrations, in a buffer containing 50 mM HEPES, 50 mM NaCl, and 5 mM $MgCl_2$ at pH 7.4. Nucleotide dissociation was initiated by the addition of a 1000-fold molar excess of unlabeled nucleotide, and the rate of dissociation was determined by monitoring the change in fluorescence of the MANT-GMPPCP-loaded protein (excitation and emission wavelengths of 335 and 485 nm, respectively) using a SpectraMax M2 plate reader *(134)*. Each nucleotide dissociation curve was fit to a one-phase single exponential to determine k_{obs}. The dissociation rates were plotted against the effector concentrations and fit as described previously *(205)* to determine the equilibrium dissociation constant (K_D).

T_m Measurements Using CD

CD data were collected on a Jasco J-815 CD spectrometer. Far-UV CD scans were collected using a 1-mm cuvette at a concentration of 20 μM KRAS protein in a buffer containing 10 mM $KH_2PO_4^{3-}/K_2HPO_4^{3-}$, 500 μM $MgSO_4$, pH 7.2, at 20 °C. Thermal melts were obtained over a temperature range of 20–95 °C using a temperature increment of 2 °C/min. The CD signal was measured at 222 nm. T_m values were calculated by fitting the thermal denaturation data using non-linear fitting. Results are plotted as the mean ± S.D. (n = 3).

NMR Analyses

For NMR measurements, ^{13}C,^{15}N-enriched KRAS proteins were exchanged into NMR buffer (20 mM Tris-maleate (pH 6.5), 40 mM NaCl, 5 mM $MgCl_2$, and 20 μM GDP, 5% D_2O). NMR spectra were acquired at 25 °C on a Bruker Avance III 700 NMR spectrometer. 2D ^{1}H-^{15}N

HSQC experiments were recorded for both WT and K104Q KRAS bound to GDP, with 1024 and 256 complex points in the direct and indirect dimensions, respectively, 32 scans/increment, and a recovery delay of 1.0 s. Spectral widths used were 9803.992 Hz (^{1}H) and 2553.626 (^{15}N) Hz. Average ^{1}H-^{15}N chemical shift perturbations were calculated according to the square root of $((\Delta\sigma\ ^{1}H)^2 + (\Delta\sigma\ ^{15}N)^2/25)$, where $\Delta\sigma\ ^{1}$H and $\Delta\sigma\ ^{15}$N are the observed changes in ^{1}H and ^{15}N chemical shifts. Backbone resonance assignments of WT KRAS were obtained by analysis of 3D HNCA, HNCACB, CBCA(CO)NH, HNCO, and HN(CO)CA spectra recorded on ^{13}C,^{15}N-labeled WT KRAS bound to GDP. The assignment of Cα, Cβ, CO, N, and HN chemical shifts was obtained by an iterative procedure using the program MARS *(206)* and manual inspection. Backbone assignment of ^{13}C,^{15}N-enriched K104Q KRAS (0.8 mM) was obtained by collecting 3D HNCA and HNCACB data and using WT KRAS assignments. For CSI, ΔCα and ΔCβ values were calculated by subtracting experimental chemical shifts of Cα and Cβ from random coil values obtained from the ncIDP server *(207)*. The value of ΔCα-ΔCβ was calculated to cancel the systematic offset contained in ΔCα and ΔCβ and then used to predict RAS secondary structure. For ^{15}N-based backbone relaxation experiments, ^{15}N longitudinal (R_1) and transverse relaxation (R_2) rates and ^{1}H-^{15}N steady-state NOE were measured on 200 μM ^{15}N WT and K104Q KRAS-GDP samples in NMR buffer at 700 MHz. Relaxation delays were as follows: R_1measurements, 0.01, 0.1, 0.2, 0.3, 0.4, 0.6, 0.8, 1.0, 1.2, and 1.4 s; R_2 experiments, 15.01, 45, 165.11, 30.02, 135.09, 60.04, 105.07, 75.05, and 90.06 ms. The ^{15}N-(^{1}H) NOE and reference spectra were recorded in an interleaved manner with a 5.5-s ^{1}H saturation time and the equivalent recovery time for the reference experiment. Order parameters (S^2) were calculated by fitting relaxation parameters R_1, R_2, and ^{15}N-(^{1}H) NOE using the programs FAST ModelFree *(208)* and ModelFree *(209)*. Backbone NH RDCs were measured using Pf1 bacteriophage (20

mg/ml) (ASLA Biotech) with deuterium splitting of 15 Hz. The $^{1}J_{NH}$ constant was measured using an interleaved HSQC-TROSY. Spectra were processed and analyzed using NMRPipe (NIDDK, National Institutes of Health) and Sparky (University of California, San Francisco).

Cell Lines

NIH 3T3 mouse fibroblasts were obtained originally from Dr. Geoffrey Cooper (Boston University) and were maintained in Dulbecco's modified Eagle's medium (DMEM) supplemented with 10% calf serum (Colorado Calf Serum). Mouse embryonic fibroblasts devoid of endogenous *Ras* alleles (Rasless MEFs) were obtained from Dr. Mariano Barbacid (CNIO Madrid) and were maintained in DMEM supplemented with 10% calf serum *(200)*.

Rasless MEF Growth

Primary mouse embryonic fibroblast (MEFs; DU315) devoid of all endogenous RAS protein expression (*Hras*$^{-/-}$; *Nras*$^{-/-}$; *Kras*$^{lox/lox}$; RERT$^{ert/ert}$) were generated and characterized previously *(200)* and were obtained from Dr. Mariano Barbacid (CNIO, Madrid, Spain). In brief, DU315 cells were treated with 600 nM 4-hydroxytamoxifen to activate translocation of the estrogen receptor-fused Cre to the nucleus for removal of the endogenous (floxed) *Kras*. Cells were arrested in the G_1 phase after 9–11 days. Blot analyses were done to verify loss of endogenous KRAS protein expression. Cell proliferation resumed after the delivery of a *KRAS* transgene to the cells using lentiviral transduction. Transduced cells were selected using blasticidin and expanded to generate cell line pools dependent on expression of the exogenous transgene for continuous proliferation.

Anchorage-dependent Growth Assays

To monitor proliferation rates, cells were plated onto a 96-well plate at a density of 2000 cells/well. After 24, 96, and 168 h, cell proliferation was monitored using the MTT colorimetric viability assay, and absorbance was measured at 550 nm to quantify cell number.

NIH 3T3 Infection

NIH 3T3 cells were infected with the pBabe-puro retrovirus expression vectors containing cDNA sequences encoding human KRAS4B (WT, K104Q, 12V, and 12V/K104Q). Post-infection, the cultures were maintained in complete growth medium supplemented with puromycin to select for stably infected cells. Samples were collected immediately after 72 h post-selection and analyzed for signaling via Western blotting. The drug-resistant cells were further passaged and maintained in puromycin-containing growth medium. Light microscopy images were collected at 24 h (Nikon Eclipse TS100) post-selection to monitor transformation.

RAS-GTP Pull-down Assays

NIH-3T3 cells were infected with retrovirus containing cDNA for KRAS (WT, K104Q, 12V, 12V/K104Q), followed by selection in puromycin-containing growth medium, to establish mass populations of drug-resistant cells. Determination of the steady-state GTP-bound levels of each KRAS protein was performed using standard pull-down analyses as described by us previously *(210)*. Briefly, drug-resistant mass populations of cells maintained in complete calf serum-containing growth medium were collected 72 h post-infection for analyses. The cultures were lysed in detergent buffer, and the total cell lysates were then incubated with recombinant glutathione *S*-transferase (GST)-tagged CRAF RBD protein, followed by Protein G-Sepharose beads, to isolate the bound KRAS-GTP. After separation by SDS-PAGE, the level of KRAS-GTP was determined by blot analyses with anti-KRAS antibody. Total FLAG epitope-tagged KRAS was determined by blot analyses with anti-FLAG antibody using the total cellular lysate.

Retrovirus Production

Retrovirus was produced in HEK-293T cells via transfection of pBABE-puro target vector and pCL-10A1 packaging vector with calcium chloride. Cells were allowed to produce retrovirus for 24 h. Retrovirus was then harvested and placed on target cells in the presence of 2 μg/ml Polybrene. Cells were incubated with retrovirus for 8 h. Fresh medium was then placed on the cells, and antibiotic selection was applied 24 h later (2 μg/ml puromycin).

Western Blotting

Cells maintained in complete growth medium were lysed in 1% Nonidet P-40 buffer (50 mM Tris, 150 mM NaCl, 10 mM $MgCl_2$, 10% glycerol, 1% Nonidet P-40, 0.25% sodium deoxycholate, pH 7.4) and resolved using SDS-PAGE analysis. To determine the levels of effector signaling, Western blotting analyses were done using phospho-specific antibodies to ERK1/2(Thr^{202}/Tyr^{204}) and AKT(Ser^{473}), with antibodies recognizing total ERK1/2 and AKT to control for total protein expression (Cell Signaling Technologies). Antibodies for KRAS (OP24, EMD Millipore) and anti-HA epitope (16B12, Covance) were used to determine the expression levels of endogenous and exogenous KRAS, respectively. An antibody for vinculin (Sigma-Aldrich) was used to verify equivalent loading of cellular proteins.

Chapter 5. A Tool for Site-Specific Methyl-Lysine Generation and Selective Enrichment in Intact Proteins[3]

Introduction

Historically, canonical amino acid mutations have been used to study post-translational modifications (PTMs) in intact proteins. It is becoming increasingly evident that canonical amino acids are not capable of truly mimicking their PTM counterparts *(68)–(70)*. Current strategies to generate native post-translationally modified intact proteins are limited. This is especially true for methylation. Several methods have been proposed such as chemical ligation reactions and the use of unnatural amino acids, but these approaches have exhibited limited success to date *(211)*. In a physiologic setting, a methyl group would be transferred from a cofactor, such as *S*-adenosyl-L-methionine (SAM), in an S_N2 fashion where the ε-amine of the lysine would carry out nucleophilic attack on SAM to transfer the methyl group to the recipient *(212)*. This can occur multiple times, generating mono-, di- or trimethylated lysine *(212)*. Simon *et al.* have described an approach using an alkylation reaction to install methyl-lysine analogs (MLAs) in fully denatured histone tails *(213),(214)*. Unfortunately, the harsh reducing and denaturing conditions required in this method are not suitable for some functionally intact, folded proteins.

Methylation status is highly regulated in the cellular milieu, and aberrant methylation signaling has been identified in several cancers *(76),(80)*. As such, it is a reasonable assumption that lysine methyltransferases, KMTs and lysine demethylases, KDMs may be novel therapeutic targets *(97)*. However, given the limited methods to generate methylated proteins, this field

[3] Mass spectrometry analysis and associated methods were provided by Dr. Laura Herring of the UNC Michael Hooker Proteomics Center

remains largely unstudied. While MLAs are highly similar to native methyl-lysine residues, they are incorporated into the protein using a chemically reactive thiol as a linker *(213),(214)*. As such, the final product contains a carbon-sulfur bond rather than a native carbon-carbon bond, which will differ in bond length and angle *(215)*. It is not well understood if MLAs are capable of truly mimicking native lysine methylation. Experimental studies quantifying the ability of MLAs to bind to methyl-binding domains from several families have demonstrated varying conclusions to this question depending upon several factors such as sequence length, modification and binding partner *(215)*. However, as with any non-native modification, caution should be used in experimental design and interpretation. There is no experimental evidence either in support of or against the use of MLAs in functional, intact proteins. To date MLAs represent the most feasible option to study lysine methylation in functional proteins.

Methylation has been primarily studied in the context of histone regulation; however, it is a critical PTM that has been demonstrated to modulate the activity of several non-histone proteins *(78),(80)*. Methylation (and acetylation) of the tumor suppressor protein p53 are known to modulate protein activity *(78),(79)*. Recently, altered lysine methylation patterns have been identified in pancreatic cancer (PDAC) *(76),(77)*. Clinically, PDAC is one of the most challenging cancers to therapeutically treat and is one of the deadliest cancers in the U.S. annually *(123)*. Pancreatic ductal adenocarcinoma (PDAC) is known to be driven by oncogenic KRas proteins, where approximately 98% of PDAC contains activating KRas mutations *(5)*. Interestingly, several KMTs have been identified as upregulated in PDAC, and subsequent analysis verified that methylation of key players of the Ras/MAPK pathway enhanced Ras-mediated oncogenic signaling *(76),(77)*. In particular, knockdown of the KMT SMYD3 inhibited Ras-mediated tumorigenesis in mouse models of PDAC and lung cancer by inhibiting MAP3K2

methylation *(77)*. Despite decades of research, no clinically effective anti-Ras therapeutics have been developed *(24),(82),(107)*. Taken together, this may suggest that methylation plays a dynamic role in regulating the Ras/MAPK signaling cascade. As such, methylation may represent an untapped potential therapeutic target in Ras-driven cancers. To date, the current methods to generate methylated proteins have not been successful with intact, functional Ras proteins. Here, we present a method to site-specifically modify intact, functional Ras proteins with methyl-lysine analogues to generate a product structurally similar to natively methylated proteins. Given that reaction efficiency can vary greatly with the accessibility of the residue to be modified, we further provide a method using 'methyl reader' proteins and competitive small molecules to isolate and enrich for methylated populations of proteins in a variably modified sample.

Site-specific methyl-lysine analogue alkylation reaction

Immediately following cysteine-mutant KRas protein purification, proteins are prepared for methyl-lysine alkylation reactions.

1. An alkylation buffer (100mM HEPES, 50mM NaCl, 5mM $MgCl_2$, 10 mM DTT, 30 uM GDP (pH 7.8)) is chilled and sparged with N_2 for 45 minutes while stirring.
2. Ras proteins are then exchanged into this buffer and concentrated to ~ 1 mg/mL. The pH is maintained at 7.8 to mitigate multiple reactivities with methyl-lysine substrates.
    a. To install methyl-lysine analogues at buried sites in intact proteins, the addition of 250 mM GnHCl can help increase the reaction efficiency.
3. Once intact proteins are prepared in alkylation buffer, 1000x molar ratio of the methylation substrate is added to the reaction mixture.

a. Protein should be delicately pipetted up and down to ensure that methylation substrates were adequately solubilized.
b. Mono- and dimethyl substrates are commercially available (2-chloro-N-methylethanamine hydrochloride and 2-Chloro-N,N-dimethylethylamine hydrochloride, respectively).
c. Mono- and di-methyl-lysine alkylation reactions were conducted at KRas K5C, K117C and K147C.

4. Fresh, 1M DTT was made with the prepared alkylation buffer and added to the reaction at 5 mM final concentration.
5. This reaction was allowed to continue for 2 days at 4 °C.
6. Ras proteins were then desalted using PD-10 columns per manufacturer protocol (GE Healthcare) to remove excess unreacted methyl-lysine substrate and further purified via size exclusion chromatography using a Sephadex G-75 column.

Methyl-binding domain enrichment of methylated Ras

Methylated KRas proteins were further isolated and enriched using the methyl-binding domains of L3MBTL1 or L3MBTL3 (malignant brain tumor family of methyl readers, MBT) and the cognate small molecule competitive binders UNC-669 or UNC-1215, respectively (The University of North Carolina, Chapel Hill Structural Genomics Consortium, Dr. Stephen Frye) *(216),(217).* An on-bead enrichment strategy was used with Ni-NTA agarose beads and His-tagged methyl binding domain proteins.

1. Methylated KRas and His-tagged MBT proteins were dialyzed overnight into a buffer containing 20 mM HEPES, 150 mM NaCl, 5 mM $MgCl_2$, 10 μM GDP (pH 7.4).

2. The His-tagged methyl binding domain of either L3MBTL1 or L3MBTL3 (~ 5 mg/mL) was added to a nickel column and allowed to incubate on beads while nutating for 30 min at 4 °C.
    a. A five-fold higher molar ratio of His-MBT was used relative to KRas concentration to ensure binding of all alkylated protein and was maintained throughout these steps.
3. The column was then washed with the buffer above to remove any unbound His-MBT.
4. Alkylated KRas proteins (~ 1 mg/mL) were added to the column and allowed to nutate for 1 hour at 4 °C to ensure binding to the His-MBT domain.
5. The column was again washed with 20 mM HEPES, 150 mM NaCl, 5 mM $MgCl_2$, 10 μM GDP (pH 7.4) to remove unbound, non-alkylated Ras protein.
    a. This flow-through and wash step were verified as containing non-alkylated Ras protein via intact mass spectrometry.
6. To release the alkylated Ras protein from the His-MBT protein, the competitive small molecules UNC-669 and UNC-1215 were used *(216),(217)*.
    a. Small molecules were added to a methyl elution buffer (20 mM HEPES, 500 mM NaCl, 5 mM $MgCl_2$ (pH 7.4)) at 100 uM final concentration (in slight excess of the methylated protein).
7. This solution was added to the column and allowed to nutate for 2 hours at 4 °C.
8. The column was subsequently washed with the same methyl elution buffer with small molecules present.

a. The flow-through from this incubation and wash was collected, concentrated, estimated pure via SDS-PAGE gel and verified via mass spectrometry as enriched alkylated Ras protein.

9. The His-MBT domain protein was further eluted from the beads using a buffer 20mM HEPES, 150 mM NaCl, 250mM imidazole, 5mM $MgCl_2$ (pH 7.4).

Results

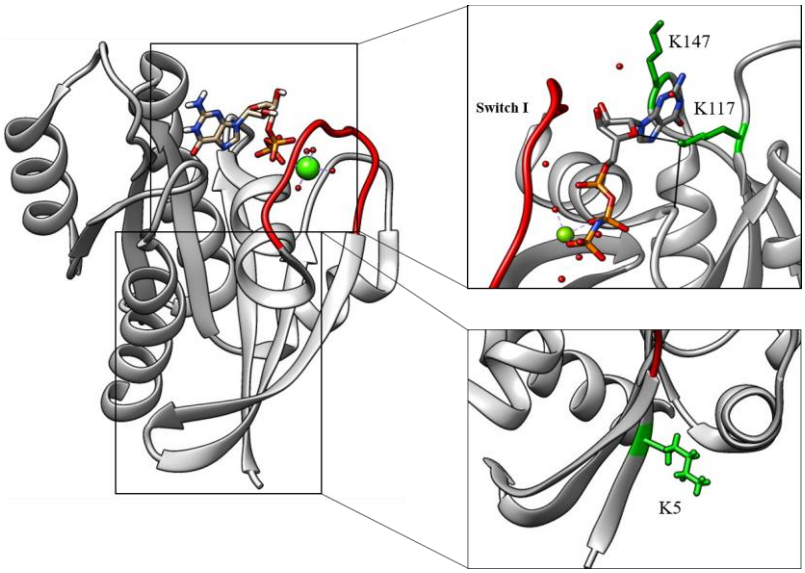

Figure 5.1 Ras methylation has been identified at several sites within the core GTPase domain

Methyl-lysine analogues are installed in Ras proteins at three locations: K5, K117 and K147. Mono- and di-methyl lysine analogues are installed at exposed and semi-buried sites within the Ras protein. K5, K117 and K147 are highly conserved in the Ras superfamily and are the sites of previously identified post-translational modifications. While K5 is more solvent exposed, K147 is known to play roles in nucleotide binding and stability. K117 mutants have been characterized as 'fast-exchange' mutants given the role of K117 in stabilizing the nucleotide base. K117 and K147 have been previously identified as sites of monoubiquitination and acetylation (K147).

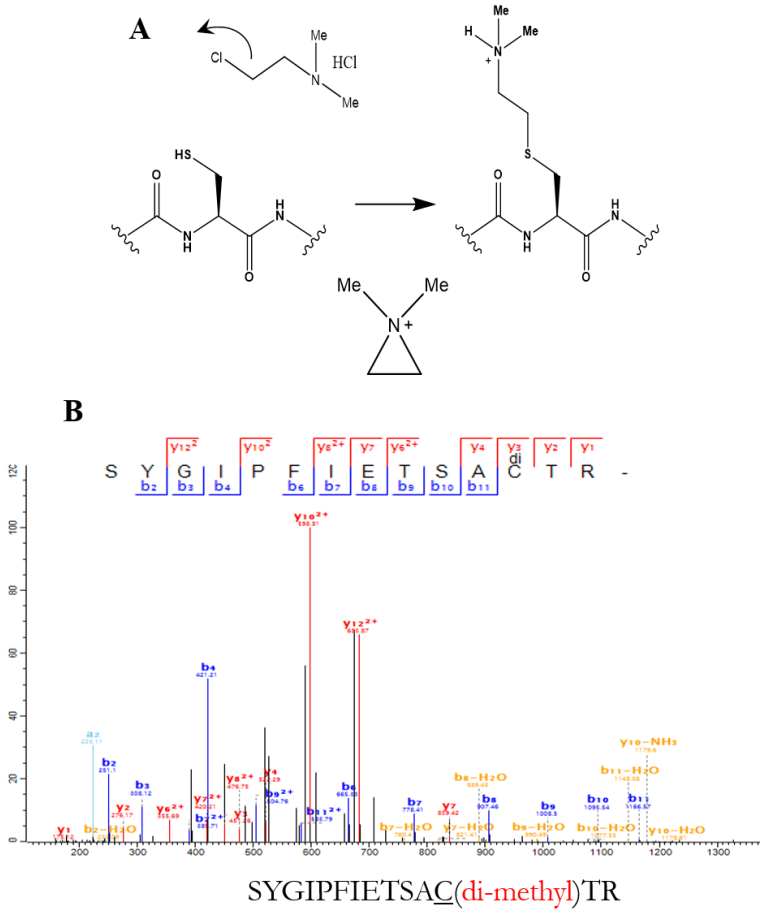

Figure 5.2 Methyl-lysine analogues are able to be installed in a site-specific manner in intact Ras protein

A. The reaction mechanism to generate a dimethyl-lysine analogue in intact protein. A reactive thiol is used to link the dimethyl-lysine analogue, generating a product that is structurally very similar to natively di-methylated lysine. B. LC-MS/MS peptide analysis of trypsin digested KRas K147C protein that has been reacted with the di-methyl lysine analogue. MS/MS spectrum of di-methylated peptide SYGIPFIETSACTR of KRAS verifies that di-methylation is identified at K147 (CID induced ions are labeled, b ions are labeled in blue, y ions are in red, b ions lost a NH_3 or H_2O molecular are labeled in yellow).

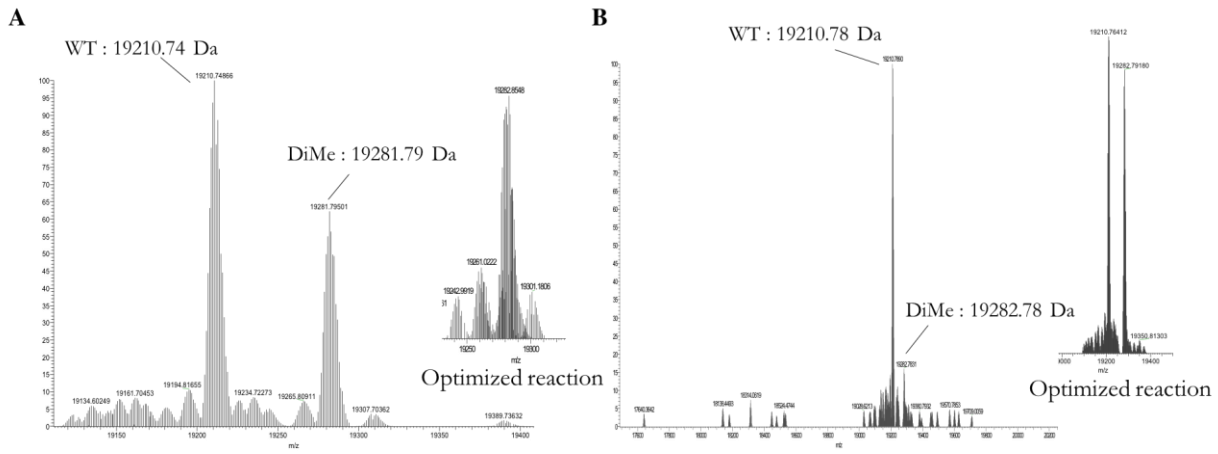

Figure 5.3 Dimethyl-lysine reaction optimization at K147 and K117 in intact KRas protein.

Intact KRas proteins were di-methylated at either K147 (A) or K117 (B). Initial reaction efficiency can be seen for each site-specific alkylation. A matrix-like reaction optimization procedure was used varying temperature, pH and concentration of GnHCl to generate final reaction methods. Di-methylation at exposed sites (K147) yields populations of protein that are fully modified. Alkylation of less exposed sites yields a mixed population of methylated and non-methylated protein.

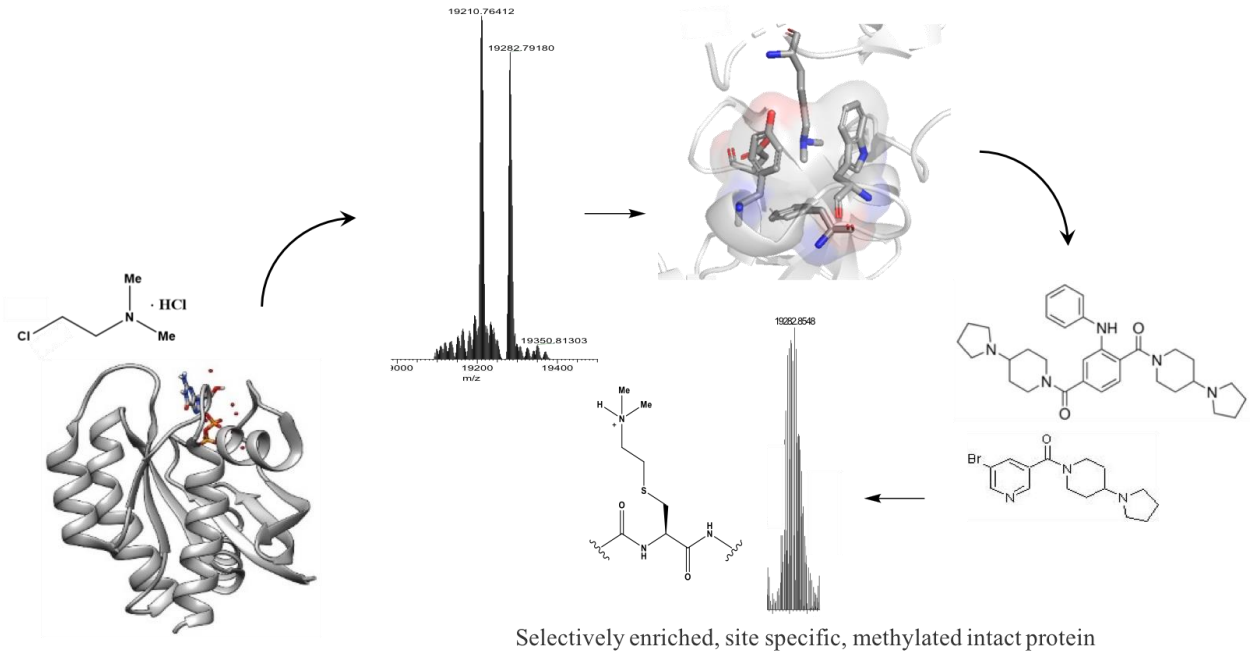

Figure 5.4 A methyl-enrichment strategy for intact methylated proteins

A methyl-enrichment strategy is presented for subsequent methylated protein isolation. The protein is first reacted with the methylated-lysine analogue. If a mixed methylated population is identified via mass spectrometry, protein can be further isolated using 'methyl reader' proteins. The MBT domains of L3MBTL1/3 can be used to selectively bind methylated lysine residues. Methylated protein can be selectively eluted with the introduction of small molecule competitive binders UNC669 and UNC1215.

Discussion

KMTs and KDMs have been identified as potential therapeutic targets in several cancers *(97)*. Given that aberrant methylation patterns have been identified in a multitude of cancers *(76),(97)*, there is a pressing need to understand how methylation is capable of regulating protein activity. While methylation has been primarily studied in the context of histone regulation, there is increasing evidence that methylation can also regulate cancer-related proteins. p53 methylation (or acetylation) is known to fine-tune its overall activation status in cancers *(78),(114)*. Further, the Ras/MAPK pathway has also been implicated in dynamic methylation regulation by the

KMT SYMD3. MAP3K2 methylation by SMYD3 was demonstrated to increase MAPK-mediated signaling and Ras-mediated tumorigenesis in mouse models of PDAC and lung cancer *(73),(77).* Aberrant methylation patterns have also been identified in the Ras-driven pancreatic ductal adenocarcinoma *(76).* Novel methylation sites have also been identified in Ras proteins (data not shown). Given the current limitations in the field of understanding how methylation regulates the activity of non-histone proteins, we sought to develop a strategy to generate site-specifically methylated intact proteins. The current strategies to generate methylated intact proteins are limited. Unlike acetylation, genetic code expansion techniques to generate methylated intact proteins have not been overarchingly successful. This is due in part to the inability to develop orthogonal tRNA/amino-acyl tRNA synthetase pairs that recognize methylated lysine exclusively *(211).* As such, genetic code expansion techniques have been used most successfully to install precursor molecules, and then methylated lysines are recovered through various chemical reactions *(211)*. These methods incorporate UV exposure or acidic conditions to generate the final product *(218)–(220),* rendering them not useful for a multitude of intact proteins.

In a method similar to Simon *et al (213),(214),* we used methyl-lysine analogues to generate methylated intact proteins that are highly similar to natively methylated proteins. Our method is unique in that we present a strategy suitable for use in intact, functional protein. While we are in the analysis phase of our research, preliminary results have demonstrated the ability to generate mono- and di-methylated intact Ras proteins at three different locations in intact KRas protein: K5, K117 and K147. Reactions have been optimized to temperature, pH and guanidinium hydrochloride concentration to facilitate the highest reaction efficiency while assuring the intact protein remain functional. However, it is important to note that these factors

may vary slightly with each protein tested. While altering the temperature and pH increases reaction efficiency significantly (data not shown), this is often met with an altered reactivity. The primary or secondary amines generated in the final product are susceptible for additional methyl-lysine linkage if the pH is increased. Increasing temperature also facilitates this process (data not shown). As such, these reactions were completed at pH no greater than 7.8 and 4 °C. For exposed sites, a reaction time of a few hours completed at 25 °C was adequate to generate methylated product. However, methylation at sites that were less exposed or more integral to protein stability required longer times and lower temperatures. The method presented here reflects these sites. Of note, this method uses the reactive thiol of a cysteine to link the methyl-lysine analogue. Therefore, exposed cysteines would be a concern for reactivity. In this example, we have used a cysteine-light version of KRas protein, where the exposed cysteines have been mutated to limit alternative reactivity *(90)*.

One limitation of our method is due to the accessibility of the site to be modified. We saw significant differences in the reaction efficiency depending on how 'exposed' the residue is and how accessible it is to modification. As such, we generated a subsequent enrichment strategy harnessing 'methyl reader' proteins and competitive small molecules to selectively enrich for methylated lysines. As the family of 'methyl reader' proteins used in this method bind methylated lysines in a relatively promiscuous manner, this method should be highly translatable for use with any methylated protein. The 'methyl reader' proteins used in this method are from the MBT (malignant brain tumor) family, L3MBTL1 and L3MBTL3. They recognize mono- and di-methyl lysines in a sequence-independent manner, where the protonated amine of the methyl-lysine is coordinated in a deep pocket through hydrogen bonding and a cation-π interaction *(221)* (also seen in **Figure 5.4**). The small molecules used in this method, UNC669 and UNC1215

(UNC structural genomics consortium) have low micromolar to nanomolar affinities for the 'methyl reader' proteins *(216),(217)* and are capable of competitively eluting the methylated Ras protein from the 'methyl reader' protein. We have completed each reaction in replicate so as to provide statistical relevance to our data. We also plan to extend the enrichment strategy to whole-cell lysates to identify the methylation site(s) in endogenous Ras proteins. In this manner, we hope the investigate the role of methylation in regulating Ras protein activity.

Materials and Methods

Cysteine-light KRas WT and cysteine mutant purification

A cysteine-light version of human KRas-4B (G12C/C51S/C80L/C118S) (residues 1–169) in a pET21 vector with an N-terminal 6-histidine tag and a TEV protease cleavage site was provided by the Shokat lab *(90)*. In brief, the exposed cysteines in Ras were mutated to reduce sensitivity to oxidants and reactivity to methyl-lysine analogue substrates in this study. This construct has been structurally and biochemically characterized as functionally similar to KRas wild type protein *(90)*. Standard mutagenesis techniques were used to generate KRas K5C, K117C and K147C constructs, and construct sequences were verified. For expression in *Escherichia coli* BL21 (DE3) cells (Novagen), cells were transformed and grown at 37 °C in Luria-Bertani (LB) medium until A_{600} of ~0.5. At this point the temperature was lowered to 18 °C, and KRas expression was induced with 0.5 mM isopropyl-β-D-1-thiogalactopyranoside (IPTG) after 30 min. Expression was continued for 16 hours. To harvest cells, the growths were pelleted at 4000 x g. They were then resuspended in a buffer containing 20 mM HEPES, 300 mM NaCl, 1 mM $MgCl_2$, 20 mM imidazole, 0.5 mM TCEP (tris(2-carboxyethyl)phosphine hydrochloride), 5% glycerol (pH 7.75), sonicated and pelleted again by centrifugation at 15,000 x g for 25 minutes. The supernatant was isolated and KRas proteins were purified using standard

Qiagen nickel affinity purification procedures. Proteins were washed with a buffer containing 20 mM HEPES, 500 mM NaCl, 5 mM $MgCl_2$, 40 mM imidazole, 0.5 mM TCEP, 5% glycerol (pH 7.75). Proteins were then eluted in a buffer containing 20 mM HEPES, 50 mM NaCl, 5 mM $MgCl_2$, 250 mM imidazole, 0.5 mM TCEP (pH 7.75). The histidine tag was cleaved during overnight dialysis at 4°C in reducing buffer (100 mM HEPES, 50 mM NaCl, 5 mM $MgCl_2$, 0.5 mM TCEP, 10 μM GDP (pH 7.8)) using TEV protease. Proteins were used immediately for methyl-lysine analogue reactions to reduce opportunity for cysteine oxidation. Following methyl-lysine reactions, Ras proteins were further purified by size exclusion chromatography using a Sephadex G-75 column. Protein purity of >95% was obtained and verified by SDS-PAGE analysis.

Methyl binding domain purification

The methyl binding domains of L3MBTL1 (residues 268-590) and L3MBTL3 (residues 225-555) (malignant brain tumor family proteins, MBT) were obtained from the Structural Genomics Consortium at the University of North Carolina, Chapel Hill courtesy of Dr. Stephen Frye. Briefly, the constructs are transformed for expression into *Escherichia coli* BL21 (DE3) cells (Novagen). They are grown at 37 °C in Luria-Bertani (LB) medium until A_{600} of ~0.5, at which point the temperature is lowered to 18 °C. Cells are induced with 0.5 mM isopropyl-β-D-1-thiogalactopyranoside (IPTG) after 30 min, and the expression was continued for 16 hours. Cells are pelleted at 4000 x g for 30 minutes, resuspended in wash buffer (50 mM sodium phosphate, 500 mM NaCl, 30 mM imidazole, cOmplete ULTRA protease inhibitor cocktail tablets (Roche) (pH 7.75)) and sonicated. Cells are pelleted at 15000 x g for 25 minutes and the supernatant is isolated. Proteins are purified using standard Ni-NTA agarose purification procedures (Qiagen). The supernatant is applied to the column and washed with the buffer above.

Elution if the protein is achieved through the addition of 500 mM imidazole to the wash buffer. Proteins were further purified by size exclusion chromatography using a Superdex 200 column in 25 mM Tris, 250 mM NaCl, 2 mM DTT, 5% glycerol (pH 7.5). Protein purity of >95% was obtained and verified by SDS-PAGE analysis. Proteins are flash frozen with 10% glycerol at 5 mg/mL.

Mass Spectrometry

All samples were analyzed by nanoLC-MS using a Waters nanoAcquity coupled to a Thermo Orbitrap Velos. The samples were injected onto a PepMap C18 (5 um particle size, 5 cm), trapping column (Thermo) then separated by in-line gradient elution onto a PepMap C18 (3 um particle size, 15 cm). Samples were eluted over a 10 min gradient from 5-90% mobile phase B, where mobile A was H20 in 0.1% formic acid and mobile phase B was ACN in 0.1% formic acid. The Orbitrap Velos was operated in full scan mode and the resolution for the precursor scan (400-2000 m/z) was set to 100,000 at 400 m/z. Data were processed in Thermo Xcalibur and Xtract within Xcalibur was used for mass deconvolution.

Chapter 6. Conclusions and Future Directions

While our work has largely contributed to the field of understanding how PTMs in the core Ras domain can modulate its activity, the questions remain of the exact molecular and cellular mechanisms behind these processes. It is clear that PTMs are capable of regulating Ras activity *(61)*, and therefore present novel therapeutic opportunities in Ras-driven cancers. In particular, acetylation has been previously identified in the core G-domain in Ras proteins at K104 and K147 *(67)–(69)*. However, there is some disagreement in the field as to whether canonical amino acids are capable of mimicking true PTMs. As such, when canonical amino acids were used as acetylation mimetics, much more severe alterations in Ras behavior were seen versus when Ras was natively acetylated *(67)–(69)*.

In collaboration with the Sers lab (Charité Universitätsmedizin Berlin), we were able to identify a novel acetylation site in Ras (K5) that was identified in CRC cell lines after treatment with the class I HDACi, Entinostat. Their work demonstrated that drug treatment primarily served to activate the protein through increased Ras-GTP bound to Raf RBDs in pulldown assays and increased signaling through the downstream MAPK pathway. Interestingly, oncogenic Ras displayed a much more resistant phenotype, exacerbating the above-mentioned behaviors. *In vitro*, we were able to generate acetylated Ras proteins using a genetic code expansion technique. We were able to determine that K5 acetylation played little role in modulating the intrinsic ability of Ras proteins to exchange or hydrolyze nucleotides. However, in the presence of the modulatory proteins, GEFs and GAPs, small defects were identified. While K5 is not noted to make direct contacts with GEFs or GAPs, it does sit very close (~5 Å) to several SOS GEF

residues *(54),(131),* where the closest residues in p120GAP are about 10 Å away *(13)*. It is possible that K5 acetylation is slightly affecting the ability of GEFs or GAPs to bind Ras and stimulate activity either through disruption of direct contacts or through disruptions in the critical switch regions that bind directly to GEFs and GAPs. We are also able to demonstrate that K5 acetylated oncogenic proteins (G12V) are able to restore the weakened affinity of G12V to the Raf RBDs, consistent with the increased signaling through the MAPK pathway identified by the Sers lab. To gain structural insight into how K5 is capable of regulating Ras activity, we conducted united atom molecular dynamic (MD) simulations of Ras in complex with the Raf RBD. In collaboration with Dr. Konstantin Popov at UNC, we were able to see that in complex with the Raf RBDs, acetylated K5 causes a significant rearrangement of the critical electrostatic binding interface between Ras and the Raf RBD. In this manner, it facilitates a much more interconnected network, which explains the tighter binding affinity observed to the Raf RBDs. One huge enigma that remains in the field is why Ras oncogenic mutants display decreased affinities to the Raf RBDs yet significantly increase MAPK signaling relative to WT protein. In this sense, a much more thorough cellular, structural and dynamic evaluation should be completed to try to understand how oncogenic mutants function to increase Ras activity. Our work focused on the class I HDACi, Entinostat. In the future, this evaluation should be extended to include selective class I or class II and pan-class HDACi to identify if a similar mechanism of Ras regulation exists. There are several studies that demonstrate that combination therapies with MEKi+HDACi or MEKi+PI3Ki+HDACi yield increased oncogenic cellular apoptosis, decreased proliferation and slowed tumor formation *(101),(102)*. HDACi could serve as novel therapeutic drugs in Ras-driven cancers, and as such, combination therapeutic studies should be extensively evaluated. Further work should also include understanding the underlying mechanism of cell

cycle arrest facilitated by Entinostat and how increased MAPK signaling is capable of driving or mitigating this process. In this manner, we may then understand better how combination therapies increase drug sensitivity in cells and xenograft models.

While K5 was identified as a novel acetylation site, it is also mutated in several 'Ras-opathies' and cancers. 'Ras-opathies' are often characterized by their ability to activate Ras as seen through increased, dysregulated MAPK signaling *(128),(170),(171)*. However, previous studies of the Noonan's syndrome KRas germline mutant, K5N were not able to determine the mechanism leading to dysregulated MAPK signaling. Cellular studies indicated a mild, at best, increase in MAPK signaling while no other changes were noted in the biochemical function of the protein. Interestingly, they did briefly describe a potential structural role for Ras activation due to K5N mutation *(128)*. In this study, I was able to determine that K5N mutation likely destabilizes the protein more predominately in the GDP-bound form. We were able to identify only small changes in the ability of the protein to exchange nucleotide in the presence of a GEF and in the ability of the protein to load nucleotides, primarily in the GDP-bound form. However, NMR and computational analysis demonstrated significant alterations in the GDP-bound form of the K5N mutant. ^{1}H-^{15}N NMR HSQCs identified significant chemical shift perturbations in the GDP-bound form of the protein, relative to WT. These mapped entirely to the effector lobe of the protein and the critical switch regions. In the active form, the K5N mutant displayed a much more similar NMR mapping to WT protein. MD simulations indicated that the K5N mutation likely disrupts the protein in the GDP-bound form primarily through causing a very electrostatically unfavorable packing network around the mutation. In dynamic evaluations of K5N, the MD simulations showed a dramatic increase in the fluctuations of SWII in the GDP-bound form, while the GTP-bound form is highly similar between the Ras proteins. Taken

together these data support the previously mentioned structural role for K5N instability in the GDP-bound form, primarily through an indirect role in disrupting nucleotide binding. Of note, we are not able to identify any differences in the ability if the K5N mutant to bind the Raf RBDs, which is a hallmark of 'Ras-opathies' *(178)*. This suggests that there is likely a defect in the protein due to K5N mutation that does not affect effector binding. If K5N mutation causes instability in the GDP-bound form, it is possible that this mutant would be more GTP-bound in the cell. By altering steady-state GTP levels in cells, the K5N mutant could potentiate signaling in Ras-mediated cascades such as the MAPK cascade. What is left unanswered is exactly how K5 regulates Ras activity. It is highly conserved, yet it is not noted to play critical roles in nucleotide binding or effector/modulatory protein binding or recognition. It is only by understanding this that we will be able to gain insight into how the K5N mutant alters protein behavior. Consistent with literature, K5 does seem to play an indirect role in coordinating and stabilizing nucleotide binding *(128)*. More extensive structural and dynamic studies will be needed to understand how mutation disruptes these processes.

As previously mentioned, acetylation has been identified in several sites in the Ras core G-domain at K104 and K147 *(67)–(69)*. In this study, we sought to determine the effect of acetylation at K104 in regulating protein activity. We were able to demonstrate that K104 is important for GEF recognition, as any mutation at this position resulted in impaired GEF-mediated nucleotide exchange. Using the acetylation mimetic, glutamine, Q we found that the K104Q displayed both GEF and GAP defects. This was consistent with NMR structural perturbations that were identified in α2 helix in Ras, which is a critical interface for GEFs and GAPs *(13),(54)*. In cells, KRas K104Q mutation was not able of altering steady state GTP-levels in RBD pulldown assays, nor was K104Q able to cause cellular transformation in NIH 3T3 cells

or efficiently rescue cells. We concluded that the GEF and GAP defects displayed in K104Q likely balanced one another, which overall did not change Ras activity. What remains unclear is whether glutamine is an adequate acetylation mimetic. When we used natively acetylated protein and again investigated the GEF activity, a much less severe defect was identified. It is becoming evident that canonical amino acids are not suitable mimetics of PTMs and as such, further studies should include natively acetylated Ras proteins.

Work in my lab and others has also identified novel methylation sites in the Ras core domain (unpublished). However, dissimilar to acetylation, there are no reliable methods to produce fully methylated, intact proteins *in vitro (211)*. A previous method to methylate histone tails has been described by *Simon and Shokat (214)*, but is not suitable for intact proteins due to the severe denaturing and reducing conditions needed. In this work, I have generated a novel method to methylate intact proteins in a site-specific manner using methyl-lysine analogues. The method involves the use of a reactive thiol to link the methyl lysine analogue to generate a product with high structural similarity to natively methylated protein. Additionally, as residue reactivity is highly dependent upon the accessibility of the site, I generated a subsequent method for methylation enrichment. This method involves the use of methyl binding domains, which bind the methylated intact protein. Subsequent exposure to competitive small molecules of the 'methyl reader' protein can cause the 'release' and of methylated protein. I will also be using this tool to probe whole-cell lysates to see if I can 'capture' methylated Ras proteins in order to identify physiological sites of methylation. Several Ras-driven cancers such as pancreatic cancer have dramatically altered methylation patterns *(76)*. With methyltransferase inhibitors on the market for the treatment of several cancers *(104),(222),(223)*, understanding how methylation regulates Ras activity may provide a novel avenue of drug targeting in Ras-driven cancers.

Final Conclusions

Herein, we have discussed the importance of G-domain PTMs in modulating Ras activity. Our data adds to a growing body of literature suggesting that Ras GTPases are particularly sensitive to modulation by PTMs and these may provide novel Ras therapeutic targeting opportunities. With HDACi and methyltransferase inhibitors currently on the market for the treatment of several cancers *(97),(104),(106),(115),(222),(223),* it is reasonable to believe that these drugs may be applicable in Ras-driven cancers as well. In order to answer these questions, more thorough mechanistic insight is needed into how acetylation (HDACi) and methylation (methyltransferase inhibitors) modulate Ras activity. As such, future work should include detailed *in vivo* an *in vitro* work aiming to characterize the mechanisms behind acetylation and methylation regulation of Ras activity. We would further suggest cell-based drug screens with combination therapy approaches, as stronger anti-tumorigenic properties have been described in the contact of HDACi treatment when combined with MEK and PI3K inhibitors *(101),(102).* This could then be extended to organoid and mouse models. Interestingly, upon Entinostat treatment (class I HDACi), only K5 was identified as being acetylated (Chapter 2). This suggests that K5 may be the physiologic site of acetylation. While it is highly conserved in the Ras superfamily, the role of K5 is modulating Ras activity is not well understood. In addition, the role of K5 mutations found in cancers and 'Ras-opathies' should be more thoroughly characterized in cellular and structural experiments as they may also provide novel mechanisms of activation and hence novel therapeutic targeting opportunities (Chapter 3). The role of methylation is largely unknown in Ras proteins. Using the methylation and enrichment strategy developed, it may be possible for the first time to provide insight in how methylation regulates Ras activity (Chapter 5). As pancreatic cancer has displayed aberrantly dysregulated methylation

patterns *(76)*, and it is nearly 100% driven by oncogenic Ras *(5)*, it is possible that methyltransferase inhibitors may also be successful in Ras-driven cancers. Future work should therefore include the biochemical and biophysical characterization of methylated Ras proteins (mono- and di-methyl at the 3 sites described in Chapter 5. As the physiologic sites of methylation in Ras remain unknown, the methylation enrichment strategy described in Chapter 5 could be applied to whole-cell lysates to identify endogenous Ras methylation sites.

REFERENCES

1. Vetter, I. R. The Structure of the G Domain of the Ras Superfamily. In *Ras Superfamily Small G Proteins: Biology and Mechanisms 1: General Features, Signaling*; 2014. https://doi.org/10.1007/978-3-7091-1806-1_2.

2. Colicelli, J. Human RAS Superfamily Proteins and Related GTPases. *Sci. Signal.* **2004**, *2004* (250), re13-re13. https://doi.org/10.1126/stke.2502004re13.

3. Rojas, A. M.; Valencia, A. Evolution of the Ras Superfamily of GTPases. In *Ras Superfamily Small G Proteins: Biology and Mechanisms 1: General Features, Signaling*; 2014. https://doi.org/10.1007/978-3-7091-1806-1_1.

4. Cox, A. D.; Der, C. J. Ras History The Saga Continues. *Small GTPases* **2010**, *1* (1), 2–27. https://doi.org/10.4161/sgtp.1.1.12178.

5. Hobbs, G. A.; Der, C. J.; Rossman, K. L. RAS Isoforms and Mutations in Cancer at a Glance. *J. Cell Sci.* **2016**, *129* (7), 1287–1292. https://doi.org/10.1242/jcs.182873.

6. John, J.; Rensland, H.; Schlichting, I.; Vetter, I.; Borasio, G. D.; Goody, R. S.; Wittinghofer, A. Kinetic and Structural Analysis of the Mg2+-Binding Site of the Guanine Nucleotide-Binding Protein P21H-Ras. *J. Biol. Chem.* **1993**. https://doi.org/10.1016/j.gie.2012.05.011.

7. Rojas, J. M.; Oliva, J. L.; Santos, E. Mammalian Son of Sevenless Guanine Nucleotide Exchange Factors: Old Concepts and New Perspectives. *Genes Cancer* **2011**, *2* (3), 298–305. https://doi.org/10.1177/1947601911408078.

8. Vigil, D.; Cherfils, J.; Rossman, K. L.; Der, C. J. Ras Superfamily GEFs and GAPs: Validated and Tractable Targets for Cancer Therapy? *Nat. Rev. Cancer* **2010**, *10* (12), 842–857. https://doi.org/10.1038/nrc2960.

9. Cherfils, J. GEFs and GAPs: Mechanisms and Structures. In *Ras Superfamily Small G Proteins: Biology and Mechanisms 1*; Springer Vienna: Vienna, 2014; pp 51–63. https://doi.org/10.1007/978-3-7091-1806-1_3.

10. Hennig, A.; Markwart, R.; Esparza-Franco, M. A.; Ladds, G.; Rubio, I. Ras Activation Revisited: Role of GEF and GAP Systems. *Biol. Chem.* **2015**, *396* (8), 831–848. https://doi.org/10.1515/hsz-2014-0257.

11. Kotting, C.; Kallenbach, A.; Suveyzdis, Y.; Wittinghofer, A.; Gerwert, K. The GAP Arginine Finger Movement into the Catalytic Site of Ras Increases the Activation Entropy. *Proc. Natl. Acad. Sci.* **2008**, *105* (17), 6260–6265. https://doi.org/10.1073/pnas.0712095105.

12. Ahmadian, M. R.; Stege, P.; Scheffzek, K.; Wittinghofer, A. Confirmation of the Arginine-Finger Hypothesis for the GAP-Stimulated GTP-Hydrolysis Reaction of Ras.

Nat. Struct. Biol. **1997**, *4* (9), 686–689. https://doi.org/10.1038/nsb0997-686.

13. Scheffzek, K.; Ahmadian, M. R.; Kabsch, W.; Wiesmüller, L.; Lautwein, A.; Schmitz, F.; Wittinghofer, A. The Ras-RasGAP Complex: Structural Basis for GTPase Activation and Its Loss in Oncogenic Ras Mutants. *Science (80-.).* **1997**, *277* (5324), 333–338.

14. Malumbres, M.; Barbacid, M. Correction: RAS Oncogenes: The First 30 Years. *Nat. Rev. Cancer* **2003**, *3* (9), 708–708. https://doi.org/10.1038/nrc1193.

15. Herrmann, C.; Martin, G. A.; Wittinghofer, A. Quantitative Analysis of the Complex between P21ras and the Ras-Binding Domain of the Human Raf-1 Protein Kinase. *J. Biol. Chem.* **1995**, *270* (7), 2901–2905.

16. Mott, H. R.; Owen, D. Structures of Ras Superfamily Effector Complexes: What Have We Learnt in Two Decades? *Crit. Rev. Biochem. Mol. Biol.* **2015**, *50* (2), 85–133. https://doi.org/10.3109/10409238.2014.999191.

17. Hunter, J. C.; Manandhar, A.; Carrasco, M. a.; Gurbani, D.; Gondi, S.; Westover, K. D. Biochemical and Structural Analysis of Common Cancer-Associated KRAS Mutations. *Mol. Cancer Res.* **2015**, *13* (9), 1325–1335. https://doi.org/10.1158/1541-7786.MCR-15-0203.

18. Harvey, J. J. An Unidentified Virus Which Causes the Rapid Production of Tumours in Mice. *Nature* **1964**, *204* (3), 1104–1105. https://doi.org/1475-2875-9-181 [pii]\n10.1186/1475-2875-9-181.

19. Scolnick, E. M.; Parks, W. P. Harvey Sarcoma Virus: A Second Murine Type C Sarcoma Virus with Rat Genetic Information. *J. Virol.* **1974**, *13* (6), 1211–1219.

20. Der, C. J.; Krontiris, T. G.; Cooper, G. M. Transforming Genes of Human Bladder and Lung Carcinoma Cell Lines Are Homologous to the Ras Genes of Harvey and Kirsten Sarcoma Viruses. *Proc. Natl. Acad. Sci.* **1982**, *79* (11), 3637–3640. https://doi.org/10.1073/pnas.79.11.3637.

21. Shih, C.; Weinberg, R. A. Isolation of a Transforming Sequence from a Human Bladder Carcinoma Cell Line. *Cell* **1982**. https://doi.org/10.1016/0092-8674(82)90100-3.

22. Pulciani, S.; Santos, E.; Lauver, A. V.; Long, L. K.; Aaronson, S. A.; Barbacid, M. Oncogenes in Solid Human Tumours. *Nature* **1982**. https://doi.org/10.1038/300539a0.

23. Goldfarb, M.; Shimizu, K.; Perucho, M.; Wigler, M. Isolation and Preliminary Characterization of a Human Transforming Gene from T24 Bladder Carcinoma Cells. *Nature* **1982**. https://doi.org/10.1038/296404a0.

24. Lazo, J. S.; Sharlow, E. R. Drugging Undruggable Molecular Cancer Targets. *Annu. Rev. Pharmacol. Toxicol.* **2016**. https://doi.org/10.1146/annurev-pharmtox-010715-103440.

25. Tate, J. G.; Bamford, S.; Jubb, H. C.; Sondka, Z.; Beare, D. M.; Bindal, N.; Boutselakis,

H.; Cole, C. G.; Creatore, C.; Dawson, E.; et al. COSMIC: The Catalogue Of Somatic Mutations In Cancer. *Nucleic Acids Res.* **2018**, *47* (October 2018), 941–947. https://doi.org/10.1093/nar/gky1015.

26. Prior, I. A.; Lewis, P. D.; Mattos, C. A Comprehensive Survey of Ras Mutations in Cancer. *Cancer Res.* **2012**, *72* (10), 2457–2467. https://doi.org/10.1158/0008-5472.CAN-11-2612.

27. Hayes, T. K.; Der, C. J. Mutant and Wild-Type Ras: Co-Conspirators in Cancer. *Cancer Discov.* **2013**, *3* (1), 24–27. https://doi.org/10.1158/2159-8290.CD-12-0521.

28. Burd, C. E.; Liu, W.; Huynh, M. V; Waqas, M. a; Gillahan, J. E.; Clark, K. S.; Fu, K.; Martin, B. L.; Jeck, W. R.; Souroullas, G. P.; et al. Mutation-Specific RAS Oncogenicity Explains NRAS Codon 61 Selection in Melanoma. *Cancer Discov.* **2014**, *4* (12), 1418–1429. https://doi.org/10.1158/2159-8290.CD-14-0729.

29. Prior, I. A.; Lewis, P. D.; Mattos, C. A Comprehensive Survey of Ras Mutations in Cancer. *Cancer Res.* **2012**, *72* (10), 2457–2467. https://doi.org/10.1158/0008-5472.CAN-11-2612.

30. Buhrman, G.; Wink, G.; Mattos, C. Transformation Efficiency of RasQ61 Mutants Linked to Structural Features of the Switch Regions in the Presence of Raf. *Structure* **2007**, *15* (12), 1618–1629. https://doi.org/10.1016/j.str.2007.10.011.

31. Smith, M. J.; Neel, B. G.; Ikura, M. NMR-Based Functional Profiling of RASopathies and Oncogenic RAS Mutations. *Proc. Natl. Acad. Sci.* **2013**, *110* (12), 4574–4579. https://doi.org/10.1073/pnas.1218173110.

32. Ihle, N. T.; Byers, L. A.; Kim, E. S.; Saintigny, P.; Lee, J. J.; Blumenschein, G. R.; Tsao, A.; Liu, S.; Larsen, J. E.; Wang, J.; et al. Effect of KRAS Oncogene Substitutions on Protein Behavior: Implications for Signaling and Clinical Outcome. *J. Natl. Cancer Inst.* **2012**, *104* (3), 228–239. https://doi.org/10.1093/jnci/djr523.

33. Campbell, S. L.; Khosravi-Far, R.; Rossman, K. L.; Clark, G. J.; Der, C. J. Increasing Complexity of Ras Signaling. *Oncogene* **1998**, *17* (11 Reviews), 1395–1413. https://doi.org/10.1038/sj.onc.1202174.

34. Kapoor, S.; Weise, K.; Erlkamp, M.; Triola, G.; Waldmann, H.; Winter, R. The Role of G-Domain Orientation and Nucleotide State on the Ras Isoform-Specific Membrane Interaction. *Eur. Biophys. J.* **2012**, *41* (10), 801–813. https://doi.org/10.1007/s00249-012-0841-5.

35. Freedman, T. S.; Sondermann, H.; Friedland, G. D.; Kortemme, T.; Bar-Sagi, D.; Marqusee, S.; Kuriyan, J. A Ras-Induced Conformational Switch in the Ras Activator Son of Sevenless. *Proc. Natl. Acad. Sci.* **2006**, *103* (45), 16692–16697. https://doi.org/10.1073/pnas.0608127103.

36. Margarit, S. M.; Sondermann, H.; Hall, B. E.; Nagar, B.; Hoelz, A.; Pirruccello, M.; Bar-

Sagi, D.; Kuriyan, J. Structural Evidence for Feedback Activation by Ras·GTP of the Ras-Specific Nucleotide Exchange Factor SOS. *Cell* **2003**, *112* (5), 685–695. https://doi.org/10.1016/S0092-8674(03)00149-1.

37. Prior, I. A.; Hancock, J. F. Ras Trafficking, Localization and Compartmentalized Signalling. *Seminars in Cell and Developmental Biology*. 2012. https://doi.org/10.1016/j.semcdb.2011.09.002.

38. Buhrman, G.; Holzapfel, G.; Fetics, S.; Mattos, C. Allosteric Modulation of Ras Positions Q61 for a Direct Role in Catalysis. *Proc. Natl. Acad. Sci.* **2010**, *107* (11), 4931–4936. https://doi.org/10.1073/pnas.0912226107.

39. Baussand, J.; Kleinjung, J. Specific Conformational States of Ras GTPase upon Effector Binding. *J. Chem. Theory Comput.* **2013**, *9* (1), 738–749. https://doi.org/10.1021/ct3007265.

40. Gohlke, H.; Kiel, C.; Case, D. A. Insights into Protein-Protein Binding by Binding Free Energy Calculation and Free Energy Decomposition for the Ras-Raf and Ras-RalGDS Complexes. *J. Mol. Biol.* **2003**. https://doi.org/10.1016/S0022-2836(03)00610-7.

41. Vetter, I. R. The Guanine Nucleotide-Binding Switch in Three Dimensions. *Science (80-.).* **2001**, *294* (5545), 1299–1304. https://doi.org/10.1126/science.1062023.

42. Morrison, D. K.; Cutler, R. E. The Complexity of Raf-1 Regulation. *Current Opinion in Cell Biology*. 1997, pp 174–179. https://doi.org/10.1016/S0955-0674(97)80060-9.

43. Fridman, M.; Maruta, H.; Gonez, J.; Walker, F.; Treutlein, H.; Zeng, J.; Burgess, A. Point Mutants of C-Raf-1 RBD with Elevated Binding to v-Ha-Ras. *J. Biol. Chem.* **2000**, *275* (39), 30363–30371. https://doi.org/10.1074/jbc.M003193200.

44. Hall, B. E.; Bar-Sagi, D.; Nassar, N. The Structural Basis for the Transition from Ras-GTP to Ras-GDP. *Proc. Natl. Acad. Sci.* **2002**, *99* (19), 12138–12142.

45. Ma, J.; Karplus, M. *Molecular Switch in Signal Transduction: Reaction Paths of the Conformational Changes in Ras P21*; 1997; Vol. 94.

46. Schubbert, S.; Bollag, G.; Lyubynska, N.; Nguyen, H.; Kratz, C. P.; Zenker, M.; Niemeyer, C. M.; Molven, A.; Shannon, K. Biochemical and Functional Characterization of Germ Line KRAS Mutations. *Mol. Cell. Biol.* **2007**, *27* (22), 7765–7770. https://doi.org/10.1128/MCB.00965-07.

47. Janakiraman, M.; Vakiani, E.; Zeng, Z.; Pratilas, C. A.; Taylor, B. S.; Chitale, D.; Halilovic, E.; Wilson, M.; Huberman, K.; Cezar, J.; et al. Genomic and Biological Characterization of Exon 4 KRAS Mutations in Human Cancer. *Cancer Res.* **2010**, *70* (14), 5901–5911. https://doi.org/10.1158/0008-5472.CAN-10-0192.

48. Kraulis, P. J.; Domaille, P. J.; Campbell-Burk, S. L.; Van Aken, T.; Laue, E. D. Solution Structure and Dynamics of Ras P21.GDP Determined by Heteronuclear Three- and Four-

Dimensional NMR Spectroscopy. *Biochemistry* **1994**, *33* (12), 3515–3531. https://doi.org/10.1021/bi00178a008.

49. Lu, S.; Jang, H.; Muratcioglu, S.; Gursoy, A.; Keskin, O.; Nussinov, R.; Zhang, J. Ras Conformational Ensembles, Allostery, and Signaling. *Chemical Reviews*. 2016, pp 6607–6665. https://doi.org/10.1021/acs.chemrev.5b00542.

50. Pacold, M. E.; Suire, S.; Perisic, O.; Lara-Gonzalez, S.; Davis, C. T.; Walker, E. H.; Hawkins, P. T.; Stephens, L.; Eccleston, J. F.; Williams, R. L. Crystal Structure and Functional Analysis of Ras Binding to Its Effector Phosphoinositide 3-Kinase γ. *Cell* **2000**, *103* (6), 931–944. https://doi.org/10.1016/S0092-8674(00)00196-3.

51. Fridman, M.; Walker, F.; Catimel, B.; Domagala, T.; Nice, E.; Burgess, A. C-Raf-1 RBD Associates with a Subset of Active v-H-Ras. *Biochemistry* **2000**, *39* (50), 15603–15611. https://doi.org/10.1021/bi001224x.

52. Kiel, C.; Filchtinski, D.; Spoerner, M.; Schreiber, G.; Kalbitzer, H. R.; Herrmann, C. Improved Binding of Raf to RasGDP Is Correlated with Biological Activity. *J. Biol. Chem.* **2009**, *284* (46), 31893. https://doi.org/10.1074/jbc.M109.031153.

53. Geyer, M.; Wittinghofer, A. GEFs, GAPs, GDIs and Effectors: Taking a Closer (3D) Look at the Regulation of Ras-Related GTP-Binding Proteins. *Curr. Opin. Struct. Biol.* **1997**, *7* (6), 786–792. https://doi.org/10.1016/S0959-440X(97)80147-9.

54. Boriack-Sjodin, P. A.; Margarit, S. M.; Bar-Sagi, D.; Kuriyan, J. The Structural Basis of the Activation of Ras by Sos. *Nature* **1998**, *394* (6691), 337–343. https://doi.org/10.1038/28548.

55. Fetics, S. K.; Guterres, H.; Kearney, B. M.; Buhrman, G.; Ma, B.; Nussinov, R.; Mattos, C. Allosteric Effects of the Oncogenic RasQ61L Mutant on Raf-RBD. *Structure* **2015**, *23* (3), 505–516. https://doi.org/10.1016/j.str.2014.12.017.

56. Kiel, C.; Serrano, L.; Herrmann, C. A Detailed Thermodynamic Analysis of Ras/Effector Complex Interfaces. *J. Mol. Biol.* **2004**, *340* (5), 1039–1058. https://doi.org/10.1016/j.jmb.2004.05.050.

57. Parker, J. a; Mattos, C. The Ras-Membrane Interface: Isoform-Specific Differences in the Catalytic Domain. *Mol. Cancer Res.* **2015**, 595–604. https://doi.org/10.1158/1541-7786.MCR-14-0535.

58. Henis, Y. I.; Hancock, J. F.; Prior, I. A. Ras Acylation, Compartmentalization and Signaling Nanoclusters. *Mol. Membr. Biol.* **2009**, *26* (1), 80–92. https://doi.org/10.1080/09687680802649582.

59. Ahearn, I.; Zhou, M.; Philips, M. R. Posttranslational Modifications of RAS Proteins. *Cold Spring Harb. Perspect. Med.* **2018**, *8* (11), 1–18. https://doi.org/10.1101/cshperspect.a031484.

60. Fiordalisi, J. J.; Cox, A. D. Farnesyltransferase Inhibitors. In *Handbook of Cell Signaling*; Bradshaw, R. A., Dennis, E. A., Eds.; Elsevier, 2010; pp 1819–1826. https://doi.org/10.1016/B978-0-12-374145-5.00222-9.

61. Ahearn, I. M.; Haigis, K.; Bar-Sagi, D.; Philips, M. R. Regulating the Regulator: Post-Translational Modification of RAS. *Nat. Rev. Mol. Cell Biol.* **2012**, *13* (1), 39–51. https://doi.org/10.1038/nrm3255.

62. Sasaki, A. T.; Carracedo, A.; Locasale, J. W.; Anastasiou, D.; Takeuchi, K.; Kahoud, E. R.; Haviv, S.; Asara, J. M.; Pandolfi, P. P.; Cantley, L. C. Ubiquitination of K-Ras Enhances Activation and Facilitates Binding to Select Downstream Effectors. *Sci. Signal.* **2011**, *4* (163), ra13. https://doi.org/10.1126/scisignal.2001518.

63. Baker, R.; Lewis, S. M.; Sasaki, A. T.; Wilkerson, E. M.; Locasale, J. W.; Cantley, L. C.; Kuhlman, B.; Dohlman, H. G.; Campbell, S. L. Site-Specific Monoubiquitination Activates Ras by Impeding GTPase-Activating Protein Function. *Nat. Struct. Mol. Biol.* **2013**, *20* (1), 46–52. https://doi.org/10.1038/nsmb.2430.

64. Thurman, R.; Siraliev-Perez, E.; Campbell, S. L. RAS Ubiquitylation Modulates Effector Interactions. *Small GTPases* **2017**, *0* (0), 1–6. https://doi.org/10.1080/21541248.2017.1371267.

65. Baker, R.; Wilkerson, E. M.; Sumita, K.; Isom, D. G.; Sasaki, A. T.; Dohlman, H. G.; Campbell, S. L. Differences in the Regulation of K-Ras and H-Ras Isoforms by Monoubiquitination. *J. Biol. Chem.* **2013**, *288* (52), 36856–36862. https://doi.org/10.1074/jbc.C113.525691.

66. Sjoblom, T.; Jones, S.; Wood, L. D.; Parsons, D. W.; Lin, J.; Barber, T. D.; Mandelker, D.; Leary, R. J.; Ptak, J.; Silliman, N.; et al. The Consensus Coding Sequences of Human Breast and Colorectal Cancers. *Science (80-.).* **2006**, *314* (5797), 268–274. https://doi.org/10.1126/science.1133427.

67. Yang, M. H.; Nickerson, S.; Kim, E. T.; Liot, C.; Laurent, G.; Spang, R.; Philips, M. R.; Shan, Y.; Shaw, D. E.; Bar-Sagi, D.; et al. Regulation of RAS Oncogenicity by Acetylation. *Proc. Natl. Acad. Sci.* **2012**, *109* (27), 10843–10848. https://doi.org/10.1073/pnas.1201487109.

68. Knyphausen, P.; Lang, F.; Baldus, L.; Extra, A.; Lammers, M. Insights into K-Ras 4B Regulation by Post-Translational Lysine Acetylation. *Biol. Chem.* **2016**, *397* (10), 1071–1085. https://doi.org/10.1515/hsz-2016-0118.

69. Yin, G.; Kistler, S.; George, S. D.; Kuhlmann, N.; Garvey, L.; Huynh, M.; Bagni, R. K.; Lammers, M.; Der, C. J.; Campbell, S. L. A KRAS GTPase K104Q Mutant Retains Downstream Signaling by Offsetting Defects in Regulation. *J. Biol. Chem.* **2017**, *292* (11), 4446–4456. https://doi.org/10.1074/jbc.M116.762435.

70. Fujimoto, H.; Higuchi, M.; Koike, M.; Ode, H.; Pinak, M.; Bunta, J. K.; Nemoto, T.; Sakudoh, T.; Honda, N.; Maekawa, H.; et al. A Possible Overestimation of the Effect of

Acetylation on Lysine Residues in KQ Mutant Analysis. *J. Comput. Chem.* **2012**, *33* (3), 239–246. https://doi.org/10.1002/jcc.21956.

71. Li, J.; Zhang, Z.; Dai, Z.; Popkie, A. P.; Plass, C.; Morrison, C.; Wang, Y.; You, M. RASSF1A Promoter Methylation and Kras2 Mutations in Non Small Cell Lung Cancer. *Neoplasia* **2003**. https://doi.org/NO_DOI.

72. Oliveira, C.; Velho, S.; Domingo, E.; Preto, A.; Hofstra, R. M. W.; Hamelin, R.; Yamamoto, H.; Seruca, R.; Schwartz, S. Concomitant RASSF1A Hypermethylation and KRAS/BRAF Mutations Occur Preferentially in MSI Sporadic Colorectal Cancer. *Oncogene* **2005**, *24* (51), 7630–7634. https://doi.org/10.1038/sj.onc.1208906.

73. Ferrarelli, L. K. MAPK Methylation Potentiates RAS Signaling. *Sci. Signal.* **2014**, *7* (330), ec162-ec162. https://doi.org/10.1126/scisignal.2005593.

74. MacLeod, A. R.; Rouleau, J.; Szyf, M. Regulation of DNA Methylation by the Ras Signaling Pathway. *J. Biol. Chem.* **1995**. https://doi.org/10.1074/jbc.270.19.11327.

75. Philips, M. R. Methotrexate and Ras Methylation: A New Trick for an Old Drug? *Sci. Signal.* **2004**, *2004* (225), pe13-pe13. https://doi.org/10.1126/stke.2252004pe13.

76. Roth, G. S.; Casanova, A. G.; Lemonnier, N.; Reynoird, N. Lysine Methylation Signaling in Pancreatic Cancer. *Current Opinion in Oncology*. 2018. https://doi.org/10.1097/CCO.0000000000000421.

77. Mazur, P. K.; Reynoird, N.; Khatri, P.; Jansen, P. W. T. C.; Wilkinson, A. W.; Liu, S.; Barbash, O.; Van Aller, G. S.; Huddleston, M.; Dhanak, D.; et al. SMYD3 Links Lysine Methylation of MAP3K2 to Ras-Driven Cancer. *Nature* **2014**, *510* (7504), 283–287. https://doi.org/10.1038/nature13320.

78. Chuikov, S.; Kurash, J. K.; Wilson, J. R.; Xiao, B.; Justin, N.; Ivanov, G. S.; McKinney, K.; Tempst, P.; Prives, C.; Gamblin, S. J.; et al. Regulation of P53 Activity through Lysine Methylation. *Nature* **2004**, *432* (7015), 353–360. https://doi.org/10.1038/nature03117.

79. Brooks, C. L.; Gu, W. The Impact of Acetylation and Deacetylation on the P53 Pathway. *Protein Cell* **2011**, *2* (6), 456–462. https://doi.org/10.1007/s13238-011-1063-9.

80. Li, J.; Zhang, Z.; Dai, Z.; Popkie, A. P.; Plass, C.; Morrison, C.; Wang, Y.; You, M. RASSF1A Promoter Methylation and Kras2 Mutations in Non Small Cell Lung Cancer. *Neoplasia* **2003**, *5* (4), 362–366. https://doi.org/10.1016/S1476-5586(03)80029-5.

81. Clanton, D.; Hattori, S.; Shih, T. Mutations of the Ras Gene Product P21 That Abolish Guanine Nucleotide Binding. *Proc. …* **1986**. https://doi.org/10.1073/pnas.83.14.5076.

82. Cox, A. D.; Fesik, S. W.; Kimmelman, A. C.; Luo, J.; Der, C. J. Drugging the Undruggable RAS: Mission Possible? *Nat. Rev. Drug Discov.* **2014**, *13* (11), 828–851. https://doi.org/10.1038/nrd4389.

83. Papke, B.; Der, C. J. Drugging RAS: Know the Enemy. *Science (80-.).* **2017**, *355* (6330), 1158–1163. https://doi.org/10.1126/science.aam7622.

84. Haklai, R.; Elad-Sfadia, G.; Egozi, Y.; Kloog, Y. Orally Administered FTS (Salirasib) Inhibits Human Pancreatic Tumor Growth in Nude Mice. *Cancer Chemother. Pharmacol.* **2007**, *61* (1), 89–96. https://doi.org/10.1007/s00280-007-0451-6.

85. Charette, N.; De Saeger, C.; Lannoy, V.; Horsmans, Y.; Leclercq, I.; Stärkel, P. Salirasib Inhibits the Growth of Hepatocarcinoma Cell Lines in Vitro and Tumor Growth in Vivo through Ras and MTOR Inhibition. *Mol. Cancer* **2010**, *9* (1), 256. https://doi.org/10.1186/1476-4598-9-256.

86. Baines, A. T.; Xu, D.; Der, C. J. Inhibition of Ras for Cancer Treatment: The Search Continues. *Future Med. Chem.* **2011**, *3* (14), 1787–1808. https://doi.org/10.4155/fmc.11.121.

87. Laheru, D.; Shah, P.; Rajeshkumar, N. V; McAllister, F.; Taylor, G.; Goldsweig, H.; Le, D. T.; Donehower, R.; Jimeno, A.; Linden, S.; et al. Integrated Preclinical and Clinical Development of S-Trans, Trans-Farnesylthiosalicylic Acid (FTS, Salirasib) in Pancreatic Cancer. *Invest. New Drugs* **2012**, *30* (6), 2391–2399. https://doi.org/10.1007/s10637-012-9818-6.

88. Riely, G. J.; Johnson, M. L.; Medina, C.; Rizvi, N. A.; Miller, V. A.; Kris, M. G.; Pietanza, M. C.; Azzoli, C. G.; Krug, L. M.; Pao, W.; et al. A Phase II Trial of Salirasib in Patients with Lung Adenocarcinomas with KRAS Mutations. *J. Thorac. Oncol.* **2011**, *6* (8), 1435–1437. https://doi.org/10.1097/JTO.0b013e318223c099.

89. Furuse, J.; Kurata, T.; Okano, N.; Fujisaka, Y.; Naruge, D.; Shimizu, T.; Kitamura, H.; Iwasa, T.; Nagashima, F.; Nakagawa, K. An Early Clinical Trial of Salirasib, an Oral RAS Inhibitor, in Japanese Patients with Relapsed/Refractory Solid Tumors. *Cancer Chemother. Pharmacol.* **2018**, *82* (3), 511–519. https://doi.org/10.1007/s00280-018-3618-4.

90. Ostrem, J. M.; Peters, U.; Sos, M. L.; Wells, J. A.; Shokat, K. M. K-Ras(G12C) Inhibitors Allosterically Control GTP Affinity and Effector Interactions. *Nature* **2013**, *503* (7477), 548–551. https://doi.org/10.1038/nature12796.

91. Shima, F.; Yoshikawa, Y.; Ye, M.; Araki, M.; Matsumoto, S.; Liao, J.; Hu, L.; Sugimoto, T.; Ijiri, Y.; Takeda, A.; et al. In Silico Discovery of Small-Molecule Ras Inhibitors That Display Antitumor Activity by Blocking the Ras-Effector Interaction. *Proc. Natl. Acad. Sci.* **2013**, *110* (20), 8182–8187. https://doi.org/10.1073/pnas.1217730110.

92. Westcott, P. M. K.; To, M. D. The Genetics and Biology of KRAS in Lung Cancer. *Chin. J. Cancer* **2013**, *32* (2), 63–70. https://doi.org/10.5732/cjc.012.10098.

93. Janes, M. R.; Zhang, J.; Li, L.-S.; Hansen, R.; Peters, U.; Guo, X.; Chen, Y.; Babbar, A.; Firdaus, S. J.; Darjania, L.; et al. Targeting KRAS Mutant Cancers with a Covalent G12C-Specific Inhibitor. *Cell* **2018**, *172* (3), 578–589.e17.

https://doi.org/10.1016/j.cell.2018.01.006.

94. Hunter, J. C.; Gurbani, D.; Ficarro, S. B.; Carrasco, M. a.; Lim, S. M.; Choi, H. G.; Xie, T.; Marto, J. a.; Chen, Z.; Gray, N. S.; et al. In Situ Selectivity Profiling and Crystal Structure of SML-8-73-1, an Active Site Inhibitor of Oncogenic K-Ras G12C. *Proc. Natl. Acad. Sci.* **2014**, *111* (24), 8895–8900. https://doi.org/10.1073/pnas.1404639111.

95. Lu, S.; Jang, H.; Gu, S.; Zhang, J.; Nussinov, R. Drugging Ras GTPase: A Comprehensive Mechanistic and Signaling Structural View. *Chem. Soc. Rev.* **2016**. https://doi.org/10.1039/C5CS00911A.

96. West, A. C.; Johnstone, R. W. New and Emerging HDAC Inhibitors for Cancer Treatment. *J. Clin. Invest.* **2014**, *124* (1), 30–39. https://doi.org/10.1172/JCI69738.

97. McGrath, J.; Trojer, P. Targeting Histone Lysine Methylation in Cancer. *Pharmacol. Ther.* **2015**, *150*, 1–22. https://doi.org/10.1016/j.pharmthera.2015.01.002.

98. Bhullar, K. S.; Lagarón, N. O.; McGowan, E. M.; Parmar, I.; Jha, A.; Hubbard, B. P.; Rupasinghe, H. P. V. Kinase-Targeted Cancer Therapies: Progress, Challenges and Future Directions. *Mol. Cancer* **2018**, *17* (1), 48. https://doi.org/10.1186/s12943-018-0804-2.

99. Gross, S.; Rahal, R.; Stransky, N.; Lengauer, C.; Hoeflich, K. P. Targeting Cancer with Kinase Inhibitors. *J. Clin. Invest.* **2015**, *125* (5), 1780–1789. https://doi.org/10.1172/JCI76094.

100. Malone, C. F.; Emerson, C.; Ingraham, R.; Barbosa, W.; Guerra, S.; Yoon, H.; Liu, L. L.; Michor, F.; Haigis, M.; Macleod, K. F.; et al. MTOR and HDAC Inhibitors Converge on the TXNIP/Thioredoxin Pathway to Cause Catastrophic Oxidative Stress and Regression of RAS-Driven Tumors. *Cancer Discov.* **2017**, *7* (12), 1450–1463. https://doi.org/10.1158/2159-8290.CD-17-0177.

101. Ischenko, I.; Petrenko, O.; Hayman, M. J. A MEK/PI3K/HDAC Inhibitor Combination Therapy for KRAS Mutant Pancreatic Cancer Cells. *Oncotarget* **2015**, *6* (18). https://doi.org/10.18632/oncotarget.4538.

102. Yamada, T.; Amann, J. M.; Tanimoto, A.; Taniguchi, H.; Shukuya, T.; Timmers, C.; Yano, S.; Shilo, K.; Carbone, D. P. Histone Deacetylase Inhibition Enhances the Antitumor Activity of a MEK Inhibitor in Lung Cancer Cells Harboring RAS Mutations. *Mol. Cancer Ther.* **2018**, *17* (1), 17–25. https://doi.org/10.1158/1535-7163.MCT-17-0146.

103. McCabe, M. T.; Mohammad, H. P.; Barbash, O.; Kruger, R. G. Targeting Histone Methylation in Cancer. *Cancer J. (United States)* **2017**, *23* (5), 292–301. https://doi.org/10.1097/PPO.0000000000000283.

104. Kaniskan, H. Ü.; Martini, M. L.; Jin, J. Inhibitors of Protein Methyltransferases and Demethylases. *Chem. Rev.* **2018**, *118* (3), 989–1068. https://doi.org/10.1021/acs.chemrev.6b00801.

105. Singh, B. N.; Zhang, G.; Hwa, Y. L.; Li, J.; Dowdy, S. C.; Jiang, S. W. Nonhistone Protein Acetylation as Cancer Therapy Targets. *Expert Review of Anticancer Therapy*. 2010. https://doi.org/10.1586/era.10.62.

106. Slingerland, M.; Guchelaar, H.-J.; Gelderblom, H. Histone Deacetylase Inhibitors: An Overview of the Clinical Studies in Solid Tumors. *Anticancer. Drugs* **2014**, *25* (2), 140–149. https://doi.org/10.1097/CAD.0000000000000040.

107. Stephen, A. G.; Esposito, D.; Bagni, R. K.; McCormick, F. Dragging Ras Back in the Ring. *Cancer Cell* **2014**, *25* (3), 272–281. https://doi.org/10.1016/j.ccr.2014.02.017.

108. Arrington, A. K.; Heinrich, E. L.; Lee, W.; Duldulao, M.; Patel, S.; Sanchez, J.; Garcia-Aguilar, J.; Kim, J. Prognostic and Predictive Roles of KRAS Mutation in Colorectal Cancer. *International Journal of Molecular Sciences*. 2012. https://doi.org/10.3390/ijms131012153.

109. Palomba, G.; Doneddu, V.; Cossu, A.; Paliogiannis, P.; Manca, A.; Casula, M.; Colombino, M.; Lanzillo, A.; Defraia, E.; Pazzola, A.; et al. Prognostic Impact of KRAS, NRAS, BRAF, and PIK3CA Mutations in Primary Colorectal Carcinomas: A Population-Based Study. *J. Transl. Med.* **2016**. https://doi.org/10.1186/s12967-016-1053-z.

110. Sakuma, T.; Uzawa, K.; Onda, T.; Shiiba, M.; Yokoe, H.; Shibahara, T.; Tanzawa, H. Aberrant Expression of Histone Deacetylase 6 in Oral Squamous Cell Carcinoma. *Int. J. Oncol.* **2006**. https://doi.org/10.3892/ijo.29.1.117.

111. Polevoda, B.; Sherman, F. N(α)-Terminal Acetylation of Eukaryotic Proteins. *Journal of Biological Chemistry*. 2000. https://doi.org/10.1074/jbc.R000023200.

112. Ropero, S.; Esteller, M. The Role of Histone Deacetylases (HDACs) in Human Cancer. *Molecular Oncology*. 2007. https://doi.org/10.1016/j.molonc.2007.01.001.

113. Bowman, G. D.; Poirier, M. G. Post-Translational Modifications of Histones That Influence Nucleosome Dynamics. *Chem. Rev.* **2015**, *115* (6), 2274–2295. https://doi.org/10.1021/cr500350x.

114. Reed, S.; Quelle, D. P53 Acetylation: Regulation and Consequences. *Cancers (Basel).* **2014**, *7* (1), 30–69. https://doi.org/10.3390/cancers7010030.

115. Qiu, T.; Zhou, L.; Zhu, W.; Wang, T.; Wang, J.; Shu, Y.; Liu, P. Effects of Treatment with Histone Deacetylase Inhibitors in Solid Tumors: A Review Based on 30 Clinical Trials. *Futur. Oncol.* **2013**, *9* (2), 255–269. https://doi.org/10.2217/fon.12.173.

116. Song, H. Y.; Biancucci, M.; Kang, H. J.; O'Callaghan, C.; Park, S. H.; Principe, D. R.; Jiang, H.; Yan, Y.; Satchell, K. F.; Raparia, K.; et al. SIRT2 Deletion Enhances KRAS-Induced Tumorigenesis in Vivo by Regulating K147 Acetylation Status. *Oncotarget* **2016**, No. September. https://doi.org/10.18632/oncotarget.12015.

117. Yang, M. H.; Laurent, G.; Bause, A. S.; Spang, R.; German, N.; Haigis, M. C.; Haigis, K.

M. HDAC6 and SIRT2 Regulate the Acetylation State and Oncogenic Activity of Mutant K-RAS. *Mol. Cancer Res.* **2013**, *11* (9), 1072–1077. https://doi.org/10.1158/1541-7786.MCR-13-0040-T.

118. Song, H.; Li, C. W.; Labaff, A. M.; Lim, S. O.; Li, L. Y.; Kan, S. F.; Chen, Y.; Zhang, K.; Lang, J.; Xie, X.; et al. Acetylation of EGF Receptor Contributes to Tumor Cell Resistance to Histone Deacetylase Inhibitors. *Biochem. Biophys. Res. Commun.* **2011**. https://doi.org/10.1016/j.bbrc.2010.11.064.

119. Zhu, P.; Martin, E.; Mengwasser, J.; Schlag, P.; Janssen, K.-P.; Göttlicher, M. Induction of HDAC2 Expression upon Loss of APC in Colorectal Tumorigenesis. *Cancer Cell* **2004**, *5* (5), 455–463. https://doi.org/10.1016/S1535-6108(04)00114-X.

120. Wilson, A. J.; Byun, D.-S.; Popova, N.; Murray, L. B.; L'Italien, K.; Sowa, Y.; Arango, D.; Velcich, A.; Augenlicht, L. H.; Mariadason, J. M. Histone Deacetylase 3 (HDAC3) and Other Class I HDACs Regulate Colon Cell Maturation and P21 Expression and Are Deregulated in Human Colon Cancer. *J. Biol. Chem.* **2006**, *281* (19), 13548–13558. https://doi.org/10.1074/jbc.M510023200.

121. Weichert, W.; Roske, A.; Niesporek, S.; Noske, A.; Buckendahl, A.-C.; Dietel, M.; Gekeler, V.; Boehm, M.; Beckers, T.; Denkert, C. Class I Histone Deacetylase Expression Has Independent Prognostic Impact in Human Colorectal Cancer: Specific Role of Class I Histone Deacetylases In Vitro and In Vivo. *Clin. Cancer Res.* **2008**, *14* (6), 1669–1677. https://doi.org/10.1158/1078-0432.CCR-07-0990.

122. Kaler, P.; Sasazuki, T.; Shirasawa, S.; Augenlicht, L.; Klampfer, L. HDAC2 Deficiency Sensitizes Colon Cancer Cells to TNFα-Induced Apoptosis through Inhibition of NF-KB Activity. *Exp. Cell Res.* **2008**, *314* (7), 1507–1518. https://doi.org/10.1016/j.yexcr.2008.01.010.

123. Siegel, R. L.; Miller, K. D.; Jemal, A. Cancer Statistics, 2017. *CA. Cancer J. Clin.* **2017**, *67* (1), 7–30. https://doi.org/10.3322/caac.21387.

124. Jones, P. A.; Issa, J. P. J.; Baylin, S. Targeting the Cancer Epigenome for Therapy. *Nature Reviews Genetics*. 2016. https://doi.org/10.1038/nrg.2016.93.

125. Song, H. Y.; Biancucci, M.; Kang, H.; O'Callaghan, C.; Park, S.-H.; Principe, D. R.; Jiang, H.; Yan, Y.; Satchell, K. F.; Raparia, K.; et al. SIRT2 Deletion Enhances KRAS-Induced Tumorigenesis in Vivo by Regulating K147 Acetylation Status. *Oncotarget* **2016**. https://doi.org/10.18632/oncotarget.12015.

126. Yang, M. H.; Laurent, G.; Bause, A. S.; Spang, R.; German, N.; Haigis, M. C.; Haigis, K. M. HDAC6 and SIRT2 Regulate the Acetylation State and Oncogenic Activity of Mutant K-RAS. *Mol. Cancer Res.* **2013**, *11* (9), 1072–1077. https://doi.org/10.1158/1541-7786.MCR-13-0040-T.

127. Taylor, S. J.; Shalloway, D. Cell Cycle-Dependent Activation of Ras. *Curr. Biol.* **1996**, *6* (12), 1621–1627.

128. Gremer, L.; Merbitz-Zahradnik, T.; Dvorsky, R.; Cirstea, I. C.; Kratz, C. P.; Zenker, M.; Wittinghofer, A.; Ahmadian, M. R. Germline KRAS Mutations Cause Aberrant Biochemical and Physical Properties Leading to Developmental Disorders. *Hum. Mutat.* **2011**, *32* (1), 33–43. https://doi.org/10.1002/humu.21377.

129. Zenker, M.; Lehmann, K.; Schulz, A. L.; Barth, H.; Hansmann, D.; Koenig, R.; Korinthenberg, R.; Kreiss-Nachtsheim, M.; Meinecke, P.; Morlot, S.; et al. Expansion of the Genotypic and Phenotypic Spectrum in Patients with KRAS Germline Mutations. *J. Med. Genet.* **2007**, *44* (2), 131–135. https://doi.org/10.1136/jmg.2006.046300.

130. Bertola, D. R.; Pereira, A. C.; Brasil, A. S.; Albano, L. M. J.; Kim, C. A.; Krieger, J. E. Further Evidence of Genetic Heterogeneity in Costello Syndrome: Involvement of the KRAS Gene. *J. Hum. Genet.* **2007**, *52* (6), 521–526. https://doi.org/10.1007/s10038-007-0146-1.

131. Sondermann, H.; Soisson, S. M.; Boykevisch, S.; Yang, S.-S.; Bar-Sagi, D.; Kuriyan, J. Structural Analysis of Autoinhibition in the Ras Activator Son of Sevenless. *Cell* **2004**, *119* (3), 393–405. https://doi.org/10.1016/j.cell.2004.10.005.

132. Neumann, H.; Hancock, S. M.; Buning, R.; Routh, A.; Chapman, L.; Somers, J.; Owen-Hughes, T.; van Noort, J.; Rhodes, D.; Chin, J. W. A Method for Genetically Installing Site-Specific Acetylation in Recombinant Histones Defines the Effects of H3 K56 Acetylation. *Mol. Cell* **2009**, *36* (1), 153–163. https://doi.org/10.1016/j.molcel.2009.07.027.

133. Neumann, H.; Peak-Chew, S. Y.; Chin, J. W. Genetically Encoding N(Epsilon)-Acetyllysine in Recombinant Proteins. *Nat. Chem. Biol.* **2008**, *4* (4), 232–234. https://doi.org/10.1038/nchembio.73.

134. Lenzen, C.; Cool, R. H.; Wittinghofer, A. Analysis of Intrinsic and CDC25-Stimulated Guanine Nucleotide Exchange of P21ras-Nucleotide Complexes by Fluorescence Measurements. *Methods Enzymol.* **1995**, *255* (C), 95–109. https://doi.org/10.1016/S0076-6879(95)55012-7.

135. Lenzen, C.; Cool, R. H.; Prinz, H.; Kuhlmann, J.; Wittinghofer, A. Kinetic Analysis by Fluorescence of the Interaction between Ras and the Catalytic Domain of the Guanine Nucleotide Exchange Factor Cdc25. *Biochemistry* **1998**, *37* (20), 7420–7430. https://doi.org/10.1021/bi972621j.

136. Scheffzek, K.; Lautwein, A.; Kabsch, W.; Reza Ahmadian, M.; Wittinghofer, A. Crystal Structure of the GTPase-Activating Domain of Human P120GAP and Implications for the Interaction with Ras. *Nature* **1996**, *384* (6609), 591–596. https://doi.org/10.1038/384591a0.

137. Daura, X.; Gademann, K.; Jaun, B.; Seebach, D.; van Gunsteren, W. F.; Mark, A. E. Peptide Folding: When Simulation Meets Experiment. *Angew. Chemie Int. Ed.* **1999**, *38* (1/2), 236–240. https://doi.org/10.1002/(SICI)1521-3773(19990115)38:1/2<236::AID-ANIE236>3.3.CO;2-D.

138. Honig, B.; Nicholls, A. Classical Electrostatics in Biology and Chemistry. *Science (80-.).* **1995**, *268* (5214), 1144–1149. https://doi.org/10.1126/science.7761829.

139. Kumar, S.; Nussinov, R. Salt Bridge Stability in Monomeric Proteins. *J. Mol. Biol.* **1999**, *293* (5), 1241–1255. https://doi.org/10.1006/jmbi.1999.3218.

140. Kumar, S.; Tsai, C.-J.; Nussinov, R. Factors Enhancing Protein Thermostability. *Protein Eng. Des. Sel.* **2000**, *13* (3), 179–191. https://doi.org/10.1093/protein/13.3.179.

141. Humphrey, W.; Dalke, A.; Schulten, K. VMD: Visual Molecular Dynamics. *J. Mol. Graph.* **1996**. https://doi.org/10.1016/0263-7855(96)00018-5.

142. Prince, H. M.; Bishton, M. J.; Harrison, S. J. Clinical Studies of Histone Deacetylase Inhibitors. *Clin. Cancer Res.* **2009**, *15* (12), 3958–3969. https://doi.org/10.1158/1078-0432.CCR-08-2785.

143. Saito, A.; Yamashita, T.; Mariko, Y.; Nosaka, Y.; Tsuchiya, K.; Ando, T.; Suzuki, T.; Tsuruo, T.; Nakanishi, O. A Synthetic Inhibitor of Histone Deacetylase, MS-27-275, with Marked in Vivo Antitumor Activity against Human Tumors. *Proc. Natl. Acad. Sci. U. S. A.* **1999**, *96* (8), 4592–4597.

144. Gartel, A. L.; Radhakrishnan, S. K. Lost in Transcription: P21 Repression, Mechanisms, and Consequences. *Cancer Research*. 2005. https://doi.org/10.1158/0008-5472.CAN-04-3995.

145. Glozak, M. A.; Seto, E. Histone Deacetylases and Cancer. *Oncogene* **2007**, *26* (37), 5420–5432. https://doi.org/10.1038/sj.onc.1210610.

146. Saji, S.; Kawakami, M.; Hayashi, S.-I.; Yoshida, N.; Hirose, M.; Horiguchi, S.-I.; Itoh, A.; Funata, N.; Schreiber, S. L.; Yoshida, M.; et al. Significance of HDAC6 Regulation via Estrogen Signaling for Cell Motility and Prognosis in Estrogen Receptor-Positive Breast Cancer. *Oncogene* **2005**, *24* (28), 4531–4539. https://doi.org/10.1038/sj.onc.1208646.

147. Yardley, D. A.; Ismail-Khan, R. R.; Melichar, B.; Lichinitser, M.; Munster, P. N.; Klein, P. M.; Cruickshank, S.; Miller, K. D.; Lee, M. J.; Trepel, J. B. Randomized Phase II, Double-Blind, Placebo-Controlled Study of Exemestane with or without Entinostat in Postmenopausal Women with Locally Recurrent or Metastatic Estrogen Receptor-Positive Breast Cancer Progressing on Treatment with a Nonsteroidal Aromata. *J. Clin. Oncol.* **2013**. https://doi.org/10.1200/JCO.2012.43.7251.

148. Blagosklonny, M. V; Pardee, A. B. The Restriction Point of the Cell Cycle. *Cell Cycle* **2002**, *1* (2), 102–109. https://doi.org/10.4161/cc.1.2.108.

149. Goel, S.; DeCristo, M. J.; McAllister, S. S.; Zhao, J. J. CDK4/6 Inhibition in Cancer: Beyond Cell Cycle Arrest. *Trends Cell Biol.* **2018**, *28* (11), 911–925. https://doi.org/10.1016/j.tcb.2018.07.002.

150. Orlando, S.; Gallastegui, E.; Besson, A.; Abril, G.; Aligué, R.; Pujol, M. J.; Bachs, O. P27

Kip1 and P21 Cip1 Collaborate in the Regulation of Transcription by Recruiting Cyclin–Cdk Complexes on the Promoters of Target Genes. *Nucleic Acids Res.* **2015**, *43* (14), 6860–6873. https://doi.org/10.1093/nar/gkv593.

151. de Boor, S.; Knyphausen, P.; Kuhlmann, N.; Wroblowski, S.; Brenig, J.; Scislowski, L.; Baldus, L.; Nolte, H.; Krüger, M.; Lammers, M. Small GTP-Binding Protein Ran Is Regulated by Posttranslational Lysine Acetylation. *Proc. Natl. Acad. Sci.* **2015**, *112* (28), E3679–E3688. https://doi.org/10.1073/pnas.1505995112.

152. Avalos, J. L.; Bever, K. M.; Wolberger, C. Mechanism of Sirtuin Inhibition by Nicotinamide: Altering the NAD+cosubstrate Specificity of a Sir2 Enzyme. *Mol. Cell* **2005**, *17* (6), 855–868. https://doi.org/10.1016/j.molcel.2005.02.022.

153. Abouelfetouh, A.; Kuhn, M. L.; Hu, L. I.; Scholle, M. D.; Sorensen, D. J.; Sahu, A. K.; Becher, D.; Antelmann, H.; Mrksich, M.; Anderson, W. F.; et al. The E. Coli Sirtuin CobB Shows No Preference for Enzymatic and Nonenzymatic Lysine Acetylation Substrate Sites. *Microbiologyopen* **2015**, *4* (1), 66–83. https://doi.org/10.1002/mbo3.223.

154. Shutes, A.; Der, C. J. Real-Time In Vitro Measurement of Intrinsic and Ras GAP-Mediated GTP Hydrolysis. In *Methods in Enzymology*; 2006; Vol. 81, pp 9–22. https://doi.org/10.1016/S0076-6879(05)07002-3.

155. Gu, H.; Lalonde, S.; Okumoto, S.; Looger, L. L.; Scharff-Poulsen, A. M.; Grossman, A. R.; Kossmann, J.; Jakobsen, I.; Frommer, W. B. A Novel Analytical Method for in Vivo Phosphate Tracking. *FEBS Lett.* **2006**, *580* (25), 5885–5893. https://doi.org/10.1016/j.febslet.2006.09.048.

156. Brune, M.; Hunter, J. L.; Corrie, J. E. T.; Webb, M. R. Direct, Real-Time Measurement of Rapid Inorganic Phosphate Release Using a Novel Fluorescent Probe and Its Application to Actomyosin Subfragment 1 ATPase. *Biochemistry* **1994**. https://doi.org/10.1021/bi00193a013.

157. Bunney, T. D.; Harris, R.; Gandarillas, N. L.; Josephs, M. B.; Roe, S. M.; Sorli, S. C.; Paterson, H. F.; Rodrigues-Lima, F.; Esposito, D.; Ponting, C. P.; et al. Structural and Mechanistic Insights into Ras Association Domains of Phospholipase C Epsilon. *Mol. Cell* **2006**, *21* (4), 495–507. https://doi.org/10.1016/j.molcel.2006.01.008.

158. Margreitter, C.; Petrov, D.; Zagrovic, B. Vienna-PTM Web Server: A Toolkit for MD Simulations of Protein Post-Translational Modifications. *Nucleic Acids Res.* **2013**, *41* (Web Server issue). https://doi.org/10.1093/nar/gkt416.

159. Margreitter, C.; Reif, M. M.; Oostenbrink, C. Update on Phosphate and Charged Post-Translationally Modified Amino Acid Parameters in the GROMOS Force Field. *J. Comput. Chem.* **2017**, *38* (10), 714–720. https://doi.org/10.1002/jcc.24733.

160. Petrov, D.; Margreitter, C.; Grandits, M.; Oostenbrink, C.; Zagrovic, B. A Systematic Framework for Molecular Dynamics Simulations of Protein Post-Translational Modifications. *Plos Comput. Biol.* **2013**, *9* (7). https://doi.org/ARTN e1003154\rDOI

10.1371/journal.pcbi.1003154.

161. Koziara, K. B.; Stroet, M.; Malde, A. K.; Mark, A. E. Testing and Validation of the Automated Topology Builder (ATB) Version 2.0: Prediction of Hydration Free Enthalpies. *J. Comput. Aided. Mol. Des.* **2014**, *28* (3), 221–233. https://doi.org/10.1007/s10822-014-9713-7.

162. Malde, A. K.; Zuo, L.; Breeze, M.; Stroet, M.; Poger, D.; Nair, P. C.; Oostenbrink, C.; Mark, A. E. An Automated Force Field Topology Builder (ATB) and Repository: Version 1.0. *J. Chem. Theory Comput.* **2011**, *7* (12), 4026–4037. https://doi.org/10.1021/ct200196m.

163. Abraham, M. J.; Murtola, T.; Schulz, R.; Páll, S.; Smith, J. C.; Hess, B.; Lindahl, E. GROMACS: High Performance Molecular Simulations through Multi-Level Parallelism from Laptops to Supercomputers. *SoftwareX* **2015**, *1–2*, 19–25. https://doi.org/10.1016/j.softx.2015.06.001.

164. Huang, W.; Lin, Z.; Van Gunsteren, W. F. Validation of the GROMOS 54A7 Force Field with Respect to β-Peptide Folding. *J. Chem. Theory Comput.* **2011**. https://doi.org/10.1021/ct100747y.

165. Darden, T.; York, D.; Pedersen, L. Particle Mesh Ewald: An N·log(N) Method for Ewald Sums in Large Systems. *J. Chem. Phys.* **1993**. https://doi.org/10.1063/1.464397.

166. Essmann, U.; Perera, L.; Berkowitz, M. L.; Darden, T.; Lee, H.; Pedersen, L. G. A Smooth Particle Mesh Ewald Method. *J. Chem. Phys.* **1995**. https://doi.org/10.1063/1.470117.

167. Baker, N. A.; Sept, D.; Joseph, S.; Holst, M. J.; McCammon, J. A. Electrostatics of Nanosystems: Application to Microtubules and the Ribosome. *Proc. Natl. Acad. Sci.* **2001**, *98* (18), 10037–10041. https://doi.org/10.1073/pnas.181342398.

168. Kumari, R.; Kumar, R.; Lynn, A. G_mmpbsa —A GROMACS Tool for High-Throughput MM-PBSA Calculations. *J. Chem. Inf. Model.* **2014**, *54* (7), 1951–1962. https://doi.org/10.1021/ci500020m.

169. Genheden, S.; Ryde, U. The MM/PBSA and MM/GBSA Methods to Estimate Ligand-Binding Affinities. *Expert Opin. Drug Discov.* **2015**, *10* (5), 449–461. https://doi.org/10.1517/17460441.2015.1032936.

170. Gelb, B. D.; Tartaglia, M. Noonan Syndrome and Related Disorders: Dysregulated RAS-Mitogen Activated Protein Kinase Signal Transduction. *Hum. Mol. Genet.* **2006**, *15* (suppl_2), R220–R226. https://doi.org/10.1093/hmg/ddl197.

171. Tidyman, W. E.; Rauen, K. A. The RASopathies: Developmental Syndromes of Ras/MAPK Pathway Dysregulation. *Curr. Opin. Genet. Dev.* **2009**, *19* (3), 230–236. https://doi.org/10.1016/j.gde.2009.04.001.

172. Carta, C.; Pantaleoni, F.; Bocchinfuso, G.; Stella, L.; Vasta, I.; Sarkozy, A.; Digilio, C.; Palleschi, A.; Pizzuti, A.; Grammatico, P.; et al. Germline Missense Mutations Affecting KRAS Isoform B Are Associated with a Severe Noonan Syndrome Phenotype. *Am. J. Hum. Genet.* **2006**, *79* (1), 129–135. https://doi.org/10.1086/504394.

173. Kratz, C. P.; Niemeyer, C. M.; Zenker, M. An Unexpected New Role of Mutant Ras: Perturbation of Human Embryonic Development. *J. Mol. Med.* **2007**, *85* (3), 227–235. https://doi.org/10.1007/s00109-006-0135-4.

174. Nava, C.; Hanna, N.; Michot, C.; Pereira, S.; Pouvreau, N.; Niihori, T.; Aoki, Y.; Matsubara, Y.; Arveiler, B.; Lacombe, D.; et al. Cardio-Facio-Cutaneous and Noonan Syndromes Due to Mutations in the RAS/MAPK Signalling Pathway: Genotype Phenotype Relationships and Overlap with Costello Syndrome. *J. Med. Genet.* **2007**, *44* (12), 763–771. https://doi.org/10.1136/jmg.2007.050450.

175. Niihori, T.; Aoki, Y.; Narumi, Y.; Neri, G.; Cavé, H.; Verloes, A.; Okamoto, N.; Hennekam, R. C. M.; Gillessen-Kaesbach, G.; Wieczorek, D.; et al. Germline KRAS and BRAF Mutations in Cardio-Facio-Cutaneous Syndrome. *Nat. Genet.* **2006**, *38* (3), 294–296. https://doi.org/10.1038/ng1749.

176. Schubbert, S.; Zenker, M.; Rowe, S. L.; Böll, S.; Klein, C.; Bollag, G.; van der Burgt, I.; Musante, L.; Kalscheuer, V.; Wehner, L.-E.; et al. Germline KRAS Mutations Cause Noonan Syndrome. *Nat. Genet.* **2006**, *38* (3), 331–336. https://doi.org/10.1038/ng1748.

177. Zenker, M.; Lehmann, K.; Schulz, A. L.; Barth, H.; Hansmann, D.; Koenig, R.; Korinthenberg, R.; Kreiss-Nachtsheim, M.; Meinecke, P.; Morlot, S.; et al. Expansion of the Genotypic and Phenotypic Spectrum in Patients with KRAS Germline Mutations. *J. Med. Genet.* **2006**, *44* (2), 131–135. https://doi.org/10.1136/jmg.2006.046300.

178. Tartaglia, M.; Gelb, B. D. Noonan Syndrome and Related Disorders: Genetics and Pathogenesis. *Annu. Rev. Genomics Hum. Genet.* **2005**, *6* (1), 45–68. https://doi.org/10.1146/annurev.genom.6.080604.162305.

179. Dance, M.; Montagner, A.; Salles, J.-P.; Yart, A.; Raynal, P. The Molecular Functions of Shp2 in the Ras/Mitogen-Activated Protein Kinase (ERK1/2) Pathway. *Cell. Signal.* **2008**, *20* (3), 453–459. https://doi.org/10.1016/j.cellsig.2007.10.002.

180. Rauen, K. A.; Schoyer, L.; Schill, L.; Stronach, B.; Albeck, J.; Andresen, B. S.; Cavé, H.; Ellis, M.; Fruchtman, S. M.; Gelb, B. D.; et al. Proceedings of the Fifth International RASopathies Symposium: When Development and Cancer Intersect. *Am. J. Med. Genet. Part A* **2018**, *176* (12), 2924–2929. https://doi.org/10.1002/ajmg.a.40632.

181. Lee, S. H.; Lee, J. W.; Soung, Y. H.; Kim, H. S.; Park, W. S.; Kim, S. Y.; Lee, J. H.; Park, J. Y.; Cho, Y. G.; Kim, C. J.; et al. BRAF and KRAS Mutations in Stomach Cancer. *Oncogene* **2003**, *22* (44), 6942–6945. https://doi.org/10.1038/sj.onc.1206749.

182. Yoshida, K.; Sanada, M.; Shiraishi, Y.; Nowak, D.; Nagata, Y.; Yamamoto, R.; Sato, Y.; Sato-Otsubo, A.; Kon, A.; Nagasaki, M.; et al. Frequent Pathway Mutations of Splicing

Machinery in Myelodysplasia. *Nature* **2011**, *478* (7367), 64–69. https://doi.org/10.1038/nature10496.

183. Zehir, A.; Benayed, R.; Shah, R. H.; Syed, A.; Middha, S.; Kim, H. R.; Srinivasan, P.; Gao, J.; Chakravarty, D.; Devlin, S. M.; et al. Mutational Landscape of Metastatic Cancer Revealed from Prospective Clinical Sequencing of 10,000 Patients. *Nat. Med.* **2017**, *23* (6), 703–713. https://doi.org/10.1038/nm.4333.

184. Le Calvez-Kelm, F.; Foll, M.; Wozniak, M. B.; Delhomme, T. M.; Durand, G.; Chopard, P.; Pertesi, M.; Fabianova, E.; Adamcakova, Z.; Holcatova, I.; et al. KRas Mutations in Blood Circulating Cell-Free DNA: A Pancreatic Cancer Case-Control. *Oncotarget* **2016**, *7* (48), 78827–78840. https://doi.org/10.18632/oncotarget.12386.

185. Lim, E. H.; Zhang, S.-L.; Yu, K.; Nga, M.-E.; Ahmed, D. A.; Agasthian, T.; Wong, P.-S.; Chua, G.-C.; Wong, D.; Tan, L.; et al. An Alternative Approach to Determining Therapeutic Choices in Advanced Non-Small Cell Lung Carcinoma (NSCLC): Maximizing the Diagnostic Procedure and the Use of Low-Volume Lung Biopsies. *J. Thorac. Oncol.* **2007**, *2* (5), 387–396. https://doi.org/10.1097/01.JTO.0000268671.49378.c2.

186. Wittinghofer, A. *Ras Superfamily Small G Proteins: Biology and Mechanisms 1*; Wittinghofer, A., Ed.; Springer Vienna: Vienna, 2014. https://doi.org/10.1007/978-3-7091-1806-1.

187. Lee, W.; Tonelli, M.; Markley, J. L. NMRFAM-SPARKY: Enhanced Software for Biomolecular NMR Spectroscopy. *Bioinformatics* **2015**. https://doi.org/10.1093/bioinformatics/btu830.

188. Pettersen, E. F.; Goddard, T. D.; Huang, C. C.; Couch, G. S.; Greenblatt, D. M.; Meng, E. C.; Ferrin, T. E. UCSF Chimera—A Visualization System for Exploratory Research and Analysis. *J Comput Chem* **2004**, *25*, 1605–1612. https://doi.org/10.1002/jcc.20084.

189. Lenzen, B. C.; Cool, R. H.; Wittinghofer, A. Analysis of Intrinsic CDC25-Stimulated Guanine Nucleotide Exchange of P21Ras Nucleotide Complexes by Fluorescence Measurements. **1995**, *255* (1992), 95–109.

190. Campbell-Burk, S. L.; Domaillea, P. J.; Starovasnik, M. A.; Boucher, W.; Laue, E. D. Sequential Assignment of the Backbone Nuclei (1H,15N And13C) of c-H-Ras P21 (1–166).GDP Using a Novel 4D NMR Strategy. *J. Biomol. NMR* **1992**, *2* (6), 639–646. https://doi.org/10.1007/BF02192852.

191. Wang, J.; Wang, W.; Kollman, P. a; Case, D. a. Antechamber, An Accessory Software Package For Molecular Mechanical Calculations. *J. Am. Chem. Soc* **2001**, *222*, U403. https://doi.org/10.1016/j.jmgm.2005.12.005.

192. Wittinghofer, A.; Pal, E. F. The Structure of Ras Protein: A Model for a Universal Molecular Switch. *Trends Biochem. Sci.* **1991**, *16*, 382–387. https://doi.org/10.1016/0968-0004(91)90156-P.

193. McCormick, F.; Wittinghofer, A. Interactions between Ras Proteins and Their Effectors. *Curr. Opin. Biotechnol.* **1996**, *7* (4), 449–456. https://doi.org/10.1016/S0958-1669(96)80123-6.

194. Wittinghofer, A.; Vetter, I. R. Structure-Function Relationships of the G Domain, a Canonical Switch Motif. *Annu. Rev. Biochem.* **2011**, *80* (1), 943–971. https://doi.org/10.1146/annurev-biochem-062708-134043.

195. Sattler, M. Heteronuclear Multidimensional NMR Experiments for the Structure Determination of Proteins in Solution Employing Pulsed Field Gradients. *Prog. Nucl. Magn. Reson. Spectrosc.* **1999**, *34* (2), 93–158. https://doi.org/10.1016/S0079-6565(98)00025-9.

196. Wishart, D.; Sykes, B. The 13C Chemical-Shift Index: A Simple Method for the Identification of Protein Secondary Structure Using 13C Chemical-Shift Data. *J. Biomol. NMR* **1994**, *4* (2), 171–180. https://doi.org/10.1007/BF00175245.

197. Terada, T.; Ito, Y.; Shirouzu, M.; Tateno, M.; Hashimoto, K.; Kigawa, T.; Ebisuzaki, T.; Takio, K.; Shibata, T.; Yokoyama, S.; et al. Nuclear Magnetic Resonance and Molecular Dynamics Studies on the Interactions of the Ras-Binding Domain of Raf-1 with Wild-Type and Mutant Ras Proteins. *J. Mol. Biol.* **1999**, *286* (1), 219–232. https://doi.org/10.1006/jmbi.1998.2472.

198. Long, D.; Marshall, C. B.; Bouvignies, G.; Mazhab-Jafari, M. T.; Smith, M. J.; Ikura, M.; Kay, L. E. A Comparative CEST NMR Study of Slow Conformational Dynamics of Small GTPases Complexed with GTP and GTP Analogues. *Angew. Chemie Int. Ed.* **2013**, *52* (41), 10771–10774. https://doi.org/10.1002/anie.201305434.

199. Lipari, G.; Szabo, A. Model-Free Approach to the Interpretation of Nuclear Magnetic Resonance Relaxation in Macromolecules. *J. Am. Chem. Soc.* **1982**, *104*, 4546–4559.

200. Drosten, M.; Dhawahir, A.; Sum, E. Y. M.; Urosevic, J.; Lechuga, C. G.; Esteban, L. M.; Castellano, E.; Guerra, C.; Santos, E.; Barbacid, M. Genetic Analysis of Ras Signalling Pathways in Cell Proliferation, Migration and Survival. *EMBO J.* **2010**, *29* (6), 1091–1104. https://doi.org/10.1038/emboj.2010.7.

201. Hall, B. E.; Yang, S. S.; Boriack-Sjodin, P. A.; Kuriyan, J.; Bar-Sagi, D. Structure-Based Mutagenesis Reveals Distinct Functions for Ras Switch 1 and Switch 2 in Sos-Catalyzed Guanine Nucleotide Exchange. *J. Biol. Chem.* **2001**, *276* (29), 27629–27637. https://doi.org/10.1074/jbc.M101727200.

202. Khosravi-Far, R.; White, M. A.; Westwick, J. K.; Solski, P. A.; Chrzanowska-Wodnicka, M.; Van Aelst, L.; Wigler, M. H.; Der, C. J. Oncogenic Ras Activation of Raf/Mitogen-Activated Protein Kinase-Independent Pathways Is Sufficient to Cause Tumorigenic Transformation. *Mol. Cell. Biol.* **1996**, *16* (7), 3923–3933.

203. Iwig, J. S.; Vercoulen, Y.; Das, R.; Barros, T.; Limnander, A.; Che, Y.; Pelton, J. G.; Wemmer, D. E.; Roose, J. P.; Kuriyan, J. Structural Analysis of Autoinhibition in the Ras-

Specific Exchange Factor RasGRP1. *Elife* **2013**, *2*, 1–28. https://doi.org/10.7554/eLife.00813.

204. Spencer-Smith, R.; Koide, A.; Zhou, Y.; Eguchi, R. R.; Sha, F.; Gajwani, P.; Santana, D.; Gupta, A.; Jacobs, M.; Herrero-Garcia, E.; et al. Inhibition of RAS Function through Targeting an Allosteric Regulatory Site. *Nat. Chem. Biol.* **2017**, *13* (1), 62–68. https://doi.org/10.1038/nchembio.2231.

205. Herrmann, C.; Horn, G.; Spaargaren, M.; Wittinghofer, A. Differential Interaction of the Ras Family GTP-Binding Proteins H-Ras, Rap1A, and R-Ras with the Putative Effector Molecules Raf Kinase and Ral-Guanine Nucleotide Exchange Factor. *J. Biol. Chem.* **1996**, *271* (12), 6794–6800. https://doi.org/10.1074/jbc.271.12.6794.

206. Jung, Y. S.; Zweckstetter, M. Mars - Robust Automatic Backbone Assignment of Proteins. *J. Biomol. NMR* **2004**. https://doi.org/10.1023/B:JNMR.0000042954.99056.ad.

207. Tamiola, K.; Acar, B.; Mulder, F. A. A. Sequence-Specific Random Coil Chemical Shifts of Intrinsically Disordered Proteins. *J. Am. Chem. Soc.* **2010**, *132* (51), 18000–18003. https://doi.org/10.1021/ja105656t.

208. Cole, R.; Loria, J. P. FAST-Modelfree: A Program for Rapid Automated Analysis of Solution NMR Spin-Relaxation Data. *J. Biomol. NMR* **2003**, *26* (3), 203–213.

209. Mandel, A. M.; Akke, M.; Palmer, III, A. G. Backbone Dynamics OfEscherichia ColiRibonuclease HI: Correlations with Structure and Function in an Active Enzyme. *J. Mol. Biol.* **1995**, *246* (1), 144–163. https://doi.org/10.1006/jmbi.1994.0073.

210. Lambert, J. M.; Lambert, Q. T.; Reuther, G. W.; Malliri, A.; Siderovski, D. P.; Sondek, J.; Collard, J. G.; Der, C. J. Tiam1 Mediates Ras Activation of Rac by a PI(3)K-Independent Mechanism. *Nat. Cell Biol.* **2002**, *4* (8), 621–625. https://doi.org/10.1038/ncb833.

211. Chen, H.; Venkat, S.; McGuire, P.; Gan, Q.; Fan, C. Recent Development of Genetic Code Expansion for Posttranslational Modification Studies. *Molecules* **2018**, *23* (7), 1662. https://doi.org/10.3390/molecules23071662.

212. Smith, B. C.; Denu, J. M. Chemical Mechanisms of Histone Lysine and Arginine Modifications. *Biochimica et Biophysica Acta - Gene Regulatory Mechanisms*. 2009. https://doi.org/10.1016/j.bbagrm.2008.06.005.

213. Simon, M. D.; Chu, F.; Racki, L. R.; de la Cruz, C. C.; Burlingame, A. L.; Panning, B.; Narlikar, G. J.; Shokat, K. M. The Site-Specific Installation of Methyl-Lysine Analogs into Recombinant Histones. *Cell* **2007**, *128* (5), 1003–1012. https://doi.org/10.1016/j.cell.2006.12.041.

214. Simon, M. D.; Shokat, K. M. *A Method to Site-Specifically Incorporate Methyl-Lysine Analogues into Recombinant Proteins*, 1st ed.; Elsevier Inc., 2012; Vol. 512. https://doi.org/10.1016/B978-0-12-391940-3.00003-2.

215. Seeliger, D.; Soeroes, S.; Klingberg, R.; Schwarzer, D.; Grubmüller, H.; Fischle, W. Quantitative Assessment of Protein Interaction with Methyl-Lysine Analogues by Hybrid Computational and Experimental Approaches. *ACS Chem. Biol.* **2012**, *7* (1), 150–154. https://doi.org/10.1021/cb200363r.

216. James, L. I.; Barsyte-Lovejoy, D.; Zhong, N.; Krichevsky, L.; Korboukh, V. K.; Herold, J. M.; MacNevin, C. J.; Norris, J. L.; Sagum, C. A.; Tempel, W.; et al. Discovery of a Chemical Probe for the L3MBTL3 Methyllysine Reader Domain. *Nat. Chem. Biol.* **2013**, *9* (3), 184–191. https://doi.org/10.1038/nchembio.1157.

217. Herold, J. M.; Wigle, T. J.; Norris, J. L.; Lam, R.; Korboukh, V. K.; Gao, C.; Ingerman, L. A.; Kireev, D. B.; Senisterra, G.; Vedadi, M.; et al. Small-Molecule Ligands of Methyl-Lysine Binding Proteins. *J. Med. Chem.* **2011**. https://doi.org/10.1021/jm200045v.

218. Nguyen, D. P.; Garcia Alai, M. M.; Kapadnis, P. B.; Neumann, H.; Chin, J. W. Genetically Encoding N(Epsilon)-Methyl-L-Lysine in Recombinant Histones. *J. Am. Chem. Soc.* **2009**, *131* (40), 14194–14195. https://doi.org/10.1021/ja906603s.

219. Groff, D.; Chen, P. R.; Peters, F. B.; Schultz, P. G. A Genetically Encoded ε-N-Methyl Lysine in Mammalian Cells. *ChemBioChem* **2010**, *11* (8), 1066–1068. https://doi.org/10.1002/cbic.200900690.

220. Wang, Y.-S.; Wu, B.; Wang, Z.; Huang, Y.; Wan, W.; Russell, W. K.; Pai, P.-J.; Moe, Y. N.; Russell, D. H.; Liu, W. R. A Genetically Encoded Photocaged Nε-Methyl-l-Lysine. *Mol. Biosyst.* **2010**, *6* (9), 1557. https://doi.org/10.1039/c002155e.

221. Gao, C.; Herold, J. M.; Kireev, D.; Wigle, T.; Norris, J. L.; Frye, S. Biophysical Probes Reveal a "Compromise" Nature of the Methyl-Lysine Binding Pocket in L3MBTL1. *J. Am. Chem. Soc.* **2011**, *133* (14), 5357–5362. https://doi.org/10.1021/ja110432e.

222. Brueckner, B.; Lyko, F. DNA Methyltransferase Inhibitors: Old and New Drugs for an Epigenetic Cancer Therapy. *Trends in Pharmacological Sciences*. 2004. https://doi.org/10.1016/j.tips.2004.09.004.

223. Brueckner, B.; Kuck, D.; Lyko, F. DNA Methyltransferase Inhibitors for Cancer Therapy. *Cancer J.* **2007**, *13* (1), 17–22. https://doi.org/10.1097/PPO.0b013e31803c7245.